



U.S. Department of
Transportation

**Federal Railroad
Administration**

Performance Evaluation of Concrete Railroad Ties on the Northeast Corridor

Office of Research
and Development
Washington, DC 20590



NOTICE

This document is disseminated under the sponsorship of the Department of Transportation in the interest of information exchange. The United States Government assumes no liability for its contents or use thereof. Any opinions, findings and conclusions, or recommendations expressed in this material do not necessarily reflect the views or policies of the United States Government, nor does mention of trade names, commercial products, or organizations imply endorsement by the United States Government. The United States Government assumes no liability for the content or use of the material contained in this document.

NOTICE

The United States Government does not endorse products or manufacturers. Trade or manufacturers' names appear herein solely because they are considered essential to the objective of this report.

REPORT DOCUMENTATION PAGE*Form Approved
OMB No. 0704-0188*

Public reporting burden for this collection of information is estimated to average 1 hour per response, including the time for reviewing instructions, searching existing data sources, gathering and maintaining the data needed, and completing and reviewing the collection of information. Send comments regarding this burden estimate or any other aspect of this collection of information, including suggestions for reducing this burden, to Washington Headquarters Services, Directorate for Information Operations and Reports, 1215 Jefferson Davis Highway, Suite 1204, Arlington, VA 22202-4302, and to the Office of Management and Budget, Paperwork Reduction Project (0704-0188), Washington, DC 20503.

1. AGENCY USE ONLY (Leave blank)		2. REPORT DATE March 2014	3. REPORT TYPE AND DATES COVERED Final Report	
4. TITLE AND SUBTITLE Performance Evaluation of Concrete Railroad Ties on the Northeast Corridor			5. FUNDING NUMBERS	
6. AUTHOR(S) and FRA COTR Ronald A. Mayville, Liying Jiang, Matthew Sherman				
7. PERFORMING ORGANIZATION NAME(S) AND ADDRESS(ES) Simpson Gumpertz & Heger Inc. 41 Seyon Street Waltham, MA 02453			8. PERFORMING ORGANIZATION REPORT NUMBER	
9. SPONSORING/MONITORING AGENCY NAME(S) AND ADDRESS(ES) Federal Railroad Administration Office of Passenger and Freight Programs Office of Research and Development Washington, DC 20590			10. SPONSORING/MONITORING AGENCY REPORT NUMBER DOT/FRA/RPD-14/03	
11. SUPPLEMENTARY NOTES				
12a. DISTRIBUTION/AVAILABILITY STATEMENT This document is available to the public through the FRA Web site at www.fra.dot.gov , or by calling (202) 493-1300.			12b. DISTRIBUTION CODE	
13. ABSTRACT (Maximum 200 words) Simpson Gumpertz & Heger Inc. conducted an investigation into the factors that caused widespread failure in prestressed concrete railroad ties on the Northeast Corridor. The problem was apparent in ties manufactured and installed circa 1994–1998. The work included a literature search, review of existing studies, field investigation, laboratory analyses, including petrography and mechanical testing, finite element analysis, and field testing. We evaluated ties that cracked (pre-2003 ties) and ties that did not crack (post-2003 and San-Vel ties). The results show that the predominant mode of cracking, horizontal cracks in the top row of tendons, is a result of a combination of high stresses from prestressing forces and alkali-silica reaction (ASR) induced pressure. Train wheel loading contributes to crack growth but does not appear to be the cause of crack initiation. Delayed Ettringite Formation (DEF) and freeze-thaw cycling do not appear to contribute to the cracking.				
14. SUBJECT TERMS Concrete railroad ties, alkali-silica reaction (ASR), delayed ettringite formation (DEF), impact echo, material analysis, prestressing tendons, degradation mechanisms, petrographic analyses, bursting and splitting forces, transfer strength and length			15. NUMBER OF PAGES 171	
			16. PRICE CODE	
17. SECURITY CLASSIFICATION OF REPORT Unclassified	18. SECURITY CLASSIFICATION OF THIS PAGE Unclassified	19. SECURITY CLASSIFICATION OF ABSTRACT Unclassified	20. LIMITATION OF ABSTRACT	

NSN 7540-01-280-5500

Standard Form 298 (Rev. 2-89)
Prescribed by ANSI Std. Z39-18
298-102

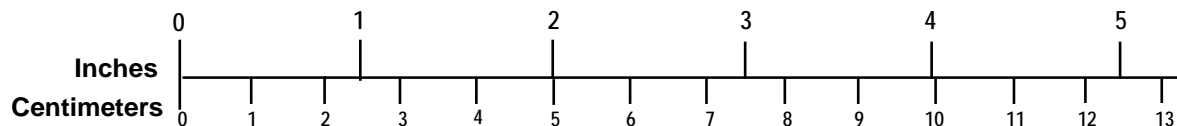
METRIC/ENGLISH CONVERSION FACTORS

ENGLISH TO METRIC

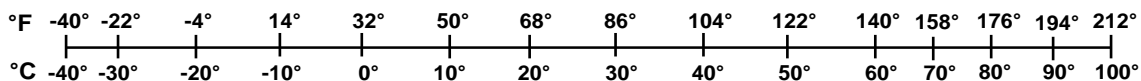
METRIC TO ENGLISH

<p>LENGTH (APPROXIMATE)</p> <p>1 inch (in) = 2.5 centimeters (cm)</p> <p>1 foot (ft) = 30 centimeters (cm)</p> <p>1 yard (yd) = 0.9 meter (m)</p> <p>1 mile (mi) = 1.6 kilometers (km)</p>	<p>LENGTH (APPROXIMATE)</p> <p>1 millimeter (mm) = 0.04 inch (in)</p> <p>1 centimeter (cm) = 0.4 inch (in)</p> <p>1 meter (m) = 3.3 feet (ft)</p> <p>1 meter (m) = 1.1 yards (yd)</p> <p>1 kilometer (km) = 0.6 mile (mi)</p>
<p>AREA (APPROXIMATE)</p> <p>1 square inch (sq in, in²) = 6.5 square centimeters (cm²)</p> <p>1 square foot (sq ft, ft²) = 0.09 square meter (m²)</p> <p>1 square yard (sq yd, yd²) = 0.8 square meter (m²)</p> <p>1 square mile (sq mi, mi²) = 2.6 square kilometers (km²)</p> <p>1 acre = 0.4 hectare (he) = 4,000 square meters (m²)</p>	<p>AREA (APPROXIMATE)</p> <p>1 square centimeter (cm²) = 0.16 square inch (sq in, in²)</p> <p>1 square meter (m²) = 1.2 square yards (sq yd, yd²)</p> <p>1 square kilometer (km²) = 0.4 square mile (sq mi, mi²)</p> <p>10,000 square meters (m²) = 1 hectare (ha) = 2.5 acres</p>
<p>MASS - WEIGHT (APPROXIMATE)</p> <p>1 ounce (oz) = 28 grams (gm)</p> <p>1 pound (lb) = 0.45 kilogram (kg)</p> <p>1 short ton = 2,000 pounds (lb) = 0.9 tonne (t)</p>	<p>MASS - WEIGHT (APPROXIMATE)</p> <p>1 gram (gm) = 0.036 ounce (oz)</p> <p>1 kilogram (kg) = 2.2 pounds (lb)</p> <p>1 tonne (t) = 1,000 kilograms (kg) = 1.1 short tons</p>
<p>VOLUME (APPROXIMATE)</p> <p>1 teaspoon (tsp) = 5 milliliters (ml)</p> <p>1 tablespoon (tbsp) = 15 milliliters (ml)</p> <p>1 fluid ounce (fl oz) = 30 milliliters (ml)</p> <p>1 cup (c) = 0.24 liter (l)</p> <p>1 pint (pt) = 0.47 liter (l)</p> <p>1 quart (qt) = 0.96 liter (l)</p> <p>1 gallon (gal) = 3.8 liters (l)</p> <p>1 cubic foot (cu ft, ft³) = 0.03 cubic meter (m³)</p> <p>1 cubic yard (cu yd, yd³) = 0.76 cubic meter (m³)</p>	<p>VOLUME (APPROXIMATE)</p> <p>1 milliliter (ml) = 0.03 fluid ounce (fl oz)</p> <p>1 liter (l) = 2.1 pints (pt)</p> <p>1 liter (l) = 1.06 quarts (qt)</p> <p>1 liter (l) = 0.26 gallon (gal)</p> <p>1 cubic meter (m³) = 36 cubic feet (cu ft, ft³)</p> <p>1 cubic meter (m³) = 1.3 cubic yards (cu yd, yd³)</p>
<p>TEMPERATURE (EXACT)</p> <p>$[(x-32)(5/9)] \text{ }^\circ\text{F} = y \text{ }^\circ\text{C}$</p>	<p>TEMPERATURE (EXACT)</p> <p>$[(9/5)y + 32] \text{ }^\circ\text{C} = x \text{ }^\circ\text{F}$</p>

QUICK INCH - CENTIMETER LENGTH CONVERSION



QUICK FAHRENHEIT - CELSIUS TEMPERATURE CONVERSION



For more exact and or other conversion factors, see NIST Miscellaneous Publication 286, Units of Weights and Measures. Price \$2.50 SD Catalog No. C13 10286

Updated 6/17/98

Contents

Executive Summary	1
1. Introduction.....	4
2. Description of the Problem	6
3. Case Studies	8
3.1 Overview	8
3.2 Examination of Ties in Track	10
3.3 Sources of Ties for Case Study Laboratory Analysis.....	13
3.4 General Approach for Examining Ties	14
3.5 Case Study Tie Conditions	17
4. Materials Analysis	22
4.1 Prestressing Tendons	22
4.2 Concrete Tie Manufacturing and Potential Concerns	25
4.3 Concrete Material Degradation Mechanisms	27
4.4 Review of Amtrak Material Specifications	31
4.5 Review of Studies of the Ties by Others	36
4.6 SGH Petrographic Examinations.....	38
4.7 Discussions and Findings Relative to Petrographic, SEM/EDS, and Air-Void System Testing.....	57
5. Mechanical Testing.....	63
5.1 Modulus and Compressive Strength.....	63
5.2 Tensile (Splitting) Strength	67
5.3 Tie Flexural Strength.....	68
6. Loads.....	74
6.1 Field Test.....	74
6.2 Other Load Data	90
7. Stresses in Concrete Ties	93
7.1 Concrete Tie Design.....	93
7.2 Finite Element Analysis of Prestressing Loads	96
7.3 Some Parametric Analyses for the Prestress Condition	109
7.4 Stresses from Other Loads	114
7.5 Strength Considerations	126
7.6 Discussion on the Vertical Location at which Cracks Occur	129
8. Evaluation of Contributing Factors.....	132
8.1 Cracking of pre-2003 Ties.....	132
8.2 Expectation of Future Performance of the Post-2003 Ties	136
9. Summary and Conclusions	138
10. References.....	141

Appendices A.1 through A.4 144

Figures

Figure 2.1. Views from the Amtrak 1989 concrete tie specification drawing corresponding to the primary tie design investigated in this study.....	6
Figure 2.2. Photographs of the predominant mode of concrete tie cracking investigated in this study; the crack on the left is revealed by alcohol.	7
Figure 3.1. Views from the Amtrak 2003 concrete tie specification drawing.	9
Figure 3.2. Views from the San-Vel concrete tie specification drawing.....	10
Figure 3.3. A bridge structure near the field test site at which we nondestructively examined ties.....	11
Figure 3.4. An example of a severely cracked tie from the MBTA Old Colony Line	12
Figure 3.5. An example of a tie with a typical crack from the MBTA Old Colony Line.....	13
Figure 3.6. Photographs from the Amtrak yard in Davisville, RI, from which some of the case study ties were obtained.....	14
Figure 3.7. Photograph of one of the case study ties showing how the crack is revealed with the use of isopropyl alcohol.	15
Figure 3.8. The crack map for Tie 9.	16
Figure 3.9. The impact echo device and a sample reading.	17
Figure 3.10. The impact echo results vs. our crack rating for the case study ties	20
Figure 4.1. Example of elliptical deformations on seven-wire strands from a pre-2003 tie.....	24
Figure 4.2. Example of elongated elliptical deformations on a single-wire strand from a post-2003 tie.....	24
Figure 4.3. Example of elliptical deformations on seven-wire strands from a San-Vel tie.	25
Figure 4.4. SGH retrieving a full-depth vertical core sample from a tie	39
Figure 4.5. A magnified view of the polished cross section in Core C8-1. Note the intersecting fractures that originate in a reactive coarse aggregate particle, extend outward into the surrounding paste structure, and are partially filled with gray, subtranslucent to opaque ASR gel (yellow arrows).	43
Figure 4.6. A magnified view of the polished cross section in Core C8-1. Note the intersecting fractures that originate in a reactive chert particle, extend outward into the surrounding paste structure, and are partially filled with gray, subtranslucent to opaque (white) ASR gel (yellow arrows).	43
Figure 4.7. A magnified view of the polished cross-section in Core S1-3 showing very few air voids in the paste structure.....	45
Figure 4.8. A magnified view of the polished cross-section in Core S1-3 showing subparallel fractures in the near surface concrete (yellow arrows).	45
Figure 4.9. A magnified view of the polished cross-section in Core S1-3 showing a tight intimate bond between the tendon strands and the surrounding paste.....	46

Figure 4.10. Core sample extracted horizontally from tie 18 at a lateral crack. Red arrow points to the location where the core example was extracted; yellow arrows point to lateral crack.....	47
Figure 4.11. Core C17-3- sprayed with alcohol showing the lateral crack on the exterior surface extending into the concrete body and stopping at the second tendon.....	48
Figure 4.12. Core C8-4 showing the cracks on the circumference of the core sample at tendons (red and yellow arrows). Note that core fractured at one of the tendons during coring at one of the cracks exaggerating its width (yellow arrows).....	48
Figure 4.13. Overview of polished section from Core C8-4 showing alignment of cracks. Red arrows point to cracks (too narrow to be visible at this scale) and outline the orientation of the cracks; yellow arrows point to reactive aggregate particles. Photograph shown in as-cored orientation, side of tie to the left, top of core to top of photograph.....	51
Figure 4.14. Magnified view of the microstructure in the body of Core C8-4 showing a reactive chert aggregate particle with ASR gel. Yellow arrows outline the reaction rim around the perimeter of the aggregate as well as the locations of ASR gel that partially fills cracks that extend outward from the aggregate and partially fills fractures in the surrounding paste structure.....	52
Figure 4.15. Magnified view of the microstructure in the body of Core C17-3 showing a reactive coarse aggregate particle and ASR gel that is partially filling the crack in the aggregate as well as portions of aggregate cracks that extend outward and partially filling fractures in the surrounding paste structure.....	53
Figure 4.16. Magnified view of the microstructure in the body of Core C8-4 showing intermittent gap (yellow arrows) around one of the prestressing strands (pink).....	53
Figure 4.17. Crack condition on the polished section from Core C17-3. Red arrows point to direction and extent of cracks; yellow arrows point to the reactive aggregates.....	54
Figure 4.18. A magnified view of the polished cross-section in Core C17-3 at the tendon near the exterior surface. Red arrows point to the minor brown corrosion staining at the tendon.....	54
Figure 4.19. A magnified view of the polished cross-section in Core C17-3 showing the fracture surface – just above the tendon. Red arrows point to the tear fractures in the fracture surface.....	55
Figure 4.20. Cracking in the polished section from Core C18-3 (only the surface crack to the first tendon is illustrated). Yellow arrows point to the crack and point in the direction of the exterior surface and the first tendon – the crack goes around the aggregate particles rather than fracturing the aggregates as shown highlighted in the inset.....	55
Figure 4.21. Relationship between the severity of ASR distress and the crack rating	61
Figure 5.1. Set-up testing for the modulus of elasticity tests.....	63
Figure 5.2. Effect of time on compressive strength of concrete for moist-cured and steam-cured concrete (from [5.1]).....	66
Figure 5.3 Effect of time on compressive strength of concrete (from [5.2]).....	67

Figure 5.4. Tensile (splitting) test configuration	68
Figure 5.5. Typical Amtrak specification setup for positive rail seat moment test	69
Figure 5.6. Illustration of the SGH positive rail seat moment test configuration.....	69
Figure 5.7. Diagrams of instrumentation used in tie positive rail seat moment tests	70
Figure 5.8. The load plots for flexural strength testing of some of the case study ties	71
Figure 5.9. An example of the type of flexural crack that occurred in each of the ties from the positive rail seat moment test.....	72
Figure 5.10. An example of the type of strand slip and vertical cracking that occurred in the final stages in each of the pre-2003 ties from the positive rail seat moment test.....	73
Figure 6.1. Layout of the field test instrumentation.....	75
Figure 6.2. View of the test site from an overpass (Track 1 is at the bottom).....	76
Figure 6.3. Vertical and lateral wheel-rail load strain gages	77
Figure 6.4. Field test strain gage locations on the concrete ties (sketch).....	78
Figure 6.5. Concrete strain gage mounted to the center of a tie	78
Figure 6.6. Field test accelerometer locations on the center tie (sketch).....	79
Figure 6.7. Three accelerometers mounted to one end of the tie	79
Figure 6.8. Vertical wheel-rail force on north rail between Ties 0 and 1 for an Acela train.....	81
Figure 6.9. Vertical tie measurements on the north rail over Tie 1 for an Acela train	81
Figure 6.10. Calculation of the actual tie load for Tie 2	82
Figure 6.11. Actual vertical tie load for Tie 1 under the north rail.....	82
Figure 6.12. Vertical wheel-rail force histogram with original tie pads	83
Figure 6.13. Vertical wheel-rail load histogram comparing old and new tie pads	84
Figure 6.14. Actual vertical tie load histogram comparing old and new tie pads.....	85
Figure 6.15 Lateral wheel-rail force on the north rail between Ties 1 and 2.....	85
Figure 6.16. Lateral wheel-rail force histogram with old tie pads.....	86
Figure 6.17. Lateral wheel-rail force histogram comparing original and new tie pads	86
Figure 6.18. Tie strain on the top center of Tie 1	87
Figure 6.19. Vertical acceleration on the northeast end of Tie 1	88
Figure 6.20. Longitudinal acceleration on the north end of Tie 1	89
Figure 6.21. An overlay of vertical accelerations and wheel loads on the north end of Tie 1	89
Figure 6.22. Peak loads measured by Amtrak on the NEC (from [6.3])	92
Figure 7.1. An illustration of the analysis steps used to simulate concrete tie prestressing	98

Figure 7.2. Comparison between the calculated and measured distributions of stress along the prestressing strand for a test beam [7.8]	99
Figure 7.3. The calculated stress along the top, center prestressing strand in the pre-2003 concrete tie	100
Figure 7.4. The longitudinal stresses calculated by finite element analysis for prestressing-only in the pre-2003 ties.....	101
Figure 7.5. The calculated vertical stresses, due to prestress-only, in the pre-2003 tie at longitudinal sections 1 in, 4.3 in, and 21 in from the tie end. (Regions that are black are in compression. Regions that are gray have tensile stresses greater than 500 psi.)	102
Figure 7.6. The calculated vertical stresses along a path through the top row of strands due to prestress-only in the pre-2003 ties at a section 4.3 in from the tie end.....	103
Figure 7.7. The strut-and-tie model for visualizing stresses near the transfer point of prestressing strands in the pre-2003 tie design	104
Figure 7.8. Illustration of the outward pressure exerted by an indented strand during slippage	105
Figure 7.9. The calculated horizontal stresses along a path through the outer most two strands due to prestress-only in the pre-2003 ties at a section 4.3 in from the tie end.....	106
Figure 7.10. The calculated vertical stresses due to prestress-only in the pre- and post-2003 ties at a longitudinal section 4.2 in from the tie end. (Regions that are black are in compression. Regions that are gray have tensile stresses greater than 500 psi.)	107
Figure 7.11. The calculated vertical stresses along a path through a row of strands (top row for pre-2003, second row for post-2003) due to prestress-only in the pre- and post-2003 ties at a section 4.2 in from the tie end.....	108
Figure 7.12. Comparison of vertical stress along a path through the top strands at the location of maximum vertical stress for the pre-2003 and San-Vel ties for prestress loading only.	109
Figure 7.13. The calculated stress along a prestressing strand in a pre-2003 tie for two values of coefficient of friction between strand and concrete	110
Figure 7.14. The vertical stress contours (prestress-only) in a pre-2003 tie for two values of coefficient of friction between strand and concrete: a) $\mu = 0.5$; b) $\mu = 0.75$	110
Figure 7.15. The prestress force variation along the strand used in the transfer length (TL) study	111
Figure 7.16. The calculated variation in vertical bursting stress vs. transfer length.....	112
Figure 7.17. The location of calculated vertical bursting stress vs. transfer length.....	112
Figure 7.18. The calculated stress along a prestressing strand in a post-2003 tie for two values of concrete modulus	113
Figure 7.19. Calculated vertical stress contours from prestressing only in a post-2003 tie for two values of concrete modulus: a) $E = 3,600$ ksi; b) $E = 4,770$ ksi	114
Figure 7.20. Longitudinal stresses in the pre-2003 tie from a 52 kip positive rail seat moment test, including prestress	115

Figure 7.21. Shear stresses in the pre-2003 tie from a 52 kip positive rail seat moment test, including the prestress. The S13 stress acts along horizontal planes through the tie.	115
Figure 7.22. Longitudinal stresses in a top, center strand for both the prestress and the prestress plus positive rail seat moment loading.....	116
Figure 7.23. Vertical stresses along a transverse path through the top strands of a pre-2003 tie for both the prestress and prestress plus positive rail seat moment loading	117
Figure 7.24. The calculated shear stress distribution along a path through the top row of strands for the application of a 52 kip vertical load at the rail seat: (top plot) at 4.3 in from the tie end; (bottom plot) at 15 in from the tie end.....	118
Figure 7.25. The finite element mesh for the pre-2003 concrete tie-shoulder insert analysis ...	119
Figure 7.26. A cross-section through the pre-2003 concrete tie model showing the proximity of the shoulder insert to the reinforcing strands	120
Figure 7.27. Shear stress distribution in the pre-2003 tie with shoulder insert subjected to a 52 kip downward load at rail seat and supported on ballast	121
Figure 7.28. Vertical tensile stress distribution in the pre-2003 tie with shoulder insert subjected to a 5 kip upward load at rail seat and supported on ballast	122
Figure 7.29. The finite element model used for dynamic impact analysis	125
Figure 7.30. Vertical stress distribution at the center of the tie shortly after impact (t = 3 ms).....	125
Figure 7.31. Time history of vertical stress in the concrete tie adjacent to a top strand and at the outer surface; tension is positive.....	126
Figure 7.32. Biaxial strength results for an 8,500 psi compression strength concrete (from [7.13]).....	128
Figure 7.33. Vertical tensile stress distribution at a section of the pre-2003 tie taken perpendicular to the strands at the location of maximum bursting stress	130
Figure 7.34. Vertical tensile stress distribution at a section of the post-2003 tie taken perpendicular to the strands at the location of maximum bursting stress	131
Figure 8.1. A severe example of a tie with the predominant mode of cracking investigated in this study	132

Tables

Table 3.1. Case study ties summary.....	8
Table 3.2. Some characteristics of the different tie designs investigated	10
Table 3.3. Case study tie conditions from visual examination in the lab	18
Table 4.1. Dimension and hardness measurement results on the case study tie strands.....	23
Table 4.2. Comparison of key components of the Amtrak specifications for pre- and post-2003 ties.....	33
Table 4.3. Summary of SGH laboratory tests on selected concrete ties	38
Table 4.4. Petrographic examination summary of concrete ties from Case Studies 1 and 2: pre-2003 NEC.....	42
Table 4.5. Petrographic examination summary of horizontally oriented concrete ties from Case Study 2: pre-2003 NEC.....	49
Table 4.6. Summary of core observations and testing related to freeze-thaw evaluation	57
Table 4.7. Data used to correlate crack severity to various measures of ASR	60
Table 4.8. Summary of ASR-related observations in the pre-2003 ties	62
Table 5.1. Modulus of elasticity and compressive strength test results.....	65
Table 5.2. Tensile (splitting) test results on concrete from the case study ties.....	68
Table 5.3. Ties for the positive rail seat moment test	70
Table 5.4. Results from the positive rail seat moment test	71
Table 6.1. Rail vehicles that passed the test site during field test measurements.....	74
Table 6.2. Tie pad properties	77
Table 6.3. Typical concrete tie strains and inferred stresses and moments	87
Table 6.4. The natural frequencies and corresponding mode shapes determined from the field test data.....	90
Table 7.1. The flexural strength (to initial cracking) requirements for the Amtrak ties from the various specifications.....	94
Table 7.2. The stresses due to prestress transfer in ties calculated using PCI methods [7.2].....	95
Table 7.3. The initial flexural cracking and ultimate moments for the case study ties calculated using PCI methods [5.3]	96
Table 7.4. Calculated natural frequencies for the concrete tie.....	123
Table 7.5. Calculated and measured tensile strengths for the concrete of the Amtrak ties for different Times after Production.....	127
Table 7.6. Comparison of maximum bursting stresses and clear concrete cover to the tie side for different tie designs.....	130

Table A.2.1. Comparison of the material test schedule for pre- and post-2003 ties.....	147
Table A.4.1. Petrographic examination summary of concrete ties from Case Study 3: post-2003 NEC.....	154
Table A.4.2. Petrographic examination summary of concrete ties from Case Study 5: San Vel.....	156

Executive Summary

The study reported here was aimed at determining the factors that caused the cracking of concrete ties on the Northeast Corridor (NEC). The mode of cracking we investigated is a horizontal crack that passes through the top row of prestressed steel reinforcing strands generally near one or both ends of a tie. It is widespread in ties manufactured and installed circa 1994–1998, which we refer to as the pre-2003 ties.

Our work involved several tasks. We examined sets of ties we divided into five case studies, each with some distinguishing feature. The case studies included pre-2003 NEC ties with minor cracking or no externally visible cracking; pre-2003 NEC ties with clear visible cracking; post-2003 NEC ties made to the 2003 specification with a very different prestressing tendon configuration and modified concrete material requirements; MBTA ties from the Old Colony Line that have a design essentially identical to the pre-2003 NEC ties and which showed the same type of horizontal cracking; and San-Vel NEC ties from 1978 that have shown virtually no signs of cracking. We examined individual ties in the field and sent some to our laboratories for more detailed analysis that included petrographic evaluations and mechanical testing. We also reviewed production test reports and petrographic reports on the cracking problem generated by third parties for Amtrak. We carried out finite element analysis to investigate the effects of various tie and external loading parameters. This analysis was validated to some degree by results from a field test we conducted on a section of the NEC in Rhode Island during which we measured loads into the track as well as the loads, strains, and accelerations of the concrete ties themselves.

We found that the tie cracking was caused by a combination of factors, none of which would have caused the distress independently. The primary factors contributing to the distress were:

- A high concentration of tensile stress in the ties at the level of the prestressing steel due to the forces associated with the transfer of load from the steel to the concrete during de-tensioning of the strands during manufacturing. These stresses are greatest at the top row of tendons.
- Stresses within the concrete from the pressures caused by alkali-silica reaction (ASR) that were additive to those from the prestressing forces.

High stresses with the potential for splitting are present in all prestressed concrete members. This failure mode is addressed specifically in prestressed concrete design guides (e.g., American Society for Testing and Materials Standards) for structures and bridges, but it is not addressed by the current concrete railroad tie specifications and tie industry standards. As a result, as-built ties have little margin of safety against this splitting mode of failure at the tie end.

ASR is a recognized deterioration mechanism in concrete, and we found evidence of reactive aggregates and ASR in all ties that showed significant cracking. However, the products of the ASR were generally confined to the regions at which the cracks occurred and were not evident in

other parts of the ties. This indicates that pressures caused by ASR were additive to the pressures from the prestressing forces and caused the observed cracking to occur before the ASR progressed sufficiently to cause typical ASR pattern cracking elsewhere in the ties.

After the cracking occurred at the zone of highest stress where the ASR and prestressing stresses combined at the upper prestressing tendon level, it was easier for the cracking to propagate there rather than to form at new locations. Our work shows that this propagation was assisted by the following secondary factors, which were not initial causes of the distress:

- The deposition and swelling of ASR gel in the cracks, creating additional pressures.
- A likely shorter length over which stresses are transferred from the prestressing strands to the concrete because of more distinct strand indentations when compared, for example, with the San-Vel ties. This caused higher bursting stresses.
- External, cyclic loading from passing trains.

The performance of the San-Vel ties is notable. These ties have been in service longer than the pre-2003 ties, but have shown virtually no cracking. Our study indicates that the stresses from prestressing are lower in the San-Vel ties and the aggregate was not reactive. The factors leading to reduced stress include lower initial prestressing forces and a tapered tie end geometry. We also found evidence that: (a) the shallower and more widely spaced indentations in the San-Vel prestressing wire led to longer transfer lengths and, therefore, lower prestressing stresses; and (b) the wire used for the San-Vel ties likely experienced greater relaxation and, therefore, lower prestressing forces.

We found that the tie distress was not caused by the following factors:

- Cyclic freezing and thawing
- Delayed ettringite formation (DEF)
- Stresses from other mechanical effects, such as from fastener inserts or unusual tie vibrations

Our assessment of the post-2003 ties, with their different prestressing tendon configuration and alternate material requirements, suggests that they will not develop horizontal cracks. Although the stresses appear to be comparable adjacent to the strands and higher on the surface (bursting stresses) than for the pre-2003 ties, the concrete materials specifications had been improved to reduce or eliminate ASR. This was achieved by better screening tests and improved ASR mitigation measures. In addition, the aggregate used in the post-2003 ties that we examined is a carbonate aggregate, not susceptible to ASR.

This investigation into the complex mechanism responsible for the cracking of concrete ties along the NEC was initiated to help ensure that all potential causes were adequately addressed by

Amtrak specification changes as part of the Federal Railroad Administration's (FRA) oversight of Amtrak's operations. As stated, several significant changes were made to the Amtrak specification in 2003. These included updated provisions to protect against ASR in recognition of the fact that the material qualification tests used for the pre-2003 ties are now known to provide inadequate protection against ASR. The new specification also required higher prestressing forces to achieve the required higher flexural strengths. We do not know whether this approach was intended to mitigate the horizontal cracking problem, but our findings indicate that the higher prestressing forces reduce the (mechanical) margin against splitting.

We believe that the industry's specifications and design guidelines for concrete railroad ties should be modified to explicitly address the splitting failure mode. This would likely result in the need for stirrups (U-shaped transverse reinforcement wires) and higher cost, but we feel the reliability of long-life ties would be greatly increased. We also believe that more careful study is needed of the flexural strength requirements for different types of railroad operation and, particularly, for the NEC.

1. Introduction

In the last several years, Amtrak's inspections have detected an unexpectedly high number of concrete ties on the NEC that either have cracked along the level of the upper prestressing strands or are showing initial signs of distress, long before reaching the end of their design service life. With major concrete tie installations on the NEC dating from the late 1970s, these failing ties are neither the oldest nor the newest on the NEC.

The study reported here was aimed at identifying any manufacturing, design, or maintenance practices, or other specifications that might warrant change to help ensure that all concrete ties installed on the NEC in the future serve for their expected design life. This study supplements Amtrak's own investigations and is intended to provide an independent evaluation of Amtrak's findings.

Prestressed concrete railroad ties are supposed to provide long-term service without the problems of deterioration, splitting, maintenance, and relatively short life of timber ties. Concrete ties are marketed and presented as having service lives approaching 50 years with relatively low maintenance. Unfortunately, past and present experience has shown that this is not always the case.

In the past, premature failures due to materials-related problems have occurred early in the ties' lives. In the late 1980s and early 1990s, a well-publicized problem occurred with Amtrak's Lone Star ties up and down the eastern seaboard [1.1]. The failures manifested themselves as linear and map-pattern visible cracking of the ties that progressed into loss of prestressing force and failure of the ties. There was consensus among all investigators that the problem was due to a materials deterioration issue, although there were differences of opinion regarding the roles of ASR, freezing and thawing, and DEF in that deterioration.

In response to the Lone Star problems, precasters adjusted their fabrication procedures to avoid DEF, began to screen aggregates more closely to avoid ASR, and increased production control to ensure that freezing and thawing did not become a problem. It seemed like concrete ties could once again be used with confidence. Unfortunately, it now appears that this additional work was insufficient as new concrete tie cracking has been reported on the NEC and other locations. More than 1 million ties were supplied to Amtrak between 1990 and 2000 using the specification and manufacturing techniques developed following the Lone Star tie problems. Amtrak is now in the process of replacing essentially all of these ties because a large enough percentage has cracked to make spot replacement uneconomical. It is largely the investigation of the circa 1990–2000 ties that forms the subject of this report. The replacement ties are made to a specification written in 2003 that included significant materials and design changes to prevent cracking. Our investigation has the objective, in part, of determining whether these changes are likely to eliminate the cracking problem.

Due to the variety of potential causes, the complexity of the failure mechanisms, and the nearly complete failure of an entire generation of concrete ties, this study was conducted as part of FRA's oversight of Amtrak's operations to verify the results of Amtrak's investigation and to help ensure that modified manufacturing specifications would result in improved tie performance. During the investigation, we reviewed much of the information Amtrak obtained through its investigation of the tie cracking problem. This included reports by third parties on the characteristics of the materials used to make the ties. We then conducted work to characterize the cracking problem by collecting ties from Amtrak that had been removed from the track. We carried out our own detailed materials analysis of the ties as well as of ties made to the 2003 specification and the 1978 vintage San-Vel ties that apparently had not cracked. We also conducted mechanical tests of the concrete, the reinforcing tendons, and the ties themselves. We conducted stress analyses for various load cases and for different tie and component parameters to investigate the extent to which these parameters could contribute to the cracking problem. This effort was supported by a field test we carried out to measure loads in the ties on the NEC and to measure some tie parameters, including strains and vibration characteristics.

2. Description of the Problem

This section provides a description of the cracking problem that was the focus of our investigation. The tie design in question conforms to a set of Amtrak specifications dating back to around 1989 up to 2003 [2.1]. Figure 2.1 shows views from the specification drawing for the tie. It is a prestressed concrete member with eight 7-wire prestressing strands each prestressed to a nominal load of 17.2 kips. No stirrups or other transverse reinforcements are included in the specification or the ties themselves.

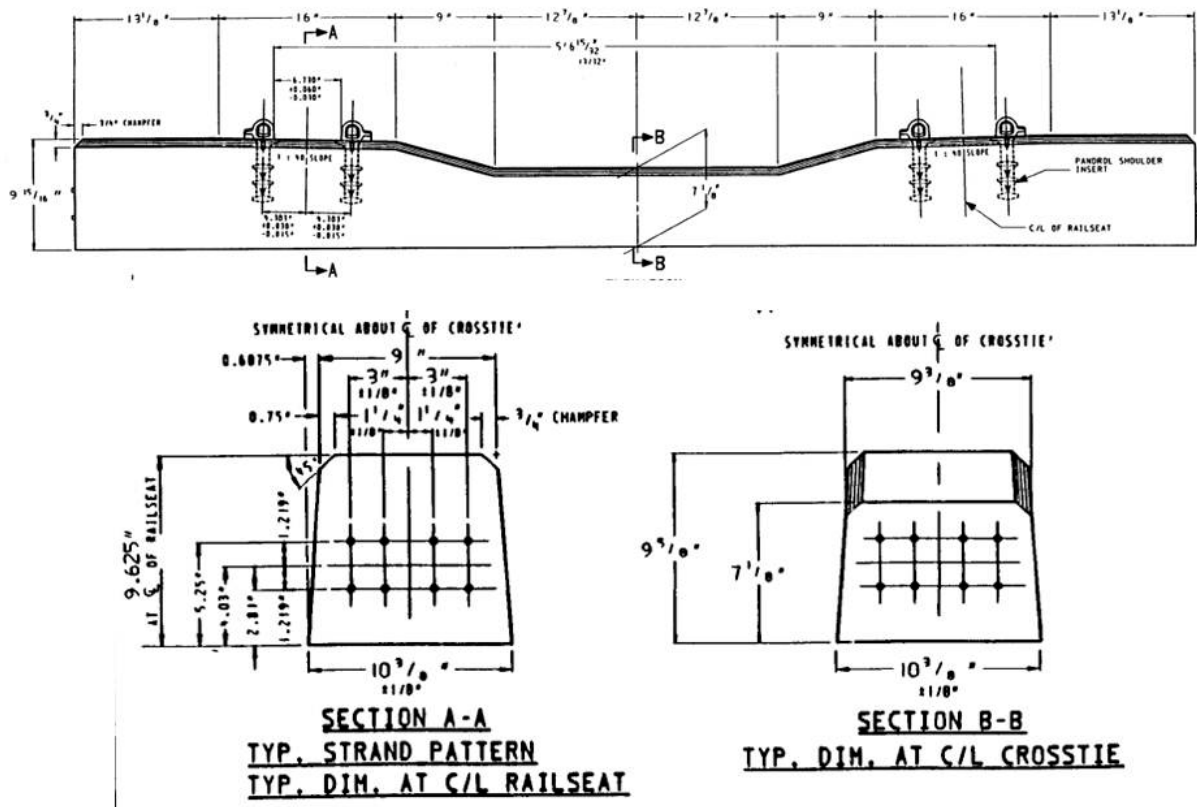


Figure 2.1. Views from the Amtrak 1989 concrete tie specification drawing corresponding to the primary tie design investigated in this study.

The predominant mode of cracking we observed in these ties from the NEC had a horizontal orientation intersecting the top row of strands, generally near the end or ends of the tie. An example of this cracking mode is shown in two different ties in Figure 2.2. Most of the ties we have examined had a crack on one or both sides. This crack is generally not visible in track because it is covered by ballast. The crack must progress substantially and turn vertically before large pieces of concrete separate from the tie. We rarely observed such severe damage. These cracks required substantial time, approximately 10 years, to become evident.



Figure 2.2. Photographs of the predominant mode of concrete tie cracking we investigated in this study; the crack on the left is revealed by alcohol.

The widespread nature of this cracking mode in our investigation is difficult to overstate. We examined a large number of concrete ties that had been removed from a 12-mile section of the NEC (MP 178-190). Approximately 70–80 percent of the ties we examined closely had a horizontal crack of the type described above. We examined another section of track as part of our field test (see Section 6). In the case of MP 168, we had great difficulty finding a tie that had no horizontal crack near at least one of its ends. Amtrak reported to us that this mode of cracking is the predominant mode of cracking associated with the ties being replaced on the entire NEC. We also conducted another investigation of the MBTA Old Colony Line consisting of 250,000 concrete ties. Part of our work in the MBTA study was to examine a subset of concrete ties as they were being removed for replacement. Approximately 50–70 percent of these ties had the same type of horizontal crack and this was by far the predominant cracking mode.

Such horizontal cracking has evidently not occurred in the newer Amtrak concrete ties (post-2003 ties) or in the older (circa 1978) San-Vel ties, although we found one report [2.2] of a horizontal crack in a San-Vel tie.

This mode of horizontal cracking, particularly when it occurs near the end of a prestressed concrete member, is generally referred to as a splitting or bursting crack and is believed to be due to the loads imparted to the concrete from the strands. We investigate this effect in detail in the sections that follow.

3. Case Studies

3.1 Overview

One of the approaches we used in investigating the causes of cracking in the NEC ties was to study ties from groups with different characteristics, including ties from other systems and ties that did not crack. We refer to these groupings as case studies. Most of the ties we examined were of the 1993–2003 vintage from the NEC, and we selected subgroups of these to form two of the case studies. We also investigated San-Vel ties, named after the company that made them (no longer in operation), which had been produced for the NEC in the late 1970s and early 1980s. Finally, we considered a set of ties used on the Old Colony Line of the Massachusetts Bay Transportation Authority (MBTA) that had a cracking problem very similar to the primary cracking problem on the NEC.

This chapter describes the general characteristics of the ties corresponding to the case studies, including their design and the form of cracking (if any). Table 3.1 lists the different case study ties.

Table 3.1. Case study ties summary.

Case Study No.	Designation	Level of Damage	Source	Year of Origin	Likely Tie Specification
1	Pre-2003; NEC	Uncracked*	MP 168, 178- 190	1993, 1994, 1998	1992 CT-10 1995 CT-10
2	Pre-2003; NEC	Cracked	MP 168, 178- 190	1993, 1994, 1998	1992 CT-10 1995 CT-10
3	Post-2003; NEC	Uncracked	MP 178-190	2003	2003 CT-10
4	MBTA	Cracked	Old Colony Line	circa 1995	MBTA spec
5	San-Vel	Uncracked	MP 166	circa 1978	AM-023

* No obvious cracking or minor cracking.

We considered three different tie designs from the NEC. We refer to the ties from the period 1993–1998 as pre-2003 ties. These ties had similar specifications [2.1] and had the geometric design shown earlier in Figure 2.1. We also investigated ties manufactured according to the 2003 specification for which several changes were made to address evidence of ASR and DEF problems. The geometry of these ties is shown in Figure 3.1. This tie has 24 single wire strands in contrast to the eight 7-wire strands of the pre-2003, MBTA, and San-Vel ties. The ties from the MBTA Old Colony Line have the same design as the pre-2003 NEC ties shown in Figure 2.1.

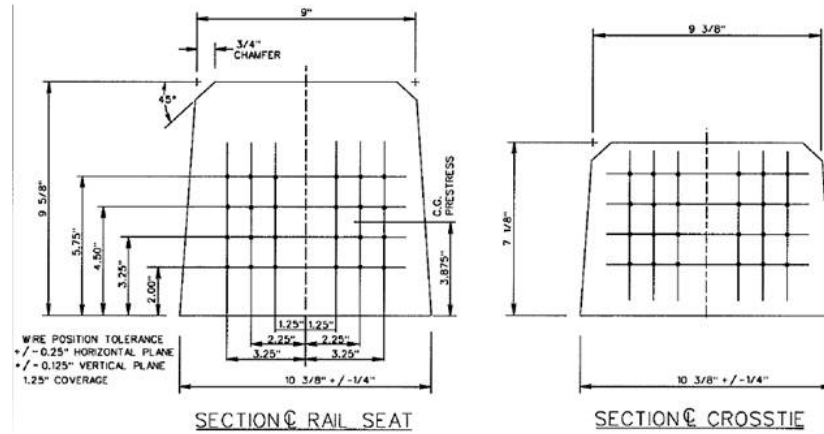
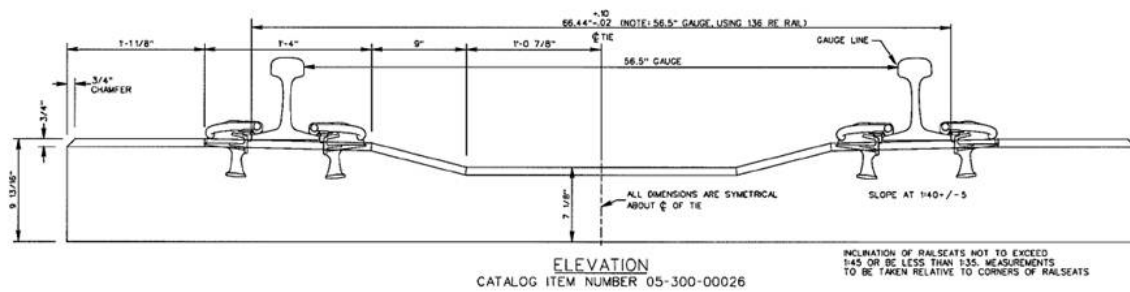


Figure 3.1. Views from the Amtrak 2003 concrete tie specification drawing.

The ties we investigated from the late 1970s and early 1980s, known as the San-Vel ties, evidently have a very good performance history with no significant signs of cracking. Figure 3.2 shows the geometric design for these ties. The San-Vel tie design is tapered at its ends and has vertical reinforcement in the form of No. 3 (0.375 in diameter) stirrups just outboard of the rail seat area. (However, these stirrups were not present in the four ties we examined in our laboratory.) Table 3.2 compares different parameters for the various ties.

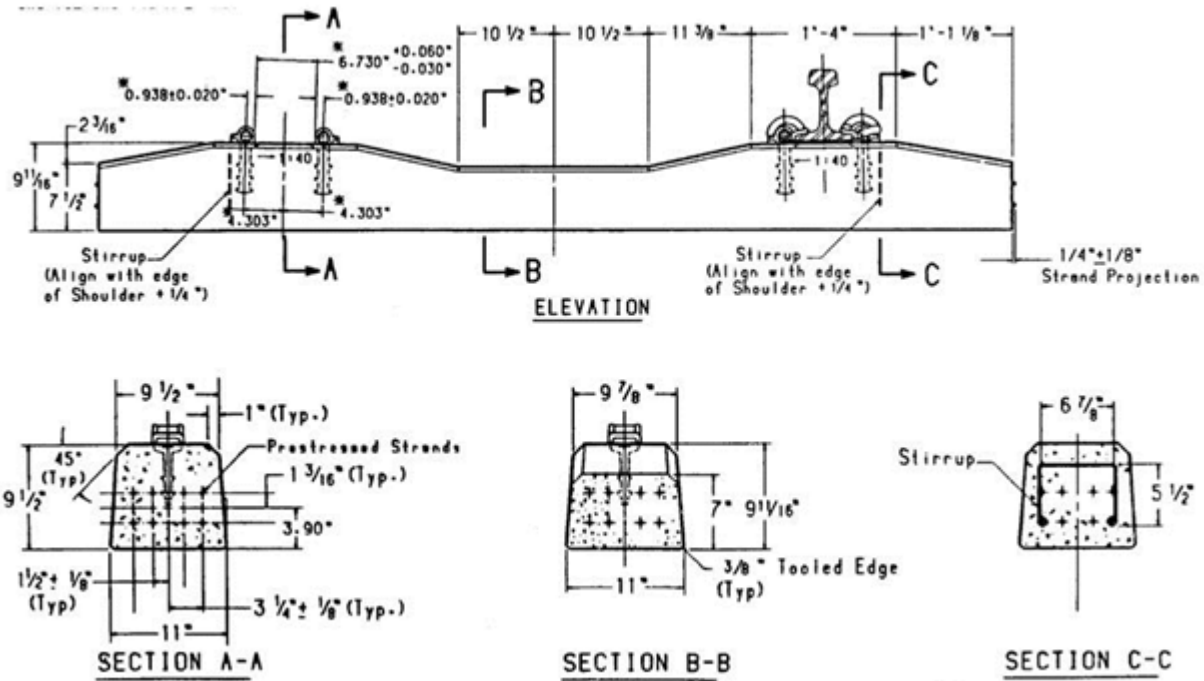


Figure 3.2. Views from the San-Vel concrete tie specification drawing.

Table 3.2. Some characteristics of the different tie designs we investigated.

Tie design	Strand type	Strand preload (kips)	Total prestress load (kips)	Cross sectional dimensions at rail seat (inches)	Minimum concrete cover to tie side (inches)
Pre-2003 (and MBTA tie)	7 wire; 0.375 in diameter	17.21	137.7	10.375 x 9.625	1.59
Post-2003	Single wire; 0.2 in diameter	6.55	157.2	10.375 x 9.625	1.39
San-Vel	7 wire; 0.375 in diameter	16.68	133.4	11 x 9.5	1.61

3.2 Examination of Ties in Track

We obtained some information about the tie cracking problem by examining ties in track. This included examination of a section of pre-2003 ties on the NEC and sections on the MBTA Old Colony Line.

3.2.1 Inspection of the Ties at the NEC Field Test Site

We carried out a detailed inspection of the section of track at which our field tests were conducted: MP 168, Track 2 (see Section 6 for the non-inspection data collected during those tests.) This inspection included visual as well as some non-destructive inspection (impact echo, described in greater detail in the next section). About one-half of the ties we examined were located under an adjacent bridge (see Figure 3.3) that had been constructed over the track approximately 5 years prior to the test. That is, the ties under the bridge had been exposed to the environment for about half of their lives. We wanted to determine whether this exposure difference led to a difference in cracking frequency and severity.



Figure 3.3. A bridge structure near the field test site at which we nondestructively examined ties.

We assessed the condition of each end of approximately 110 concrete ties using the impact echo method. Approximately half of the ties were under the bridge and half were exposed directly to the environment. All of the concrete ties appeared to be manufactured around 1994. We have established through previous programs a correlation between impact echo results and the likelihood of horizontal cracking. Using this correlation, the impact echo results indicated that 96 percent of the concrete ties not sheltered by the bridge structure had horizontal cracks and 58 percent of concrete ties sheltered by the bridge structure had horizontal cracks. We also excavated the tie-end regions at forty-one locations (approximately 20 percent of the ties tested with impact echo) to confirm the impact-echo test results and found that 92 percent of the exposed ties and 53 percent of the under-bridge ties were cracked, agreeing closely with the impact-echo test results. The impact echo data and our excavation observations suggest that at this location (Amtrak MP 168, Track 2), most of the ties are cracked and the condition of the concrete ties sheltered by the bridge structure is better than the unsheltered concrete ties. These

latter observations suggest that weathering, in the form of moisture variation, temperature fluctuation, freeze-thaw exposure, etc., is a factor that contributes to crack severity.

Six of the ties from this site, three of the exposed ties, and three from under the bridge were shipped by Amtrak to the SGH laboratory for more detailed examination.

3.2.2 Inspection of the Ties on the MBTA Old Colony Line

SGH inspected ties on several sections of track on the MBTA Old Colony Line as part of another program and some of the results are summarized here. This section of track carries commuter trains from South Station in Boston, MA, to either Plymouth or Middleboro, MA. We conducted visual examinations and some impact echo tests on ties from some of the sections on this line.

The type of cracking observed is essentially identical to what we observed on the NEC: horizontal cracks that are located at the top row of strands generally near the tie ends. Figure 3.4 shows an example of a tie removed from the line that had very severe such cracking and Figure 3.5 shows an example in which the crack is clearly visible on the side of the tie.



Figure 3.4. An example of a severely cracked tie from the MBTA Old Colony Line.



Figure 3.5. An example of a tie with a typical crack from the MBTA Old Colony Line.

We did not conduct a statistical analysis of the tie conditions, but our general observations are as follows:

- Approximately 50 percent of the concrete ties we examined had cracks.
- A horizontal crack at the level of the top row of strands was present in essentially all cracked ties we examined.
- Cracked concrete ties were found in essentially all sections of track, including exposed, under bridges, mainline track, and sidings.

3.3 Sources of Ties for Case Study Laboratory Analysis

We obtained ties for our NEC case studies from Amtrak’s tie yard in Davisville, RI, and from areas in this neighborhood. The Davisville ties had been removed from the section of track between mileposts 178 and 190 near Providence as part of Amtrak’s tie replacement program. These ties had been stacked in large piles and our team examined accessible ties from the entire lot. Figure 3.6 shows photographs from this examination. It was easy to inspect the sides of these ties, unlike those in track, and we found that more than 70–80 percent had cracks on one or both sides at the ends.

We also obtained ties from the section of track we instrumented to measure loads (MP168; see Section 6.) Three of these were the ties we instrumented, which were exposed directly to the environment. We obtained three additional ties from underneath a nearby bridge, which we were told by Amtrak had been constructed over the track around 2007; that is, the ties were fully exposed to the environment for about half of their lives. As stated previously, these ties appeared to show less cracking than their neighbors.

The San-Vel ties had been removed from Track 1 at milepost 166 as part of separate track work.



Figure 3.6. Photographs from the Amtrak yard in Davisville, RI, from which some of the case study ties were obtained.

3.4 General Approach for Examining Ties

We used the same general approach to examine all ties that were sent to us from the field. We first examined the ties in either a storage area or in track in all cases except for the San-Vel ties; the San-Vel ties were selected by Amtrak and sent to us. Amtrak or the MBTA shipped ties to SGH by truck for detailed examination. We inspected the ties to obtain or confirm, to the extent possible, the date code. In some cases, the date code was worn away because the seal had come off or faded from weathering. We confirmed that the dimensions of the ties conformed to the applicable specifications and then we examined the ties for cracking. We used both visual examination and nondestructive testing. Cracking was revealed in part by spraying the surfaces of the ties with isopropyl alcohol. The alcohol evaporates readily from the surface but takes longer to evaporate from a crack, allowing the cracks to be viewed and photographed more distinctly. Figure 3.7 shows an example of this form of crack detection.



Figure 3.7. Photograph of one of the case study ties showing how the crack is revealed with the use of isopropyl alcohol.

We mapped the cracks in each of the ties and recorded crack lengths and widths (the opening of the crack). Figure 3.8 shows an example of the mapped cracks that are typical of the ties that contained cracks.

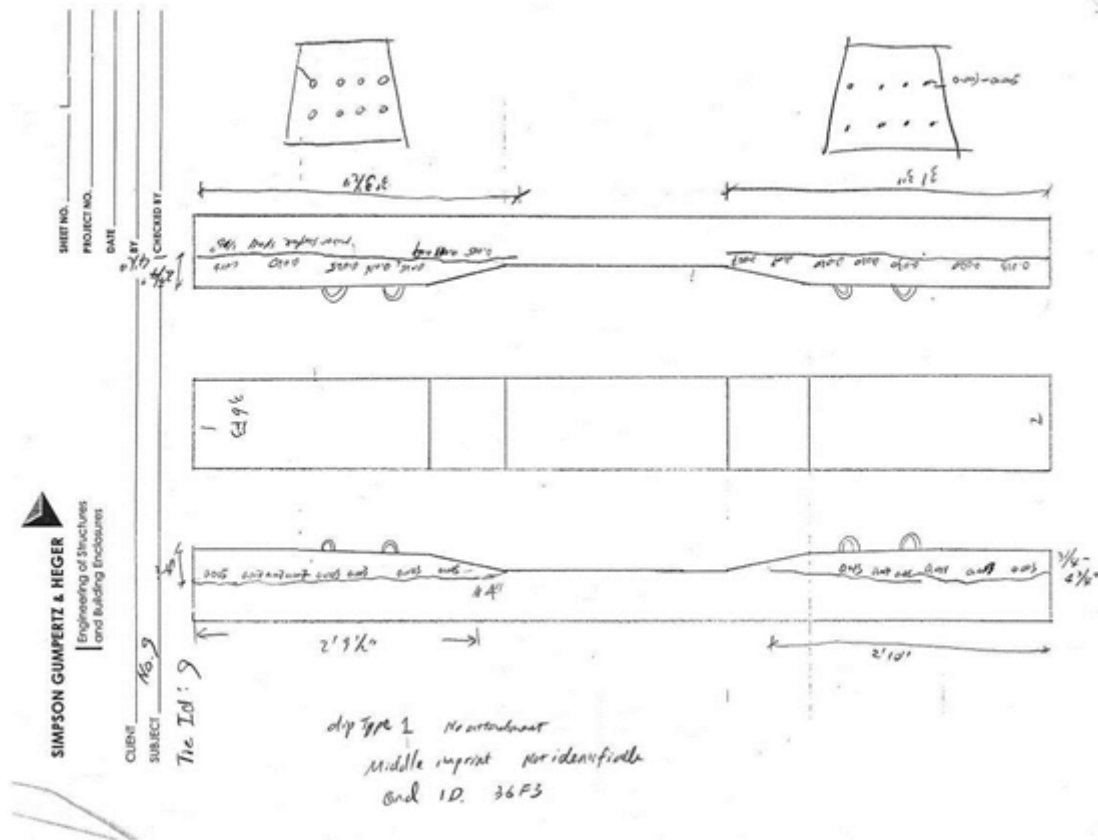


Figure 3.8. The crack map for Tie 9.

We also characterized the case study ties using the impact echo nondestructive inspection method. In the impact echo method, one introduces a transient stress pulse into a test object by mechanical impact and then monitors the surface displacements caused by the arrival of reflection of the pulse from internal defects and external boundaries (c.f. [3.1]). Figure 3.9 shows the instrument in use on a tie in the lab. The results of the test are typically displayed in terms of calculated inches of depth, rather than in the predominant signal frequency (in Hz) actually measured, because the technique is usually used to determine depth to delaminations and voids. Our past experience on concrete ties indicates that the presence of significant internal defects or cracking results in a downshift in the frequency (corresponding to an increase in the apparent thickness.)

This same impact echo technique was applied to the ties at the field test site (see Section 3.2.1).



Figure 3.9. The impact echo device and a sample reading.

3.5 Case Study Tie Conditions

Table 3.3 lists the tie conditions obtained from visual examination. We measured crack width by using a transparent plastic crack card (on which are lines of varying thicknesses). Our crack severity rating is based on a combination of the measured crack width and lengths. The rating is assigned as follows:

Rating 1: no visible crack at all

Rating 2: visible cracks with width < 0.005 in and the crack length is typically short (within 12 in)

Rating 3: visible cracks with width between 0.005 and 0.016 in and the crack length is variable

Rating 4: crack width greater than 0.016 and the crack length is extensive, typically extending from the end of tie to the shoulder of the tie

Table 3.3. Case study tie conditions from visual examination in the lab.

Case Study		Tie Number	Crack Length and Width (inches)								SGH crack severity rating
			End 1 - Side 1		End 1 - Side 2		End 2 - Side 1		End 2 - Side 2		
			Length	Width	Length	Width	Length	Width	Length	Width	
1	Pre-2003 NEC; uncracked or minor cracking	1	18-1/2	0.005	-	-	-	-	-	-	2
		2	-	-	-	-	-	-	-	-	1
		19	-	-	7-1/2	0.003	5-1/2	0.003	-	-	2
		20	-	-	-	-	-	-	11	<0.003	2
		22	6	<0.003	33-1/2	<0.003	-	-	10	<0.003	2
2	Pre-2003 NEC; cracked	3	Note 1	Note 1	Note 1	Note 1	-	-	36	0.060	4
		4	9-1/2	0.005	35	0.025	35-1/2	0.020	-	-	4
		5	35-1/2	0.013	24	0.005	38-1/2	0.011	24-3/4	0.003	3
		6	24-1/2	0.003	Note 2	0.05	-	-	Note 2	0.035	4
		7	5-1/2	0.003	33-1/2	0.016	-	-	33-1/4	0.013	3
		8	33	0.011	34	0.020	12	0.003	33-1/2	0.013	4
		9	37-1/2	0.009	39-1/2	0.025	34	0.013	39	0.030	4
		10	-	-	-	-	10	0.003	27	0.009	3
		11	-	-	31	0.003	10	0.003	17-1/2	0.003	3
		12	24	0.003	29-1/2	0.013	25-1/2	0.013	30	0.025	4
		13	34-1/2	0.016	-	-	40	0.016	-	-	3
		14	32-1/2	0.005	35-1/2	0.009	36	0.025	31	0.005	4
		17	10	<0.003	34	0.011	29	0.005	49	0.003	3
18	16	0.003	3-1/2	0.007	32	0.007	34	0.003	3		

Case Study	Tie Number	Crack Length and Width (inches)								SGH crack severity rating	
		End 1 - Side 1		End 1 - Side 2		End 2 - Side 1		End 2 - Side 2			
		Length	Width	Length	Width	Length	Width	Length	Width		
		25	30	0.005	34	0.003	35	0.005	36	0.005	3
3	Post-2003 NEC	15	-	-	-	-	-	-	-	-	1
		16	-	-	-	-	-	-	-	-	1
		21	-	-	-	-	-	-	-	-	1
		23	-	-	-	-	-	-	-	-	1
		24	-	-	-	-	-	-	-	-	1
4	MBTA	X	4	<0.003	40	0.016	4	<0.003	9	0.003	3
		Y	39	0.030	19	0.003	34	0.016	16	<0.003	4
5	San-Vel	S1	-	-	-	-	-	-	-	-	1
		S2 (Note 3)	-	-	-	-	-	-	-	-	1
		S3	-	-	-	-	-	-	-	-	1
		S4	-	-	-	-	-	-	-	-	1

- Notes:
1. Concrete spalled above the upper tendon at End 1 of Tie No. 3.
 2. Crack penetrated through the entire length of the tie.
 3. Concrete S3 shows transverse cracks on the top of tie in the middle region.

Figure 3.10 shows a correlation between the cracking severity of the case study ties inspected in our laboratory and the impact echo reading. We note a general relationship although with significant scatter.

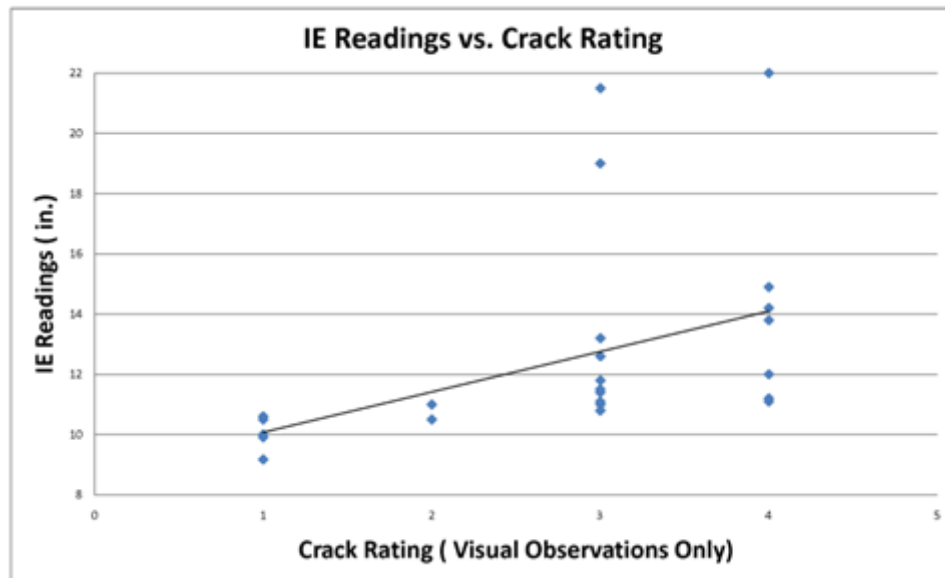


Figure 3.10. The impact echo results vs. our crack rating for the case study ties.

The impact echo tests, which measure the conditions of the interior of the ties, indicate that cracking is internal to the tie as well as evident at the surfaces.

The lab and field examinations allow us to make the following observations about the tie conditions:

Pre-2003 NEC ties

- a) The majority of these ties have some level of cracking.
- b) The cracks are nearly all horizontal, passing through the top row of strands.
- c) The cracks are present on the interior of the ties.
- d) These cracks nearly always extend to the very end of the tie.
- e) In general, the cracks do not extend to the central, tapered part of the tie, although there are a few examples in which this is the case.
- f) We found no cracks at the second row (the bottom row) of strands.
- g) Occasionally, there are vertical cracks oriented parallel to the reinforcing strands. These cracks intersect the top surface of the tie and are at the tie ends.

- h) We found no cracks that could be classified as flexural cracks (perpendicular to the reinforcing strands).
- i) There does not seem to be a correlation between cracking severity and date code for the dates to which this category applies.
- j) The ties removed from under the bridge near the field test site showed less severe cracking than those adjacent to the bridge, which were exposed to the environment for their entire life.

Post-2003, NEC ties

- k) We found no cracking in these ties—neither visually nor with impact echo.

San-Vel, NEC ties

- l) We found no cracking in these ties—neither visually nor with impact echo.

MBTA Old Colony Line ties

- m) The cracking in these ties is essentially identical to that observed in the pre-2003 NEC ties.

4. Materials Analysis

The purpose of this section is to determine the extent to which material characteristics may have contributed to the observed cracking. We first review the prestressing tendons. We then review the manner in which the ties are produced and concerns related to their production. This review is followed by a description of various potential concrete degradation mechanisms and their dependence on material and production parameters. This provides the context for evaluating Amtrak's materials and production specifications for the ties and the results of our own and others' petrographic analyses, descriptions of which are included in this section.

We find that the ASR degradation mechanism is a contributing factor to the tie cracking and that the other degradation mechanisms are not. We also find evidence that one of the reasons for the good performance of the San-Vel ties is the relatively shallow tendon indentation geometry and the likelihood that the steel used for the tendons experienced stress relaxation.

4.1 Prestressing Tendons

4.1.1 *Characterization of Prestressing Tendons*

Prestressing tendons are high-strength steel strands or wires used to strengthen the railroad tie by transferring a compressive force to the concrete and thereby reducing the risk of concrete failure under tensile loading. The prestressing tendons for the concrete ties are seven-wire strands or single wires. The concrete is cast around tendons that are under a predetermined tensile load and stress (the prestress). After the concrete cures to a specified strength, 4,250 psi in the case of the pre-2003 railroad ties, the load on the tendons is released and force is transferred to the concrete through a 'bond' mechanism that occurs over a transfer length at each end of the tendons. The bond occurs through a variety of mechanisms, including friction, adhesion, and mechanical interlock. The interlock is assisted by indentations that are rolled into the individual wires of the tendon. The stress in the tendons is high, on the order of 75 percent of the ultimate tensile strength of the tendon steel, which is typically 270 ksi. Some relaxation occurs in the tendons over time and this tends to reduce the final prestressing force and initial compressive stress in the concrete, but the degree of relaxation has been controlled with low relaxation wire since the 1980s.

We examined tendons from three of the case study ties: pre-2003, post-2003, and San-Vel. We removed the tendons from the ties by breaking the concrete with an air hammer and cutting the tendon with a cut-off wheel. We measured the wire and strand diameters and the indentation lengths, pitch, and depth using digital analysis software. The indentations of the seven-wire strands exhibit the appropriate length, pitch, and depth per ASTM A886 (Standard Specification for Steel Strand, Indented, Seven-Wire Stress-Relieved for Prestressed Concrete). The dimensional analysis results for the single wire are consistent with ASTM A881 (Standard Specification for Steel Wire, Deformed, Stress-Relieved or Low-Relaxation for Prestressed Concrete Railroad Ties).

We performed Vickers microhardness measurements on some of the wire cross-sections to estimate the tensile strength (using conversion tables). The converted tensile strengths for the single wire and for wires in the seven-wire strand exceed minimum requirements set forth in the applicable standards.

Table 4.1 compares the various measurements we made on the wires of these tendons.

Table 4.1. Dimension and hardness measurement results on the case study tie strands.

Parameter	Strand Source Tie		
	Pre-2003	Post-2003	San-Vel
Wire diameter (in)	0.129	0.207	0.130
Indentation length (in)	0.100	0.148	0.056
Indentation pitch (in)	0.225	0.228	0.246
Indentation depth (in)	0.0035	0.0030	0.0016
Wire hardness (kg/mm ²)	534	547	556
Tensile strength (converted) ksi	267	275	280

Figures 4.1-4.3 show examples of the indentations in the wires from the three tie types. There are four lines of longitudinally oriented elliptical indentations around the circumference of the wires for the pre-2003 and San-Vel strands, and there are three lines of indentations oriented at an angle to the longitudinal direction for the post-2003 ties.

We note that the indentations in the San-Vel tie wires are shorter, more widely spaced, and shallower than for the pre-2003 ties.

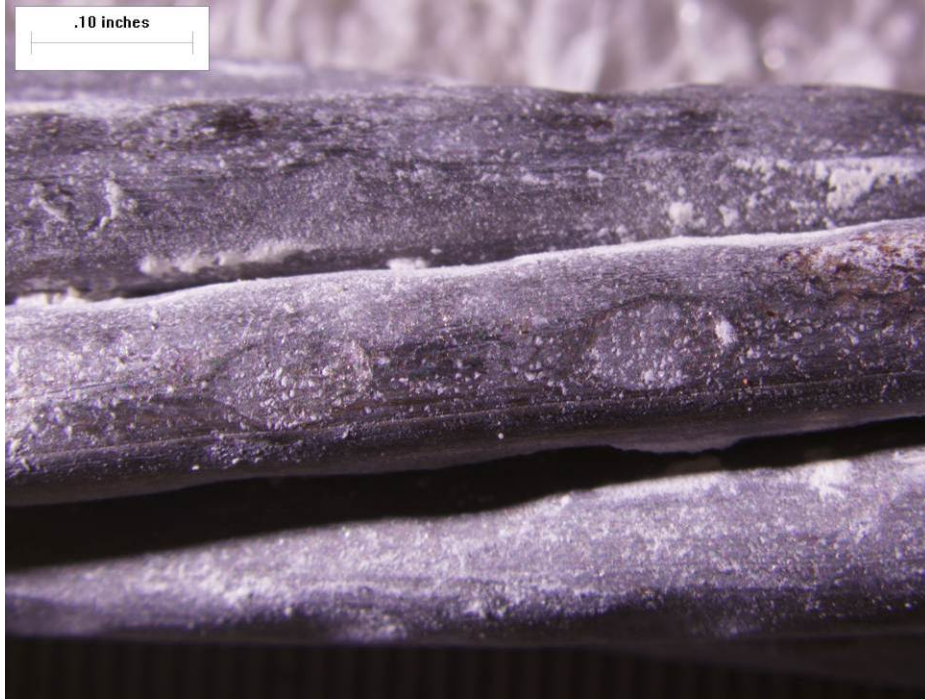


Figure 4.1. Example of elliptical deformations on seven-wire strands from a pre-2003 tie.



Figure 4.2. Example of elongated elliptical deformations on a single-wire strand from a post-2003 tie.



Figure 4.3. Example of elliptical deformations on seven-wire strands from a San-Vel tie.

We also investigated the extent to which there are differences in the relaxation properties of the different strands. We found no practical method to test for this, but our review of standards indicates that the use of low-relaxation wires in the prestressed concrete industry occurred in the late 1970s and early 1980s. This suggests the strands in the San-Vel ties, which were produced in the mid-to-late 1970s, were not made from low relaxation wires.

4.1.2 Surface Residue Testing

We conducted one type of analysis multiple times to determine whether there was any unusual contamination on the strands of the subject ties that could affect their bond to the concrete. We conducted Fourier transform infrared spectrometry (FTIR) on residues present on the strand wires from four ties: three from the pre-2003 ties (Nos. 1, 2, and 7) and one from a post-2003 tie (No. 16). The strand sections were submerged in solvent and allowed to sit for 5 minutes with stirring. We conducted these tests together with a control (solvent only). The result showed that there was no organic material.

4.2 Concrete Tie Manufacturing and Potential Concerns

We reviewed the concrete tie manufacturing process to identify potential production-related aspects that may affect the quality of the ties.

The Amtrak concrete crosstie is a pretensioned, prestressed concrete member. The tendons are stressed before the concrete is placed into the casting molds, and the stressing force is transferred to the concrete after the concrete has cured to a specified strength. The North American manufacturers of the Amtrak crosstie use the long line method, with fixed pretensioning beds and sliding molds. A more detailed review on the concrete tie manufacture method and typical sequence of production cycle are shown in Appendix A.1. As described in Appendix A.1., we identified the following items that may affect the quality of the crossties:

4.2.1 End Bars

The end bars (often called “end gate bars”) are a set of vertically stacked flat bars that provide for the vertical location of the tendons and close off the ends of the molds. If there are two rows of tendons, there are three bars—the bottom bar locates the first tendon row and closes off the bottom of the mold, the second bar sets on top of the first row of tendons and locates the second row of tendons, and the third bars sets on top of the second row of tendons and extends to the top of the mold.

Besides supporting the tendons at the correct vertical position, when extracted, the gap left between the forms provides a space for the tendon cutting saw to pass without touching the ends of the molds. The bars are usually 3/4 in wide and provide a 3/4 in nominal gap. The bars are the full width of the mold, forming the entire tie end. The small space between the bars (the diameter of the tendons) at the outside ends of the molds can be plugged to prevent grout leakage.

Potential problems associated with the end bars include:

- The bars put the tendons in rows thereby putting the tendon force in concentrated planes.
- The removal of the bars potentially disturbs the tendons at the tie ends. The bars need to be extracted before the concrete fully sets, but after the concrete solidifies enough to prevent end slumping after the bars are removed. The bars need to be pulled out perfectly level otherwise the tendons would be pried upward, potentially compromising the integrity of the bond between tendon and concrete. The bars also need to be smooth without any surface nicks or distortions. Surface imperfections could disturb the strand as the bars are removed.
- Even though the molds are held tight against the bars, concrete buildup and bar imperfection may prevent a grout-tight joint. Grout does sometimes leak out, which may affect the tendon bond locally.

4.2.2 Transfer Strength

The transfer strength is the minimum concrete strength required before the strands can be cut free of the tensioning beds. For the pre-2003 ties, the specified transfer strength was 4,250 psi.

The concrete mix and the accelerated curing cycle should be designed to achieve the transfer strength in the production cycle time with a reasonable factor of safety.

Because the specifications require only a minimum transfer strength, the actual transfer strength is frequently higher (such as when ties cure over a weekend or when the concrete is designed with too high a strength). This can create a higher risk of cracking for the following reasons:

- High strengths result in shorter transfer lengths (the length of embedded prestressing needed to transfer their prestressing loads into the concrete), which concentrates the prestressing loads in the ends of the ties rather than distributing them.
- High strength also corresponds to lower creep, providing less redistribution of the loads within the tie over time.

4.3 Concrete Material Degradation Mechanisms

Precast concrete railroad ties manufactured in plants using heat-curing and then exposed to cold temperature and water (in the form of rain and snow or ground water) while in service are vulnerable to several degradation mechanisms: cyclic freezing and thawing, DEF, external sulfate attack, and ASR. Some of these types of material deterioration have been reported to be potential causes of the cracking of concrete ties cast before 2003.

We first review the potential degradation mechanisms to identify likely mechanisms explaining the observed distress. This review also provides context for evaluating the tie specifications and for reviewing and interpreting our test results and those of others.

4.3.1 Cyclic Freezing and Thawing

The mechanism of freeze-thaw damage in concrete is quite complex, but can be summarized as follows: as the water in moist concrete freezes, it produces osmotic and hydraulic pressures in the capillaries and pores of the cement paste and aggregate. If these pressures exceed the tensile strength of the surrounding paste or aggregate, a crack will form. The cumulative effect of successive freeze-thaw cycles is the disruption of paste and aggregate, eventually causing significant expansion and deterioration of the concrete. Freeze-thaw action typically begins at the exposed surface and progresses into the concrete structure. Deterioration is typically visible in the form of scaling, cracking that is subparallel (a petrographic term meaning roughly or nearly parallel) to the exposed surfaces, and disintegration.

Resistance to freezing and thawing is improved by including air-entraining admixtures in the fresh concrete to create a system of small, closely spaced air bubbles or voids in the fresh concrete. After the concrete sets, the air voids provide free space into which the ice and water can expand during freezing, thus providing pressure relief from the bursting forces and preventing damage to the concrete. The ability of the air voids to protect the concrete depends on the distance the water must travel to the nearest air void for relief, the size of the voids, and,

to a lesser extent, the total amount of void volume. Therefore, according to ACI 201.2 – Guide to Durable Concrete, the air void system should meet the following requirements to provide sufficient protection against freezing and thawing, as determined by evaluation in accordance with ASTM C457 (Standard Test Method for Microscopical Determination of Parameters of the Air-Void System in Hardened Concrete):

- The voids must be spaced closely enough; the spacing factor (indicating the typical distance water or ice must travel to reach a void) should be no more than 0.008 in.
- The voids must be small enough; the specific surface area (the surface area of the voids relative to their volume) should be 600 in²/in³ or greater.
- The total air volume must be large enough: the total air content should be between 4.5 and 7.5 percent (for a typical 3/4 in nominal size coarse aggregate per ACI 318); however, with the advent of modern air-entraining admixtures capable of entraining very small and closely spaced air voids, this requirement can be relaxed for concretes with air void systems with sufficiently small and closely spaced voids.

In addition to an adequate entrained air system, concrete must also be sufficiently impermeable to prevent or reduce the amount of water or other deleterious materials (such as deicing salts) that can enter the concrete through the exposed surface. Recommended qualities for sufficient resistance to cyclic freezing and thawing include using a water-to-cementitious material ratio (w/cm) of 0.45 or less and replacing a portion of the portland cement with a pozzolan such as fly ash, slag, or silica fume. The general quality of the hardened concrete (including w/cm or cementitious replacement) can be evaluated by petrographic analysis.

4.3.2 Delayed-ettringite formation (DEF)

Ettringite (a form of calcium sulfoaluminate hydrate) is a normally occurring hydration product in portland cement concretes that is created by the reaction of the aluminate phases of the cement and gypsum (calcium sulfate) in the cement. The ettringite typically forms almost immediately after water is added to the cement and its formation helps to control the setting time of the cement. The formation of the ettringite is expansive, as the calcium sulfoaluminate combines with 32 water molecules to form the ettringite crystal, but this expansion is innocuous when it occurs in the plastic concrete because there is no rigid hydration structure to resist the expansion.

DEF refers to a damaging reaction in which the normal early formation of ettringite that occurs in plastic concrete is delayed or altered, leading to later ettringite formation in the hardened paste. Current research indicates that ettringite becomes unstable at approximately 158 °F (70 °C), above which it becomes unstable and breaks down into calcium monosulfate. If this occurs in concrete, the ettringite that reforms after the concrete cools creates expansive pressure during its reformation. Due to its large volume in comparison with the monosulfate, this “delayed” formation of ettringite leads to internal expansion of paste volume and damage to the hardened concrete. Microscopically, DEF is characterized by cracks within the paste, gaps at the paste-aggregate interface that are filled with larger opportunistic ettringite crystals, and accumulations of ettringite within the paste that look like bird’s nests when viewed at high magnifications under

the scanning electron microscope. Macroscopically, DEF is characterized by a map cracking pattern with no associated deposits of gel.

The precast concrete industry is especially concerned about DEF because of its use of accelerated heat curing. Because of those concerns, the precast concrete industry incorporated heat controls into its Precast/Prestressed Concrete Institute (PCI) MNL 116 – Manual for Quality Control for Plants and Productions of Precast and Prestressed Concrete Products [4.1]. The manual provides temperature control requirements for accelerated curing: maximum concrete curing temperature shall not exceed 180 °F in the concrete. In the commentary, it also states that if a known potential for ASR or DEF exists, the maximum permitted temperature is reduced to 158 °F (70 °C). For comparison, Germany and Canada limit maximum concrete temperatures to 140 °F (60 °C) [4.2].

4.3.3 External Sulfate Attack

External sulfate attack is an expansive chemical alteration of concrete paste involving the ingress of sulfate ions from external sources such as ground water, seawater, or industrial or residential wastewater. In external sulfate attack, the sulfates to which the concrete is exposed migrate into the concrete over time and react with the calcium aluminate components of the cement. This reaction causes distress in the concrete through two mechanisms. The first is the formation of expansive ettringite and gypsum in the concrete. The second is a chemical attack of the hydrated cement paste that causes it to soften and deteriorate.

In practice, the most severe deterioration occurs just above ground or exposed water level and is characterized by a loss of surface paste and extensive cracking with associated deposits of gypsum and calcium hydroxide. Below the ground or water levels, a softening of the paste structure occurs and progresses inwards, which is the most frequently observed form of deterioration. The softening of the paste structure is due to the chemical alteration and replacement of existing hydration products within the paste structure that disrupt the paste-to-aggregate bond strength of the concrete, resulting in reduced compressive strength, aggregate loss, and bulk loss of the concrete.

Depending on the level of exposure to sulfates in service, using sulfate-resistant cements (only available by special order or in certain areas of the country), reducing the permeability of the concrete (by using low water-to-cementitious material ratio and good curing), or a combination of both are practical measures to resist sulfate attack.

4.3.4 Alkali-Silica Reaction (ASR)

Concrete can also be damaged if reactive aggregate is used. The most-common form of this material-related deterioration is ASR. ASR occurs when susceptible aggregates (typically those that contain unstable noncrystalline or mechanically strained semi-crystalline silica morphologies) react with the alkalis present in the concrete. Although the very early-age

mechanics of the reaction are not well understood, the literature [4.3] describes the pressures associated with ASR formation as occurring in three phases: an “induction” phase where stresses increase prior to fracturing; a “main expansion” phase representing a period of crack development and rapid expansion of concrete; and a “late expansion” phase describing the end of propagation and the end of expansion. In the first phase of this process, some of the silica present in the aggregate reacts with alkalis and hydroxides in the concrete to dissolve the silica and to create pressures within the concrete that crack the aggregates and surrounding paste. The second phase then occurs as the reaction forms a highly absorptive alkali-silica gel within cracks and voids in the aggregate and the surrounding cement paste. The gel absorbs water and swells, creating additional pressures and expansion, further fracturing the aggregates and the surrounding cement paste. In the final phase, the available reactants are consumed or the chemistry becomes unfavorable for further gel formation or swelling and the reaction ceases or slows.

As the ASR progresses, the concrete deteriorates as the internal cracking progresses and interconnects. Extreme ASR can result in complete disintegration of the concrete. ASR will continue as long as the concrete contains a sufficient supply of alkalis and has a relative humidity above approximately 85 percent. Moisture fluctuation and freeze-thaw cycling exacerbate the disintegration.

Since ASR will occur only with the presence of three conditions (reactive forms of silica in the aggregate, high-alkali (pH) pore solution, and sufficient moisture), practical measures to avoid and control ASR include the following, which can be used singly or in combination:

- Limiting the alkali content of the concrete by using cement with very low alkali. ASTM C150 (Standard Specification for Portland Cement) recommends the optional use of a low-alkali with a cement alkali content of less than 0.60 percent; however, cases have been reported that ASR distress occurred in the concrete with cement having this range of alkali content [4.4].
- Using supplemental cementitious material to replace portions of the cement.
- Use of nonreactive aggregates. The current industry-accepted test methods to screen for alkali-silica reactive aggregate include:
 - Petrographic analysis:
 - ASTM C295 - Standard Guide for Petrographic Examination of Aggregates for Concrete. This method determines the physical and chemical characteristics of the aggregate particles to identify characteristics (e.g., crystal structure or type of material) that indicate that the material is potentially reactive.
 - ASTM C856 - Standard Practice for Petrographic Examination of Hardened Concrete. This method is used to observe hardened concrete for the general quality of the concrete and for evidence that is characteristic of DEF, ASR, cyclic freezing-thawing, etc.
 - Expansion tests: ASTM C1260 - Standard Test Method for Potential Alkali Reactivity of Aggregates (Mortar-Bar Method), ASTM C1293 (Standard Test Method for Determination of Length Change of Concrete Due to Alkali-Silica Reaction), and ASTM C1567 - Standard Test Method for Determining the Potential Alkali-Silica

Reactivity of Combinations of Cementitious Materials and Aggregate (Accelerated Mortar-Bar Method), etc. These tests subject samples of concrete or mortar made with the aggregates in question to accelerated exposure conditions to induce a rapid reaction, the effects of which are typically measured by expansion of the sample. They are used to relatively rapidly screen aggregates.

Past test methods that are no longer in use, but that were used to evaluate the reactivity of the aggregate in the pre-2003 ties include:

- ASTM C227 - Standard Test Method for Potential Alkali Reactivity of Cement-Aggregate Combinations (Mortar-Bar Method). This expansion test used mortar bars mixed with a high-alkali cement and exposed to 100 °F (38 °C) and high humidity to test for reactivity. Experience [4.4] has shown that the results of the C227 test can be misleading, with slowly reacting aggregates frequently passing the test despite poor field performance.
- ASTM C289 - Standard Test Method for Potential Alkali-Silica Reactivity of Aggregates (Chemical Method). This test immerses crushed samples of the aggregate in a sodium hydroxide solution and analyzes the resulting dissolved material for comparison with interpretation charts. The test has been found to be limited in applicability because it fails to properly identify slowly reactive aggregates and is considered useful only if used in combination with other more reliable tests.

Mixing water is not considered a significant source of alkalis in concrete, as mixing water is either potable or contains no more than 600 ppm (0.06 percent) alkali. Regardless of specification requirements, these are also practical limits, as water with alkali contents sufficient to contribute to aggregate reactions will cause problems with admixture performance, setting, and strength such that they will not be practicably usable in concrete production.

4.4 Review of Amtrak Material Specifications

In light of the discussion on concrete degradation mechanisms, we reviewed the Amtrak material specifications for concrete ties, which provide general requirements for the concrete materials, concrete mixture proportions, and quality control/assurance tests. In contrast to the abrupt change in the tie configuration from eight seven-wire strands to multiple single wires in 2003, the evolution of the tie specifications has been more gradual and incremental. In order to understand how these requirements changed over time, we reviewed the Amtrak specifications from 1983 to 2003 that are available to us. We summarize the evolution of the specifications in Table 4.2. Additional information is provided in Appendix A.2.

The effects of the evolution of the specification are summarized below:

- Cement: The specifications changed to decrease the alkali content of the concrete, with low alkali (defined by ASTM C150 as less than 0.60 percent) required in 1992, and low sulfate required in 2003. The use of low alkali cement reduces the risk of ASR, but as previously mentioned, it is not a guarantee of nonreactivity [4.4].

- **Aggregate Reactivity:** The specifications evolved significantly over time. In 1989 there was no specific requirement for aggregate reactivity (ASTM C33 does not include default reactivity requirements). In 1992, the specifications expanded to include chemical testing and petrographic examination of aggregates to identify potential reactivity. However, as discussed in Section 4.3.4, these tests have been subsequently found to be unreliable as a screening and evaluation tool. In 2003, the present-day expansion tests were added, providing a more revealing evaluation of the aggregates, as discussed in Section 4.3.4.
- **Curing:** the curing changes in the specification have been relatively unchanged since the maximum temperature requirement was introduced in 1992, presumably after the widespread Lone Star tie failures on the NEC.
- **Transfer of Pretensioning Force:** The minimum concrete strength at transfer remained vague in the specifications until 2003 when a 4,000 psi minimum strength was implemented. It is unclear how the “manner which prevents damage to the concrete tie” prior to this point was evaluated. However, tie production drawings prior to 2003 all show required transfer strengths of 4,000 or 4,250 psi, suggesting that the effect of the specification change had no effect on production practice.
- **Air Entrainment:** The air entrainment requirements are relatively unchanged, aside from an increase in the required durability factor.

Table 4.2. Comparison of key components of the Amtrak specifications for pre- and post-2003 ties.

Category	1989 Specification	1992 Specification	1995 Specification	Post-2003 Specification
Cement	ASTM C150	ASTM C150- Low alkali	ASTM C150- Low alkali	ASTM C150, Type II or Type III, low alkali, having the lowest possible alkali content, but no more than 0.60% alkali content of Na ₂ O equivalent; ASTM C265 – maximum SO ₃ as 0.5g/l; maximum SO ₃ : Al ₂ O ₃ as 1.0. Require mill certificates
Aggregate Reactivity	ASTM C33	ASTM C33 ASTM C289 or ASTM C1105 (6 months) ASTM C227 (12 months)	ASTM C33 ASTM C289 or ASTM C1105 (6 months) ASTM C227 (12 months)	ASTM C295 (3 months) ASTM C1260 (6 months) ASTM C856 (3 months) ASTM C1293(6 months) ASTM C1105 (6 months) “Duggan” (6 months) (Note 1)
Curing	Pressure steam or steam vapor accelerated—No temperature requirement	Radiant heat with a maximum bed temperature of 140 °F.	Low pressure steam or radiant heat with a maximum bed temperature of 140 °F.	PCI MNL 116 Maximum temperature within the concrete shall not exceed 140 °F.

Category	1989 Specification	1992 Specification	1995 Specification	Post-2003 Specification
Transfer of Pretensioning Force ²	Accomplished in a manner which prevents damage to the concrete tie. (Note 2)	Accomplished in a manner which prevents damage to the concrete tie.	Accomplished in a manner which prevents damage to the concrete tie.	Concrete strength at transfer should be in accordance with ACI 318, but in no case shall be less than 4000 psi.
Freeze-thaw Resistance	Air entrainment 2% to 5% ASTM C666 Durability factor: 75% at 300 cycles	Air entrainment 4% to 6% ASTM C457 (6 months) ASTM C666 (6 months) Durability factor: 90% at 300 cycles	Air entrainment 4% to 6% ASTM C457 (6 months) ASTM C666 (6 months) Durability factor: 90% at 300 cycles	Air entrainment 4% to 7% ASTM C457 (6 months) ASTM C666 (6 months) Durability factor: 90% at 300 cycles

Notation:

- ASTM C150 – Standard Specification for Portland Cement.
- ASTM C33 – Standard Specification for Concrete Aggregates.
- ASTM C265 – Standard Test Method for Water-Extractable Sulfate in Hydrated Hydraulic Cement Mortar.
- ASTM C289 – Chemical method for potential ASR of aggregate.
- ASTM C227 – Potential ASR of cement-aggregate combination.
- ASTM C295 – Petrographic examination of aggregate for concrete.
- ASTM C457– Microscopical Determination of Parameters of the Air-Void System in Hardened Concrete.
- ASTM C666 – Resistance of Concrete to Rapid Freezing and Thawing.
- ASTM C1260 – Potential ASR of aggregate, mortar bar method.
- ASTM C1293 – Length change of concrete due to ASR.
- ASTM C1105 – Length change of concrete due to ACR.
- ASTM C856 – Petrographic examination of hardened concrete.
- ACI 318 – Building Code Requirements for Structural Concrete and Commentary.
- PCI MNL 116 – Quality Control for Plants and Production of Structural Precast Concrete Products.

Note 1: The “Duggan” test was developed in 1986 and used small 1 in diameter cylinders subjected to heating and subsequent immersion in water. It was intended to test for ASR, but was later found not to be a reliable indicator of ASR vulnerability. It never became an ASTM standard.

Note 2: The 1988 Concrete Tie drawing shows a concrete strength of 4000 psi at transfer;
The 1990 Concrete Tie drawing shows a concrete strength of 4250 psi at transfer;
The 2006 Concrete Tie drawing shows a concrete strength of 4000 psi at transfer;
The 2010 Concrete Tie drawing shows a concrete strength of 4000 psi at transfer.

4.5 Review of Studies of the Ties by Others

We reviewed several reports related to the concrete tie problem prepared by other organizations to supplement our own studies. These included investigations of cracked pre-2003 ties and uncracked post-2003 ties, as well as materials tests conducted during production of the pre- and post-2003 ties.

4.5.1 Investigation of Pre-2003 Tie Cracking

We reviewed a total of four reports from CTLGroup (CTL) [4.5-4.8], two reports from Lankard Materials Laboratory (LML) [4.9, 4.10], and two reports from Valley Forge Laboratories (VFL) [4.11, 4.12]. These reports describe testing performed on samples removed after pre-2003 ties began exhibiting cracking in service. The laboratory tests, including petrographic analysis, scanning electronic microscope and energy dispersive X-ray spectroscopy unit (SEM/EDS) analysis, physical tests (compression), chemical tests (chloride tests), and Duggan tests for ASR and DEF, were performed on the concrete core samples extracted from cracked concrete ties as well as from some concrete ties that showed no visible cracking.

The test results and the findings from petrographic analysis, physical tests, chemical tests, and Duggan tests, etc. are described in Appendix A.3.

The studies conducted by CTL, LML, and VFL agree that the observed cracking is not associated with chloride-induced corrosion, cyclic freezing and thawing, or lower-than-desired compressive strength. The petrographic studies (conducted by CTL and LML) both agree that the observed horizontal splitting of the concrete ties is associated with ASR, although they do not agree on the magnitude of the effect of ASR, with LML attributing to the ASR a greater role in the observed cracking. Neither CTL nor LML associated the observed horizontal cracking with DEF-related distress, except in tie samples identified as having an atypical failure mode which exhibited widespread map cracking unlike the typical failure mode observed on the other ties.

4.5.2 Manufacturing Quality Control Testing Related to Pre-2003 Ties

We reviewed numerous concrete test reports written by CTL from 1990 to 1997, in which tests were performed on concrete specimens made during production. These tests appear to be part of a test schedule, as required by the Amtrak 1992 to 1995 specification. The testing found the following:

- ASTM C227 (Potential Alkali Reactivity of Cement-Aggregate Combinations): expansion below the 0.1 percent expansion criteria, indicating that the aggregates were non-reactive,
- ASTM C289 (Potential Alkali-Silica Reactivity of Aggregates): aggregates found to be “innocuous,”
- ASTM C457 (Microscopical Determination of Parameters of the Air-Void System in Hardened Concrete): concrete found to have a variable (from marginal to sufficient) air

content, but sufficiently low spacing factor and sufficiently high specific surface to be durable,

- ASTM C666 (Resistance of Concrete to Rapid Freezing and Thawing): concrete found to meet the specified requirements,
- ASTM C295 (Petrographic examination of aggregate for concrete): CTL tested one sample of coarse and two samples of fine aggregates. They concluded that the materials were not highly reactive. They did, however, note the presence of a small amount of chert particles, but no potentially deleterious constituents.

While the ASTM C227 and ASTM C289 test reports conducted during concrete tie manufacturing in the 1990s indicate that both the fine and coarse aggregates were nonreactive and considered innocuous, the petrographic studies conducted by CTL and LML on those ties after they had been in service (as discussed in Section 4.5.1) revealed the presence of reactive aggregate particles and evidence of ASR distress in the concrete. As discussed in Section 4.3.4, the ASTM C227 and C289 tests in use at the time of manufacture were not sensitive enough to detect a slowly reactive aggregate and they may have provided an incorrect prediction. In addition, use of the low-alkali cement may not guarantee elimination of ASR distress that may be associated with the inherent reactivity of aggregate as previously discussed. This is further discussed in Section 8.1.1 on contributing factors.

4.5.3 Information Related to Post-2003 Ties

We also reviewed a total of five reports from CTL Thompson [4.13-4.17], four reports from DRP [4.18 to 4.20, 4.21], one report from CTLGroup [4.22], one report from Hanson Aggregate [4.23], one document from Rocla [4.24], and one report from University of Illinois at Urbana-Champaign (UIUC) [4.25] associated with the post-2003 ties, after significant changes were made in the concrete materials, concrete mix design, and prestressing design. These documents are primarily laboratory test reports on the cement and aggregates used in post-2003 ties, as well as on core samples retrieved from post-2003 concrete ties, which are likely part of the test schedule required by the 2003 specification. The test results and the findings from petrographic analysis, expansion tests, Duggan tests, cyclic freezing-thawing test, and UIUC's evaluation of post-2003 specification and concrete tie production are summarized in Appendix A.3.

In summary, our review of the UIUC reports and other studies conducted by CTL and DRP indicates that concrete ties manufactured after 2003 were generally in good condition at the time of testing, with no indications of ASR or DEF distress. Furthermore, the production and materials testing information indicates that the materials used in the post-2003 ties were in compliance with the more stringent (as discussed in Section 4.3) ASR-related specifications in place at the time, including the aggressive ASTM C1260 ASR screening test; our review further shows that the as-produced concrete was resistant to damage from cyclic freezing and thawing. This is not surprising, as the petrographic testing also indicates that the post-2003 ties used a nonsilica-based dolomitic marble and a nonreactive metamorphic quartz that does not contain chert.

4.6 SGH Petrographic Examinations

We conducted petrographic examinations on samples removed from the case study ties to determine the conditions and properties of the existing concrete and to provide data and evidence of the extent to which materials-related parameters may be contributing to the cracking problem.

Table 4.3 below identifies the examined cores. For clarity, it also identifies the other mechanical tests we performed on selected concrete ties, as further described in Section 5 of this report. We do not have results from the MBTA ties to report here.

Table 4.3. Summary of SGH laboratory tests on selected concrete ties.

Tie No.	Crack Rating	Test Performed						
		Vertical Core for General Petrographic Examination	Horizontal Core for Petrographic examination – at crack	SEM /EDX	Air-void system analysis	Compression and modulus test	Splitting tensile test	Characteristic of prestressing tendons
Pre-2003 NEC; uncracked or minor cracking								
1	2	√				√	√	√
2	1	√			√	√	√	√
19	2	√				√		
20	2	√				√		
Pre-2003 NEC; cracked								
6	4	√			√	√		
7	3							√
8	4	√	√	√	√	√	√	
10	3	√				√		
11	3	√				√		
14	4	√				√		
17	3	√	√			√		
18	3	√	√			√		
Post-2003 NEC								
16	1	√			√	√	√	√
21	1	√				√		
San-Vel NEC								
S1	1	√	√ (no apparent crack)			√	√	
S2	1	√	√ (no apparent crack)			√		√

4.6.1 Sample Preparation

We extracted 3 in diameter cores from the case study ties. The purpose of the cores was to evaluate the general composition and condition of the hardened concrete, geology of the aggregate, and the presence of any ongoing expansive reactions, such as ASR, DEF, or cyclic freezing and thawing, that may be associated with the cracked ties. We extracted two types of cores: vertical and horizontal. The vertical cores were taken through the full thickness of the ties approximately 4 in from the end of the ties and centered at one of the two middle tendons (Figure 4.4). The horizontal cores were taken as partial or full-width horizontal core samples at locations at which cracks were visible on the sides, generally about 8 to 9 in from the tie end. The horizontal core included the top row of tendons and the visible crack itself (except for the San-Vel ties, which had no crack). We used these samples to conduct petrography at the site of likely crack initiation and propagation, even though these were more difficult to prepare.



Figure 4.4. SGH retrieving a full-depth vertical core sample from a tie.

We then cut nominal 3/4 to 1 inch-thick longitudinal sections from or near the centers of each of the core samples. In the case of the vertical cores, these sections were oriented so that the observed surface was perpendicular to the tie transverse direction and parallel to the tendons. The exception was the vertical core for Tie 8 for which the cut plane was perpendicular to the tendons. The cut plane for the horizontal cores was made perpendicular to the tendons. We then lapped and ground each of the sawed sections to obtain a smooth, flat cross section for our microscopic examination.

In addition, we prepared blue-dye-epoxy-impregnated ultrathin (20 to 25 μm) sections from each of the corresponding remnant core pieces in order to conduct a more detailed petrographic examination on the hardened concrete. For vertical full-depth core samples, we prepared one thin section from each core sample at the locations not including prestressing tendons. For horizontal core samples retrieved at visible cracks, we were able to prepare the thin sections perpendicular to the prestressing tendon to include the prestressing tendons, and we made three thin sections across the entire width of these concrete ties.

We examined the polished sections with the aid of a stereomicroscope at magnifications of 4 to 40X and examined the prepared ultrathin sections using a transmitted-light polarizing microscope at magnifications of 25 to 200X. Our examinations were conducted in accordance with ASTM C856 (Petrographic Examination of Hardened Concrete).

4.6.2 Petrographic Findings from Vertical Core Samples

The following is a description of our petrographic findings from these samples, classified by three categories: pre-2003 ties, post-2003 ties, San-Vel ties.

4.6.2.1 Concrete in Pre-2003 Ties

Our specific observations are described in Appendix A.4 and summarized in Table 4.4. In general, we noted the following:

- The quality of the concrete appears to be fair-to-good, with none-to-minor indications of aggregate segregation near the top surface;
- The concrete exhibits a normal-to-advanced degree of cement hydration and a very low to moderate-low water-to-cementitious materials ratio;
- The concrete contains no fly ash or slag;
- A minor component of the coarse aggregate particles (namely the diabase or diorite metamorphic rock) and of the fine aggregate (namely the chert) contain unstable or strained silica that is reactive or potentially reactive;
- We observe no indications of cyclic freeze-thaw damage, DEF, or external sulfate attack.

We found that the cracking and distress in the concrete is primarily associated with ASR, as summarized below.

- We observe very minor evidence of ASR and no evidence of ASR-related distress in core samples from Ties 2, 10, 17, and 19. This finding is based on observing only occasional dark rims around coarse aggregate particles with no aggregate fractures extending into the surrounding paste and no evidence of ASR gel formation. We did not observe lateral cracking at the top tendon elevations on both sides of Tie 2 and on the one side of Tie 10 where the core sample was retrieved; however, there is visible lateral cracking at the top tendon elevation on both sides of Ties 17 and 19. We observe that crack widths in Ties 17 and 19 are typically no more than 0.003 in.

- We observe evidence of minor ASR-related distress in the core samples from Ties 1, 11, 18, and 20, as indicated by the occasional formation of dark rims around fine and coarse aggregate particles, fractures that originate in chert particles and extend into and disrupt the surrounding paste structure, and/or the presence of ASR gel lining or completely filling air voids located adjacent to reactive aggregate particles. Note that we typically observe hairline lateral cracking (with crack widths typically no more than 0.003 in) at the top tendon elevation on both sides of these ties.
- We observe evidence of minor-to-moderate ASR-related distress in the core samples from Ties 6, 8, and 14, as indicated by the occasional to frequent formation of dark reaction rims around the perimeters of aggregate particles, occasional fractures in fine and coarse aggregate particles that extend outward from the aggregate and disrupt the surrounding paste (Figures 4.5 and 4.6), as well as fractures that are partially to completely filled with ASR gel. In particular, we note ASR gel that forms along multiple horizontal fractures at the top tendon elevation in core samples from Ties 6 and 14. The three concrete ties (6, 8, and 14) exhibit lateral cracking on both sides, with crack widths up to 0.050 in at the top tendon elevations. In each case, the cracks extend from the ends to the shoulder of each tie.
- The vertical crack on top of Tie 8 is associated with ASR-related distress.

Table 4.4. Petrographic examination summary of concrete ties from Case Studies 1 and 2: pre-2003 NEC.

Feature	Tie 1	Tie 2	Tie 19	Tie 20	Tie 6	Tie 8	Tie 10	Tie 11	Tie 14	Tie 17	Tie 18	
	Case Study 1: uncracked or minor cracking				Case Study 2: cracked							
General condition	Good: no evidence of excessive bleeding or aggregate segregation.	Fair to good: no evidence of excessive bleeding or aggregate segregation.	Good: no evidence of aggregate segregation	Good: minor evidence of aggregate segregation	Fair to good: no evidence of excessive bleeding or aggregate segregation.	Fair to good: with minor indication of aggregate segregation near the top surface	Good: no evidence of excessive bleeding or aggregate segregation.	Fair to good: with localized aggregate segregation related to placement and consolidation	Good no evidence of excessive bleeding or aggregate segregation	Fair to good: with localized aggregate segregation	Good: minor evidence of aggregate segregation	
Air content	3½% to 4½%	2½% to 3½%	2½% to 3½%	3% to 4%	1½% to 2½%.	3½% to 4½%.	2½% to 3½%	1½% to 2½%	2% to 3%	2½% to 3½%	2½% to 3½%	
Quality and distribution of air-void system	Uniformly distributed	Not well developed; non uniform distribution	Uniformly distributed	Uniformly distributed	Uniformly distributed	Variable within the core sample	Uniformly distributed	Uniformly distributed	Uniformly distributed	Uniformly distributed	Uniformly distributed	
Estimated w/cm	0.37 to 0.43	0.40 to 0.46	0.37 to 0.43	0.37 to 0.43	0.37 to 0.43	0.33 to 0.39	0.34 to 0.41	0.37 to 0.43	0.34 to 0.40	0.40 to 0.46	0.37 to 0.43	
Cement hydration	Normal to advanced	Normal to advanced	Normal to advanced	Normal to advanced	Normal to advanced	Normal to advanced	Normal to advanced	Normal to advanced	Normal to advanced	Normal to advanced	Normal to advanced	
Supplemental cementitious material?	None observed	None observed	None observed	None observed	None observed	None observed	None observed	None observed	None observed	None observed	None observed	
ASR distress level	Slight	None observed	None observed	Slight	Slight-to-moderate	Slight-to-moderate	None observed	Slight	Slight-to-Moderate	None observed	Slight	
DEF distress level	None observed	None observed	None observed	None observed	None observed	None observed	None observed	None observed	None observed	None observed	None observed	
Cyclic freeze and thaw damage?	None observed	None observed	None observed	None observed	None observed	None observed	None observed	None observed	None observed	None observed	None observed	



Figure 4.5. A magnified view of the polished cross section in Core C8-1. Note the intersecting fractures that originate in a reactive coarse aggregate particle, extend outward into the surrounding paste structure, and are partially filled with gray, subtranslucent to opaque ASR gel (yellow arrows).

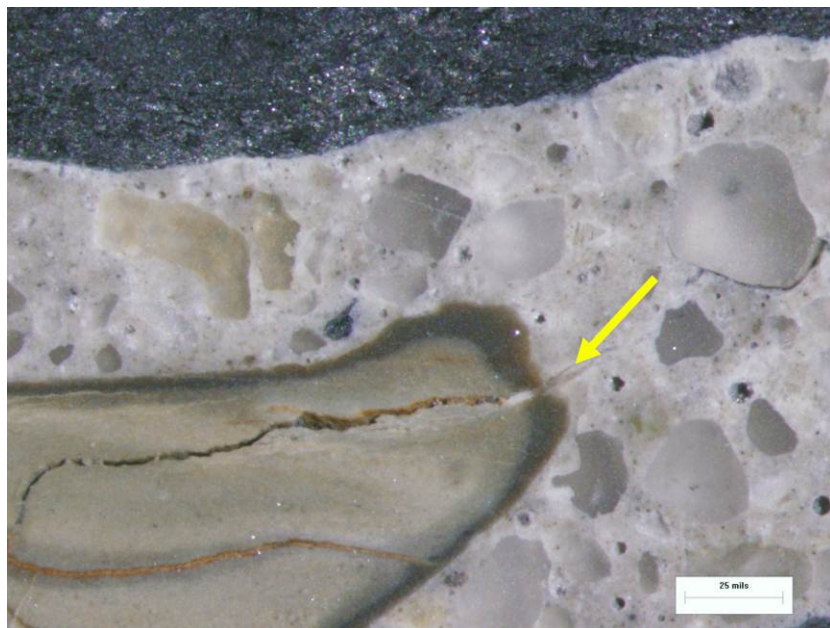


Figure 4.6. A magnified view of the polished cross section in Core C8-1. Note the intersecting fractures that originate in a reactive chert particle, extend outward into the surrounding paste structure, and are partially filled with gray, subtranslucent to opaque (white) ASR gel (yellow arrows).

4.6.2.2 Concrete in Post-2003 Ties

Our specific findings are described in Appendix A.4 and summarized below:

- In general, the quality of the concrete appears to be good with low water-to-cementitious ratio ranging from 0.32 to 0.40.
- The paste structure consists of hydrated grains of portland cement with supplemental fly ash replacement. We did not observe any evidence of retarded hydration or inadequate cement contents in the hardened concrete.
- We did not note any evidence of ASR distress, DEF distress, cyclic freeze-thaw damage, or chemical alternation of paste structure.
- The aggregate is a dolomitic limestone which does not contain silica-based materials. The aggregate therefore is not susceptible to ASR.
- The concrete mix proportions are comparable to those presented in the Amtrak concrete tie 2003 specification.

4.6.2.3 Concrete San-Vel Ties

Our findings are described in Appendix A.4 and summarized below:

- In general, the quality of the concrete appears to be good. The paste structure consists of hydrated grains of portland cement with no supplemental materials such as fly ash or slag.
- The number and frequency of air voids in the hardened concrete are very low and not indicative of intentional air entrainment (Figure 4.7). The concrete in Core S1-3 (horizontal core sample from Tie S1) appears to have suffered cyclic freeze-thaw damage near one of the two exposed lateral surfaces of the tie, as evidenced by the formation of near-horizontal cracks that are oriented subparallel to the exterior (lateral) surface of concrete tie S1 (Figure 4.8). However, we did not observe evidence of cyclic freeze-thaw damage in any of the other core samples.
- We observe evidence of a tight bond between the prestressing tendons and the surrounding paste in each of the examined core samples (Figure 4.9).
- We did not note any evidence of ASR distress, DEF distress, external sulfate attack, or other chemical alternation of the paste structure.

Specifications or pertinent documents for the production of San-Vel ties are not available to us; therefore, we do not know if air entrainment was required at the time of manufacture of these ties.

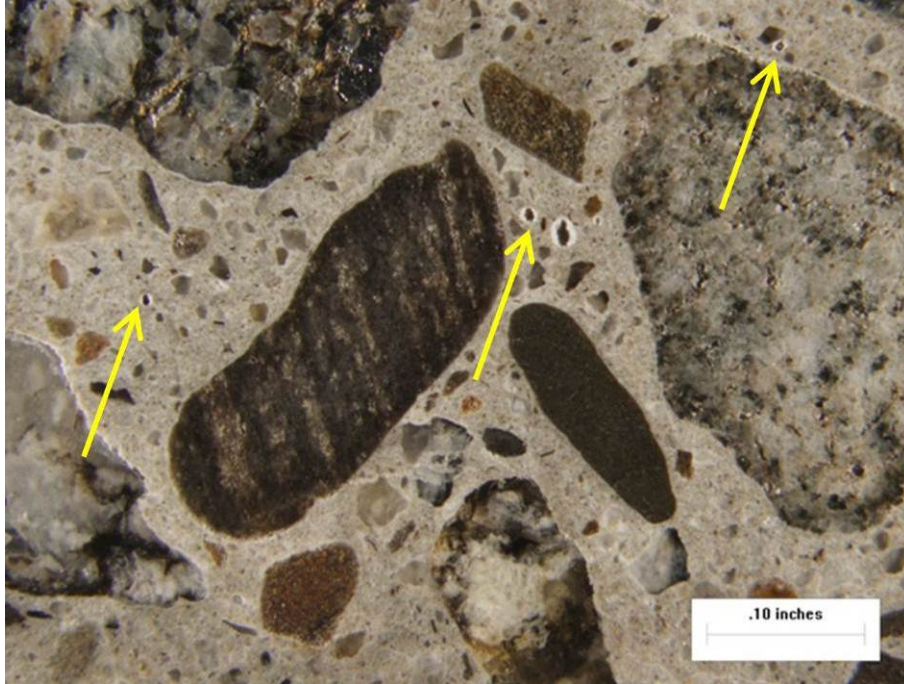


Figure 4.7. A magnified view of the polished cross-section in Core S1-3 showing very few air voids in the paste structure.

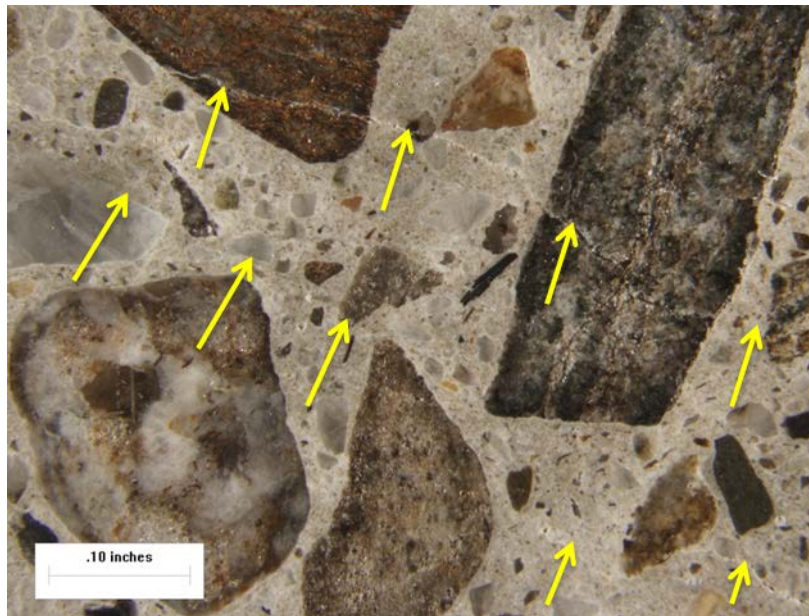


Figure 4.8. A magnified view of the polished cross-section in Core S1-3 showing subparallel fractures in the near surface concrete (yellow arrows).



Figure 4.9. A magnified view of the polished cross-section in Core S1-3 showing a tight intimate bond between the tendon strands and the surrounding paste.

4.6.3 Petrographic Findings from Horizontal Core Samples at Externally Visible Cracks

To supplement the vertical cores and to provide additional information about the concrete performance in the very-near-strand zone (which could not be clearly observed in the vertical cores because the sample preparation avoided the near strand zone), we extracted and studied partial or full depth horizontal concrete cores at externally visible cracks from Case Study 2 (pre-2003 NEC, cracked) ties 8, 17, and 18 (Figure 4.10).

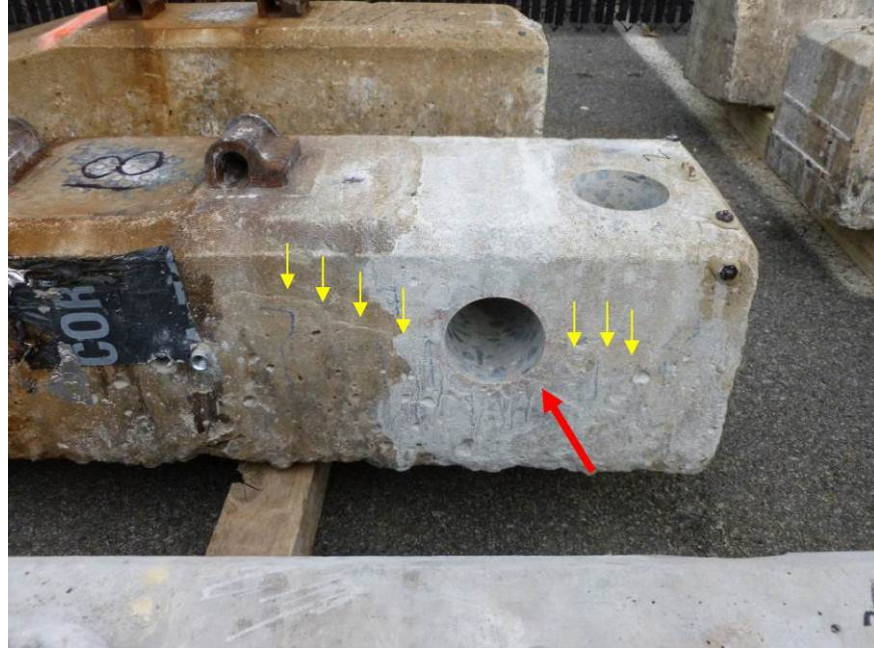


Figure 4.10. Core sample extracted horizontally from Tie 18 at a lateral crack. Red arrow points to the location where the core example was extracted; yellow arrows point to lateral crack.

We examined the three core samples after coring and noted that the visual lateral cracks at the surface typically extended to the first tendon (outermost tendon) and sometimes extended further and stopped at the second tendon (middle tendon), as shown in Figure 4.11. In addition, cracks were present on the circumference of the core sample at tendon levels, as shown in Figure 4.12. The circumferential cracks on the core are vertical cracks in the tie.



Figure 4.11. Core C17-3- sprayed with alcohol showing the lateral crack on the exterior surface extending into the concrete body and stopping at the second tendon.



Figure 4.12. Core C8-4 showing the cracks on the circumference of the core sample at tendons (red and yellow arrows). Note: That core fractured at one of the tendons during coring at one of the cracks, thus exaggerating its width (yellow arrows).

Our petrographic findings of cracking in these horizontally oriented core samples are shown in Table 4.5 and summarized below:

- There are multiple cracks visible in the polished sections, primarily within the same horizontal plane (with respect to the tie) at the upper level of tendons and within a plane that is roughly vertical within the tie. Figure 4.13 shows an example from Tie 8.
- The cracks are primarily associated with ASR-related distress, as evidenced by the presence of reactive coarse and fine aggregate particles and ASR gel partially filling paste and aggregate fractures. Figure 4.14 and Figure 4.15 show examples from Tie 8 and Tie 17, respectively.
- We did not note any corrosion deposits on the prestressing tendons, with the exception of Tie 17.
- We noted that there are occasional gaps between the prestressing tendon and the surrounding paste (Figure 4.16). We observe cement hydration product along the edge of the gap, indicating that the gap formed at an early age of the concrete and was not caused by the coring process.

Table 4.5. Petrographic examination summary of horizontally oriented concrete ties from Case Study 2: pre-2003 NEC.

Feature	Tie 8	Tie 17	Tie 18
Cracking	Multiple cracks, primarily within the plane of the upper level of tendons and other planes radial to the length of the upper tendons (Figure 4.13)	Multiple cracks, primarily in the plane of the upper level tendons but also occurring along other planes radial to the length of the upper tendons (Figure 4.17). Portions of the cracks show tearing features, indicating early-age formation (Figure 4.19)	Multiple cracks, primarily in the plane of the upper level tendons and within other planes radial to the length of the upper level tendons. The majority of the cracks extend around aggregate particles rather than fracturing them (Figure 4.20).
ASR Distress Level	ASR gel partially fills cracks in coarse and fine aggregate and paste (Figures 4.14 through Figure 4.15).	ASR gel partially fills cracks in coarse and fine aggregate and paste.	Occasionally, ASR gel partially fills the cracks. The cracks occasionally split reactive aggregate particles.

Feature	Tie 8	Tie 17	Tie 18
Corrosion	None	<p>Minor corrosion deposits on the first tendons where the crack stops (Figure 4.18). Since the corrosion product does not extend into the crack, and we found the evidence of corrosion product in an adjacent location (not connected to the large crack) that runs into a void, we believe that the corrosion predated the surface crack. However, we cannot determine if there is any relationship between the corrosion of the tendon and the crack.</p>	None
Other	<p>Occasional gaps between the prestressing tendon and the surrounding paste (Figure 4.14). Cement hydration product along the edge of the gap, indicating the gap formed at an early age.</p>	<p>Intermittent gap between the prestressing tendon and the surrounding paste. Surface crack extends to first tendon appears to have formed at a later age, as evidenced by a greater depth of the carbonation at the exterior surface than crack interface. The crack fractures multiple coarse aggregate particles along its path (Figure 4.17).</p>	<p>Intermittent gap between the prestressing tendon and the surrounding paste. Occasionally, the fine cracks show evidence of autogenous healing based on observations of secondary calcite. This indicates that the cracks occurred at a very early age.</p>



Figure 4.13. Overview of polished section from Core C8-4 showing alignment of cracks.

Red arrows point to cracks (too narrow to be visible at this scale) and outline the orientation of the cracks; yellow arrows point to reactive aggregate particles. Photograph shown in as-cored orientation, side of tie to the left, top of core to top of photograph.



Figure 4.14. Magnified view of the microstructure in the body of Core C8-4 showing a reactive chert aggregate particle with ASR gel. Yellow arrows outline the reaction rim around the perimeter of the aggregate as well as the locations of ASR gel that partially fills cracks that extend outward from the aggregate and partially fills fractures in the surrounding paste structure.

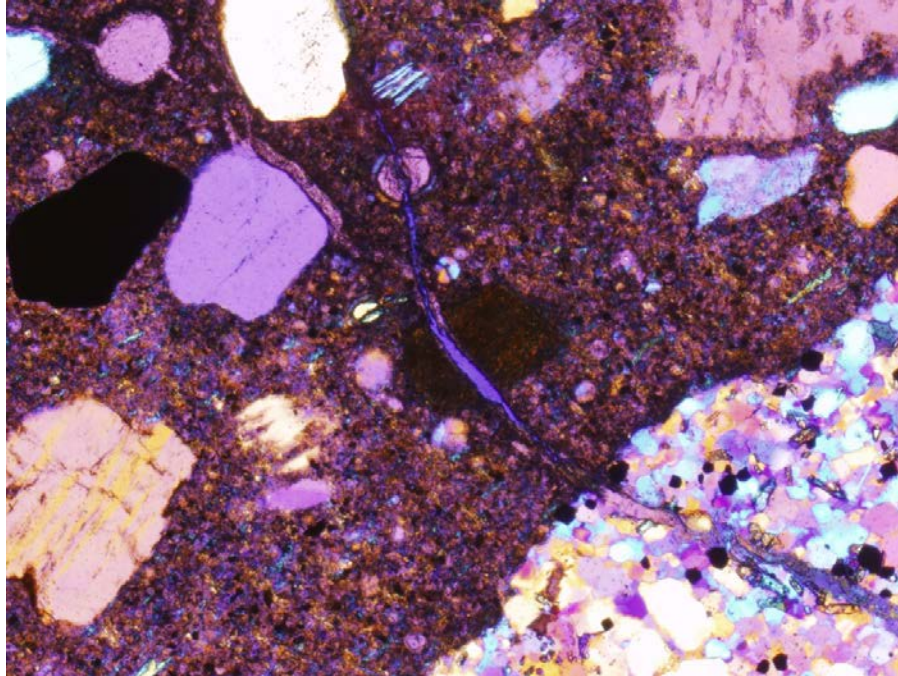


Figure 4.15. Magnified view of the microstructure in the body of Core C17-3 showing a reactive coarse aggregate particle and ASR gel that is partially filling the crack in the aggregate, as well as portions of aggregate cracks that extend outward and partially fill fractures in the surrounding paste structure.

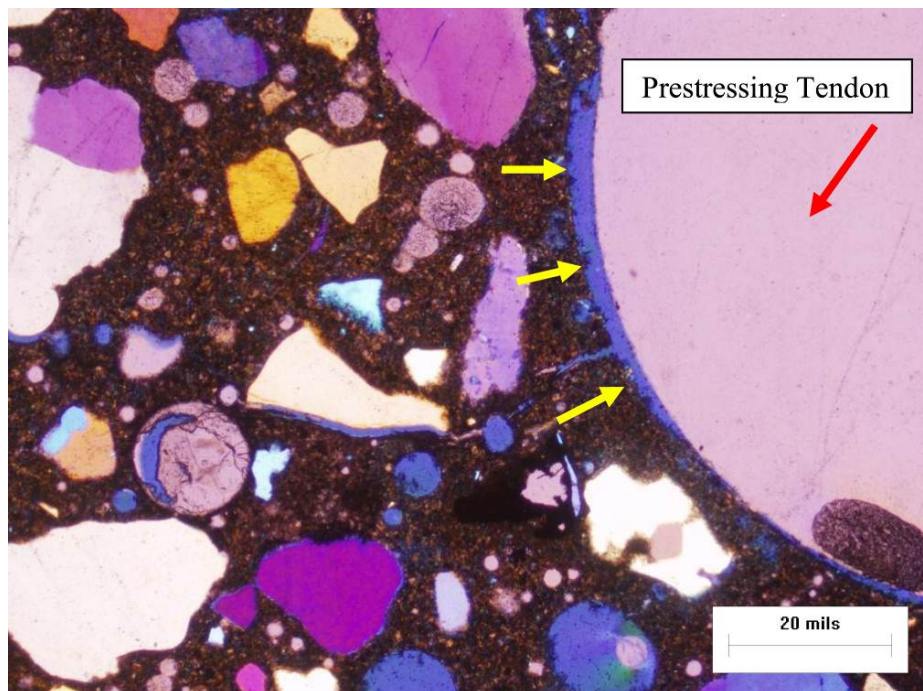


Figure 4.16. Magnified view of the microstructure in the body of Core C8-4 showing intermittent gap (yellow arrows) around one of the prestressing strands (pink).



Figure 4.17. Crack condition on the polished section from Core C17-3. Red arrows point to direction and extent of cracks; yellow arrows point to the reactive aggregates.



Figure 4.18. A magnified view of the polished cross-section in Core C17-3 at the tendon near the exterior surface. Red arrows point to the minor brown corrosion staining at the tendon.



Figure 4.19. A magnified view of the polished cross-section in Core C17-3 showing the fracture surface just above the tendon. Red arrows point to the tear fractures in the fracture surface.

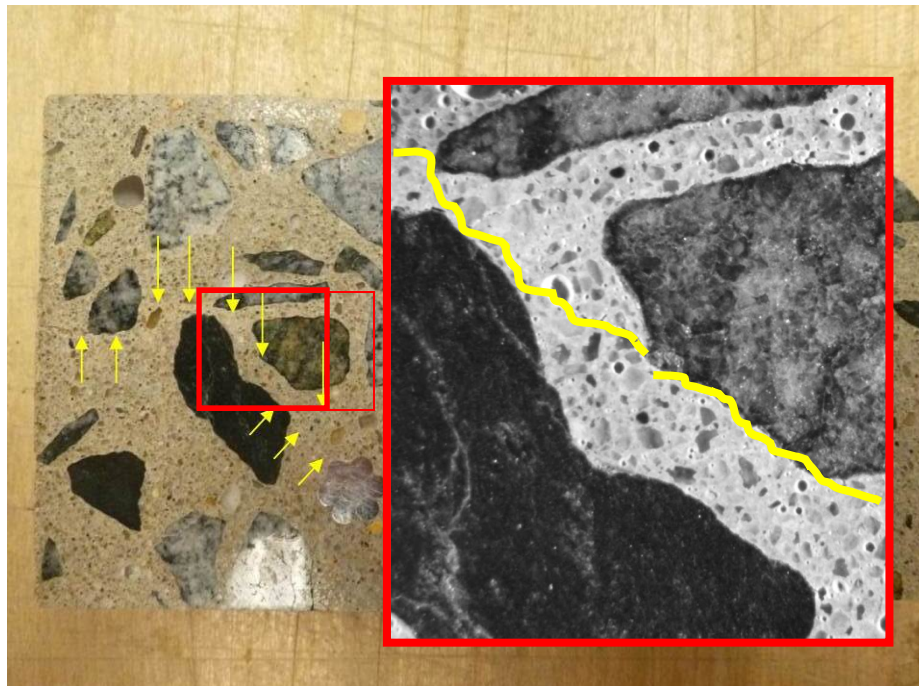


Figure 4.20. Cracking in the polished section from Core C18-3 (only the surface crack to the first tendon is illustrated). Yellow arrows point to the crack and point in the direction of the exterior surface and the first tendon. The crack goes around the aggregate particles rather than fracturing the aggregates as shown highlighted in the inset.

4.6.4 SEM/EDS Examinations – DEF Potential

Although we did not observe any characteristic symptoms of DEF distress (such as gaps at the paste-aggregate interface that are filled with larger opportunistic ettringite crystals, or frequent internal fractures in the paste structure) during our optical petrography, we conducted scanning electron microscope (SEM)-based petrography to confirm that DEF was not occurring. This was required to confirm the lack of even early-stage DEF because the ettringite formations that cause expansion within the paste frequently begin at very small scales that are distributed throughout the paste and are only visible at magnifications above 1,000X.

We examined the top portion of the polished section of core sample from Tie 8, a severely cracked tie, using our JEOL JSM-6490LV SEM equipped with an EDAX Apollo 40 Silicon Drift Detector energy dispersive X-ray spectroscopy unit (EDS). The EDS unit provides compositional information regarding the characteristic elemental constituents that cannot be discerned optically.

Our SEM/EDS examinations did not reveal any evidence of ongoing DEF distress such as ettringite (a hydrous calcium aluminum sulfate mineral) in the small fractures within the paste structure or in localized “nests” within the cement paste. This indicates that there is no DEF-related deterioration within the concrete. We did find normally occurring primary ettringite in the air voids. We did not note any other abnormal material reactions. This finding is consistent with the findings of others concerning the majority of ties studied previously, as was discussed in Section 4.5.

We did not examine concrete core samples from the remaining seven concrete ties selected for the case studies because their optical petrographic analyses did not reveal any larger-scale evidence of internal sulfate attack due to DEF or external sulfate attack that would have suggested they were any different from the concrete in Tie 8.

4.6.5 Air-Void System Analysis and Freezing-Thaw Resistance of Concrete Ties

To better understand the air void system parameters and their possible effect on tie performance, we supplemented the petrographic estimates of air content in the concrete with a quantitative assessment of the air-void system parameters on four of the vertical core samples. We made these assessments in accordance with ASTM C457 (Microscopical Determination of Parameters of the Air-Void System in Hardened Concrete), using the modified point-count method. The results of the testing are shown in Table 4.6, along with the visual observations and petrographic analyses from Table 4.4 for comparison.

Table 4.6. Summary of core observations and testing related to freeze-thaw evaluation.

	Tie 2	Tie 6	Tie 8	Tie 16	Test Method
Case Study	Pre-2003 NEC, uncracked or minor cracking	Pre-2003 NEC, cracked	Pre-2003 NEC, cracked	Post-2003 NEC	-
Tie Cracking Rating*	1	4	4	1	Visual
Surface Scaling	No	No	No	No	Visual
Pozzolonic Material?	None	None	None	Fly ash	Petrographic
Air Content	2.0%	2.3%	2.3%	3.8%	Lab Test ASTM C457
Spacing Factor (in)	0.0049	0.0084	0.0064	0.0056	Lab Test ASTM C457
Specific Surface Area (in ² /in ³)	1713	859	1275	1103	Lab Test ASTM C457
Quality of Air-Void System	Non-uniformly distributed	Well-distributed	Some variation	Well-distributed	Petrographic
Sub-Parallel Cracking	No	No	No	No	Petrographic

* See Section 3.

As further discussed in Section 4.7 below, the information from the separate analyses are generally similar and in agreement with the previous testing by others.

4.7 Discussions and Findings Relative to Petrographic, SEM/EDS, and Air-Void System Testing

The purpose of the petrographic, SEM/EDS, and air-void analyses work was to investigate and identify any evidence supporting or discounting potential materials-related phenomena that may be the cause of the observed cracking. In general, these types of phenomena include: low general overall quality which may lower the strength of the concrete, poor inherent resistance to aggressive freeze-thaw environments, external sulfate attack, or internal deleterious reactions such as DEF and ASR. Our discussion and findings related to these phenomena are given below.

4.7.1 General Concrete Quality

In general, we observe no evidence of significant manufacturing-related deficiencies such as aggregate segregation, late-age water additions, or incomplete consolidation. Similarly, there are no indications of concrete proportioning or batching errors, such as a shortage of cement or over-watering, and the overall hydration reactions are normal. The concrete exhibits a very low to

moderate water-to-cementitious ratio that we estimate to be in the range of 0.33 to 0.46, which is appropriate for high design compressive strength.

Our examinations of the core samples from ties manufactured in 2008 (Ties 16 and 21) indicate that the concrete proportions and quality are comparable to those described in the Amtrak concrete tie specification for post-2003 ties and are consistent with the mix design provided in the Amtrak UIUC Phase Report dated 4 December 2009, in terms of cement and fly ash content, cement type, mineral type of the coarse and fine aggregate particles, concrete air content, and water-to-cementitious ratio.

Based on these observations, we do not believe that manufacturing-related material deficiencies, proportioning or batching errors, or deficient hydration reactions are responsible for the observed cracking. This is consistent with the previous findings of CTL and LML.

4.7.2 Resistance to Cyclic Freezing and Thawing

Our overall observations and detailed air content measurements on pre-2003 concrete ties show that they are not undergoing damage caused by cyclic freezing and thawing, and they are not generally vulnerable to this type of distress, based on the following:

- The pre-2003 concrete ties do not exhibit symptoms of freeze-thaw damage, such as scaling or subparallel cracking.
- Although they contain low air contents and minor variations in the air-void systems, our tests indicate that the concrete has sufficient freeze-thaw resistance, with marginal to well-distributed air void systems, spacing factors at or less than 0.008 in, and specific surface areas larger than $600 \text{ in}^2/\text{in}^3$.
- Our petrographic analysis on the thin sections indicates that the water-to-cementitious material ratio (w/cm) in the concrete is generally lower than the 0.45 (maximum) typically specified for resistance to damage due to cyclic freezing and thawing.

Our studies on the post-2003 concrete ties find that they exhibit similar freeze-thaw performance as the pre-2003 ties and have improved inherent freeze-thaw resistance due to their higher air content.

Our limited study on the San-Vel ties indicates that they can be vulnerable to surface damage due to cyclic freezing and thawing, as shown by the near-surface subparallel cracking of a single one of the examined San-Vel ties. This damage is consistent with the low quality of their low air void system, which will make the San-Vel ties susceptible to cyclic freezing and thawing where they are exposed to sufficient water to become saturated. It is important to note that this minor damage is purely a surface phenomenon and has had no effect on the concrete in the region of the prestressing strands. Furthermore, despite the potential vulnerability to cyclic freezing and thawing of the San-Vel ties, it does not appear to have affected their overall performance, as shown by the reported lack of the characteristic horizontal cracking in the San-Vel tie population. This further reinforces our assessment that the observed horizontal cracking of the other ties in the NEC is not related to cyclic freezing and thawing, as the San-Vel ties have the lowest resistance to cyclic freezing and thawing, yet have very good observed performance in place.

Based on these observations, we believe that cyclic freezing and thawing is not responsible for the observed cracking in the pre-2003 ties. This is consistent with the previous findings of CTL and LML.

4.7.3 Delayed-Ettringite Formation (DEF)

We do not observe any signs of DEF in the San-Vel, pre-2003 ties, or post-2003 ties. There are no deposits of ettringite within the paste and no significant deposits of ettringite in the cracks and void spaces. Therefore, we conclude that DEF is not a cause or contributor to the observed cracking in the pre-2003 ties.

This finding is consistent with those of CTL and LML in their investigation of ties that did not exhibit widespread map cracking on the tie surfaces, indicating that all of the petrographic assessments of the typical damage condition were consistent. CTL and LML did examine a limited number of ties (we believe they have examined the same ties based on the tie designation used in their reports) that exhibited an abnormal cracking pattern over the entire tie surface, and they concluded that DEF may have been a contributor to the unusual cracking in those particular ties. We did not observe any ties meeting the CTL and LML description and did not encounter any heavily map-cracked ties in the field, so we conclude that while DEF may have occurred in those ties, it is not widespread, not a cause of the predominant horizontal cracking mode, and was likely due to isolated problems with curing temperatures or unusual material reaction.

4.7.4 External Sulfate Attack

We do not observe any signs of external sulfate attack in any of the ties examined. There are no deposits of ettringite within the paste, no softening of the cement paste, no cracking with associated deposits of gypsum or calcium hydroxide, and no significant deposits of ettringite in the cracks and void spaces. Therefore, we conclude that external sulfate attack is not a cause or contributor to the observed cracking in the pre-2003 ties.

4.7.5 Alkali-Silica Reaction

We observe that ASR is present in the pre-2003 ties and that it appears to be associated with the crack locations. In particular, we note the following regarding ASR within the ties:

- The post-2003 and the San-Vel ties (which reportedly have not experienced splitting-type failures in the field) show no indications of ASR-related distress. In the San-Vel ties, the aggregates do not appear to be ASR-susceptible, and the use of fly ash and an entirely different type of aggregate in the post-2003 ties appears to have mitigated or prevented any reaction.
- The pre-2003 ties show evidence of ongoing ASR. Specifically, we note the following:
 - There is slight-to-moderate ASR distress within the concrete (cracking that contains ASR gel deposits, aggregates with reaction rims, and deposits of ASR gel in air voids and cracks within the concrete paste). These results are consistent with the CTL and

LML reports that also find that ASR is present in the pre-2003 ties. The failure of the ASTM C227 and C289 screening tests in use during manufacture of the pre-2003 ties is not surprising, as the tests are now recognized by industry as not sensitive enough to detect a slowly reactive aggregate and may thus have provided an incorrect prediction.

- There is an apparent relationship between the degree of ASR distress in the core samples and the horizontal cracking condition on the exterior surface of the concrete ties, with both increasing concurrently as indicated in Table 4.7 and Figure 4.21. Note that the higher variability at the petrographic ASR severity rating of 0 is likely an artifact of the way the petrographic sections were prepared from the vertical cores, as previously discussed.
- The ASR distress occurs only in the immediate vicinity of the plane of the upper layer of prestressing strands, with little to no ASR observed elsewhere in the ties. In addition, the cores taken horizontally through the horizontal cracks in the ties, which provide more information around the near-tendon area, show more ASR-related features than the vertical cores, especially as related to the primary horizontal splitting cracks in the ties and the other cracks oriented radially to the tendons, as shown in Table 4.8. This indicates that the occurrence of the ASR is associated with the locations of prestressing tendons because we only observe minor evidence of ASR distress away from the tendon locations.

Section 8 provides additional analysis and discussion of this relationship between distress and tie performance in relation to other work performed as part of this investigation.

Table 4.7. Data used to correlate crack severity to various measures of ASR.

Tie ID	Crack Severity Rating at Each End* (End 1-End 2)	Petrographic ASR Severity Rating (Based on Vertical Core Samples)
1	2-1	1-Slight
2	1-1	0-None
6	4-4	2-Slight-to-Moderate
8	4-3	2-Slight-to-Moderate
11	3-2	1-Slight
10	1-3	0-None
14	3-4	2-Slight-to-Moderate
16	1-1	0-No evidence
17	3-3	0-No evidence
18	3-3	1-Slight
19	2-2	0-No evidence
20	1-2	1-Slight
21	1-1	0-No evidence
S1	1-1	0-No evidence
S2	1-1	0-No evidence

* See Section 3 for a description of the crack severity rating; for example, 2-1 means End 1 has severity = 2 and End 2 has severity = 1.

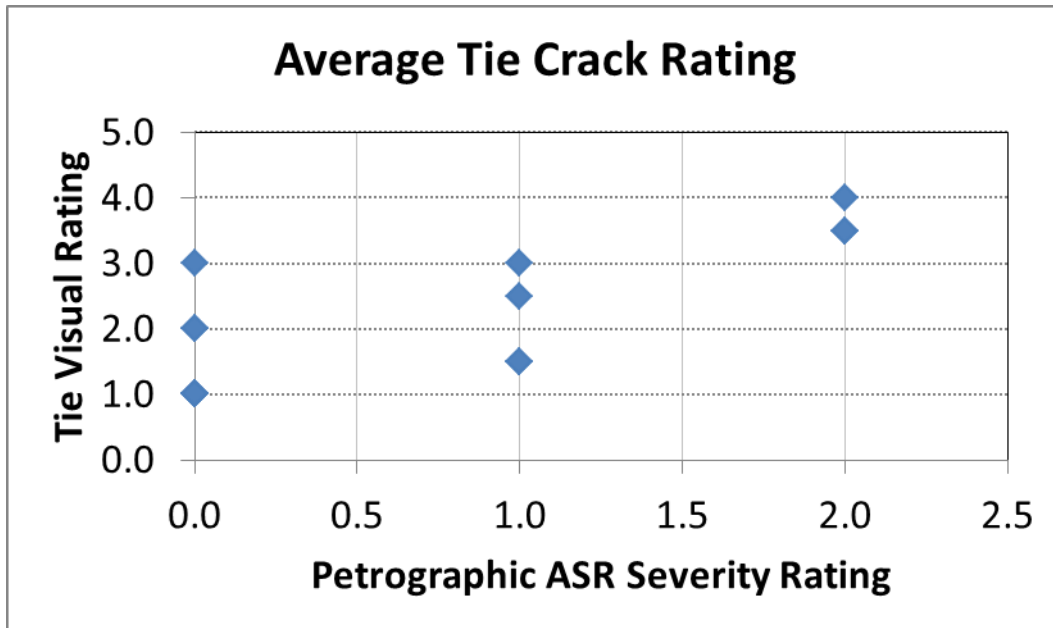


Figure 4.21. Relationship between the severity of ASR distress and the crack rating.

The visual rating is assigned as follows:

Rating 1: no visible crack at all

Rating 2: visible cracks with width <0.005 in and the crack length is typically short (within 12 in)

Rating 3: visible cracks with width between 0.005 and 0.016 in and the crack length is variable

Rating 4: crack width greater than 0.016 in and the crack length is extensive, typically extending from the end of tie to the shoulder of the tie

The petrographic ASR severity rating is assigned as follows:

Rating 0: No cracking detected - No features or characteristics associated with alkali-silica reaction (ASR) detected

Rating 1: Very slight cracking (No evidence of deleterious ASR) - A condition usually described as “microcracking.” Cracks typically up to 20 to 30 μm in width, the majority of which are visible only on interior concrete surfaces, confined mainly to the cement paste matrix, sometimes at cement/aggregate interfaces such as adhesion cracks. Cracks are short, isolated, and usually empty. No significant internal aggregate cracking, and if present, aggregate fractures are nonpropagating.

Rating 2: Slight cracking (minor or trace evidence of deleterious ASR) - Cracks 30–40 μm in width, usually isolated, not forming a network. Cracks may originate from aggregates, but do not generally propagate very far into surrounding cement matrix. Reaction rims are frequently also evident around the perimeters of the “reacting” and distressed aggregate particles. Extensive crack networks are not observed. Some internal and peripheral cracking of aggregates may be present. Cracks may also be present on the boundaries of aggregate particles as adhesion cracks. Visible ASR gel deposits in voids and cracks may be observed, but not necessarily. The cracks are generally open. The cracks and air voids within the concrete are occasionally partially filled primary and/or secondary deposits of sulfate, portlandite, or carbonate minerals.

Table 4.8 – Summary of ASR-related observations in the pre-2003 ties.

Tie ID	Core Direction	ASR Classification	Distress Features						Notes
			Rims around Aggregates	Cracking	ASR Gel	Lateral Crack at Upper Tendon Level (& Associated Crack Widths)	Vertical Cracking	Cracking on the top surface of Tie	
1	Vertical	Slight	Occasional	Occasional fracture primarily within coarse aggregates; a single fracture in paste near top tendon	Partially filled in short cracks originated with chert particles	0.003 to 0.005 at one side	No	No	
2	Vertical	None-to-Slight	Occasional	Occasional fracture primarily within coarse aggregates	None observed	None observed	No	No	
6	Vertical	Slight-to-Moderate	Occasional-to-Frequent	Occasional aggregate fractures in coarse aggregate and fine aggregate extending into the surrounding paste	Multiple fractures in the paste just above the tendon; ASR gel partially fills fractures.	0.003 to 0.050 both sides	No	No	
8	Vertical	Slight-to-Moderate	Frequent	Micro and macro fractures/cracking throughout the sample: in the paste structure and within the aggregate particles	ASR gel in the fractures throughout the full depth of the core sample	0.003 to 0.013 both sides	Yes	Yes	Vertical and topside crack associated with ASR
	Horizontal	Slight-to-Moderate	Frequent	Multiple cracks, primarily in the plane of the upper level tendons and in the plane perpendicular to the upper level of tendons – cracks associated with reactive coarse aggregates	Majority of cracks partially filled with ASR gel.	-	Within concrete body	No	Occasional gaps between prestressing tendons and surrounding paste
10	Vertical	None-to-Slight	Occasional	Occasional fracture primarily within coarse aggregates	None observed	None observed	No	No	
11	Vertical	Slight	Occasional	Occasional fracture primarily within coarse aggregates	None observed	<0.003 in both sides	No	No	
14	Vertical	Slight-to-Moderate	Frequent	Occasional aggregate fractures in coarse aggregate and fine aggregate extending into the surrounding paste	Multiple fractures and one prominent fracture in the paste structure just above the tendon elevation. Fractures filled with ASR gel.	0.003 to 0.025 in both sides	No	No	
17	Vertical	None-to-Slight	Occasional	Occasional fracture primarily within aggregate	None observed	0.003 to 0.011 in both sides	No	No	Sections made above tendon-upper tendon level
	Horizontal	Slight-to-Moderate	Occasional-to-Frequent	Multiple cracks, primarily in the plane of the upper level tendons and perpendicular to the upper level of tendons – majority are associated with reactive coarse aggregates; portions of the cracks show tearing features, indicating early-age formation	Majority cracks partially filled with ASR gel.	-	Within concrete body	No	Corrosion deposits on one tendon at intersection with surface crack; intermittent gap between the tendon and paste
18	Vertical	Slight	Occasional	Occasional fracture primarily within aggregate; two reactive cherts within the section	None observed	0.003 to 0.007 in both sides	No	No	Sections made above tendon-they do not include the concrete at upper tendon level
	Horizontal	Slight-to-Moderate	Occasional-to-Frequent	Multiple cracks, primarily in the plane of the upper level tendons and in the plane perpendicular to the tendons; cracks extend around aggregate particles rather than fracturing them.	Occasionally, cracks partially filled with ASR gel	-	Within concrete body	No	Intermittent gap between prestressing tendon and the sounding paste
19	Vertical	None-to-Slight	Occasional	Occasional fracture primarily within aggregate	None observed	No more than 0.003 in one side	No	No	Sections made above tendon
20	Vertical	Slight	Occasional	Occasional fracture primarily within aggregate	In air void	None observed	No	No	Sections made above upper tendon- level

5. Mechanical Testing

We conducted several mechanical tests to characterize the case study ties. Our goal was to determine whether there are significant differences in certain properties between ties with different levels of performance and to obtain information useful for modeling and strength evaluations. The properties we measured included elastic modulus, compression strength, tension (splitting) strength, and flexural strength of the ties themselves.

5.1 Modulus and Compressive Strength

We conducted modulus of elasticity testing to determine if the stiffness of the concrete had been affected by any type of concrete deterioration, and we tested the compressive strength to see if the compressive strength was significantly different between ties. The elastic modulus and the compressive strength of the concrete tie materials were measured from the same sample. We took this sample from the horizontal core removed from a region above the tendons. Figure 5.1 shows a photograph of one of the test samples in the test machine (in this case to measure elastic modulus). The dimensions of the samples were nominally 3 in in diameter and 5 in long. However, we used a shorter sample in those cases in which the core piece cracked from the coring operation.



Figure 5.1. Set-up testing for the modulus of elasticity tests.

We measured the modulus of elasticity of the concrete core samples in accordance with ASTM C469 (Standard Test Method for Static Modulus of Elasticity and Poisson Ratio of Concrete in Compression) using a universal testing machine. We then tested this same core in accordance with ASTM C39 (Standard Test Method for Compressive Strength of Cylindrical Concrete Specimens) using a higher capacity universal testing machine. The test results of both tests are

shown in Table 5.1 below. The ID refers to the tie number and core sample: C1-2 is from Tie 1 and is core sample 2.

Table 5.1. Modulus of elasticity and compressive strength test results.

Core ID	Compressive Strength (psi, L/D factored)	Modulus of Elasticity (10 ⁶ psi) Gage length: 2 in			
		Test Run 1	Test Run 2	Average of Two Runs	Predicted Using ACI Equation
Pre-2003 NEC, uncracked or minor cracking					
C1-2	9,900	4.66	4.90	4.78	5.67
C2-2	9,560	6.00	5.76	5.88	5.57
C19-2	10,200	4.63	4.63	4.63	5.76
C20-2	9,400	4.64	4.63	4.64	5.53
Pre-2003 NEC, cracked					
C6-2	9,710	3.59	3.86	3.72	5.62
C8-2	8,740	3.51	3.69	3.60	5.33
C10-2	9,750	4.59	4.38	4.49	5.63
C11-2	10,580	4.79	4.57	4.68	5.86
C14-2	9,610	4.16	4.44	4.30	5.59
C17-2	10,000	4.05	4.05	4.05	5.70
C18-2	7,850	3.98	3.96	3.97	5.05
Post-2003 NEC					
C16-2	9,070	6.59	6.47	6.53	5.43
C21-2	10,130	5.57	5.56	5.57	5.74
San-Vel					
S1-1	12,850	4.85	4.86	4.85	6.46
S2-1	12,190	4.67	4.63	4.65	6.29

The compression test results range from 7,850 psi to 12,850 psi, all of which are above the specified 28-day compressive strength of 7,000 psi. This level of strength is considered to be high strength.

The measured compressive strength is more than 7,000 psi, indicating that the 28-day compressive strength of the concrete most likely met the specification requirement of 7,000 psi. It is not surprising that the concrete strength is only slightly higher than 7,000 psi even after 7–14 years of aging, because although the compression strength of conventional concrete increases with time, heat-cured concrete behaves somewhat differently. The early age heating leads to significantly higher early-age strengths, but limits the maximum strength and long-term strength

gain. Nilson [5.1] provides equations to estimate the strength of similar concretes cured under moist or early-age steam curing in precasting operations; the application of the equations to a nominal 7,000 psi concrete (Figure 5.2) shows the effect of the steam curing. A similar effect is shown in Figure 5.3 from Gerwick [5.2]. Examination of these curves indicates that a minimal increase in strength over time is to be expected for heat-cured concrete.

Table 5.1 shows that the measured modulus of elasticity of the core samples varies significantly, ranging from 3.5×10^6 psi to 6.6×10^6 psi. To aid in interpreting the results of the testing, we also calculated the predicted elastic modulus based on its compressive strength, using the $E=57,000 \sqrt{f'_c}$ equation given in ACI [5.3], “Building Code and Commentary.” We note that most of the elastic modulus numbers are lower than those predicted by the ACI equation. This is consistent with our finding of indications of ASR in the concrete, because low-level ASR causes microcracking that lowers the elastic modulus (causing “softening” of the concrete) without significantly affecting strength [5.4]. However, the low measured elastic modulus values for the San-Vel ties are surprising, given their lack of observed ASR. The reason for this is not clear.

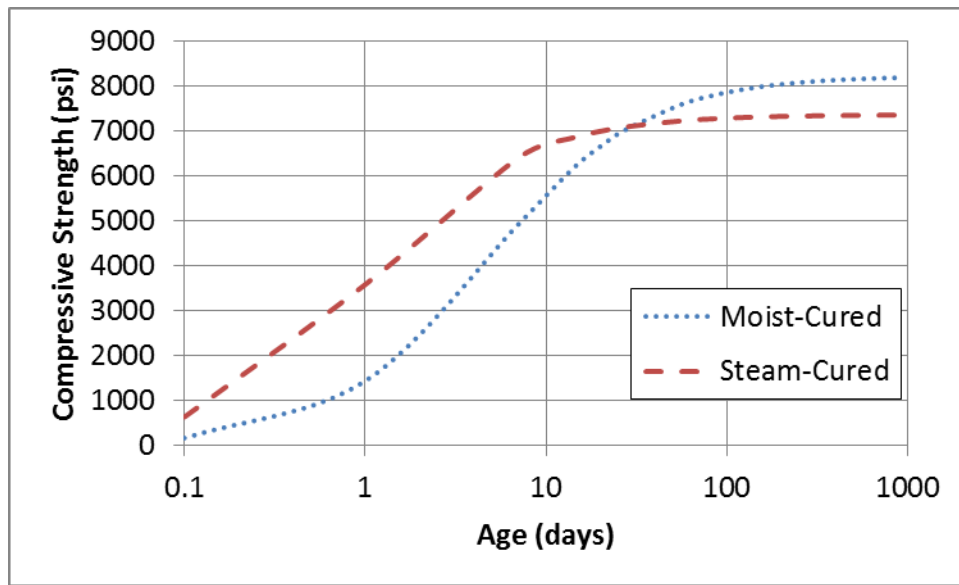


Figure 5.2. Effect of time on compressive strength of concrete for moist-cured and steam-cured concrete (from Nilson [5.1]).

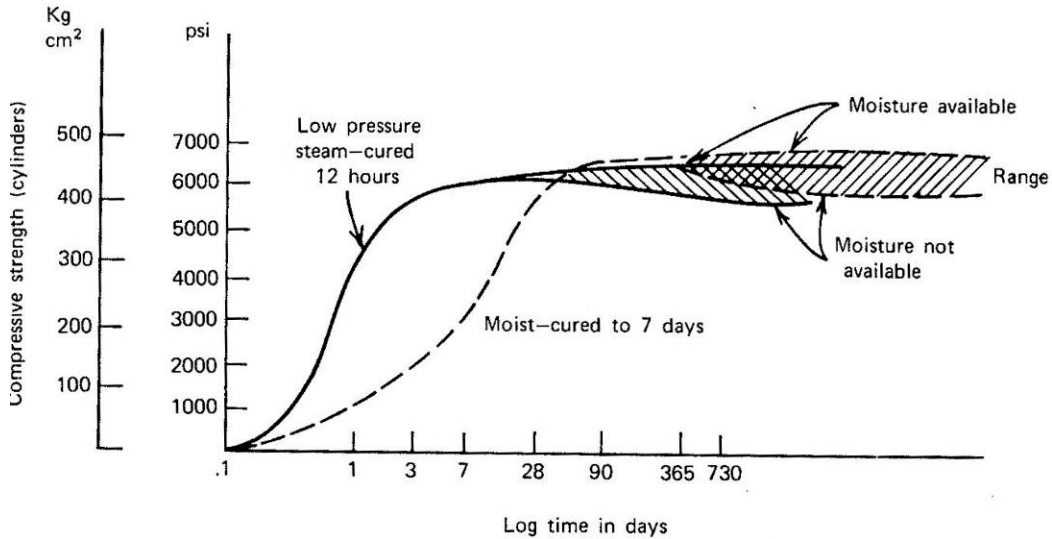


Figure 5.3. Effect of time on compressive strength of concrete (from Gerwick [5.2]).

5.2 Tensile (Splitting) Strength

We conducted a few tests to measure the tensile strength of the concrete in the ties perpendicular to the plane corresponding to the primary crack orientation we observed in the ties. We wanted to determine whether significant differences in tensile strength could explain the difference in performance. We removed 2.3–3 in diameter, 3–4 in long test samples by coring the ties above the strands at the end opposite the one from which we removed samples for compression and modulus testing. We conducted the tests according to ASTM C496 (Standard Test Method for Splitting Tensile Strength of Cylindrical Concrete Specimens). Figure 5.4 shows a photograph of the test configuration. The direction of maximum tensile stress in this test is perpendicular to the line connecting the loading points. We oriented the test specimen so that the crack plane corresponded to a horizontal plane in the tie, although this plane is above the plane of the top row of tendons. Table 5.2 lists the results of the tests. These tensile strengths are relatively high (see also Section 7) compared with the value obtained from the generally accepted formula:

$$f_t' = 7.5\sqrt{f_c'}$$

This formula gives a tensile strength of 750 psi for a 10,000 psi compression strength. (See also [5.5] and [5.6] for tensile strength values.)

The split tensile strengths are greater than expected, but there does not appear to be a significant difference between the values from the different case study ties.



Figure 5.4. Tensile (splitting) test configuration.

Table 5.2. Tensile (splitting) test results on concrete from the case study ties.

Specimen ID	Tensile Strength (psi)
Pre-2003 NEC, uncracked or minor cracking	
C1-3	910
C2-3	1,005
Pre-2003 NEC, cracked	
C8-3	965
Post-2003 NEC	
C16-3	1,015
San-Vel	
S2-2	925

5.3 Tie Flexural Strength

We performed positive rail seat moment tests on four ties in accordance with Amtrak’s concrete tie specifications. The purpose of these tests was to determine the extent to which the ties possessed the desired flexural strength even in the presence of the type of cracking that has been observed and to obtain data for comparison with our finite element model. Figure 5.5 shows the

test configuration from the 1989 Amtrak specification, and Figure 5.6 illustrates the configuration we used to conduct the tests.

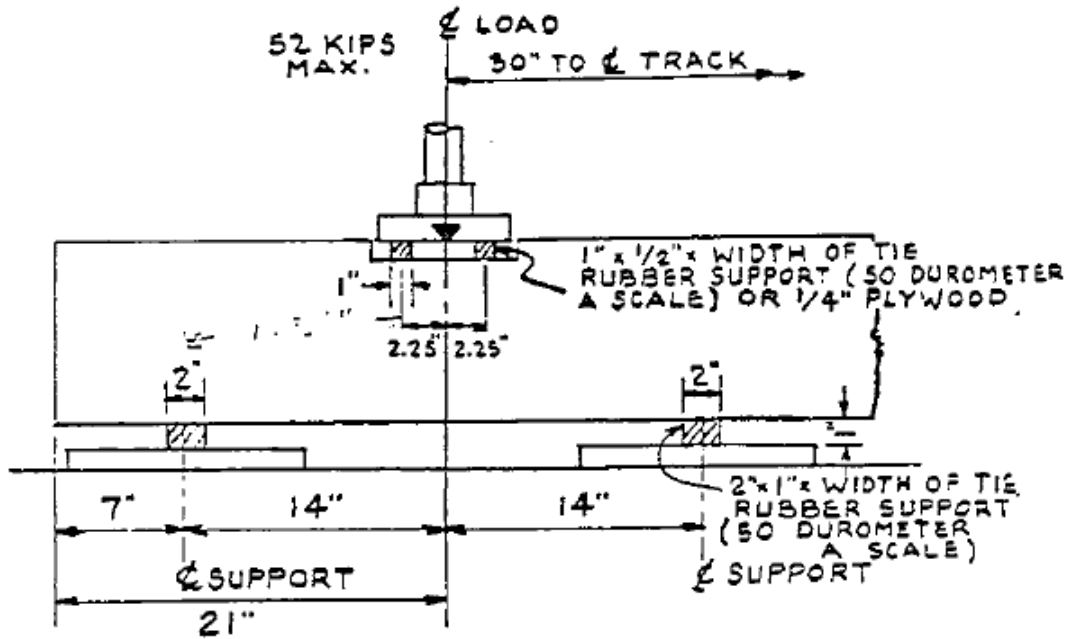


Figure 5.5. Typical Amtrak specification setup for positive rail seat moment test.

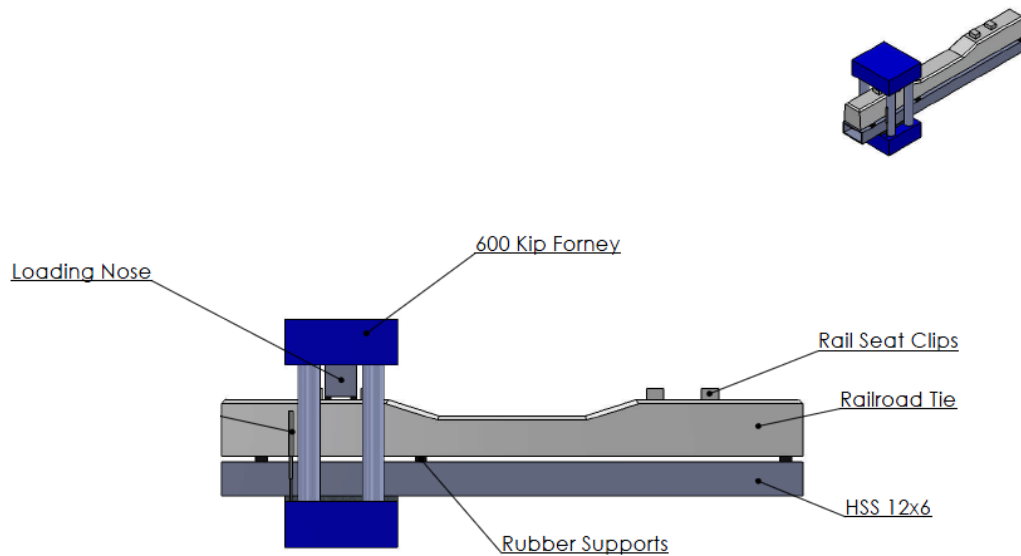


Figure 5.6. Illustration of the SGH positive rail seat moment test configuration.

Load was determined from the calibrated pressure transducer in the hydraulic actuator. We measured strains with bondable foil strain gauges at the locations shown in Figure 5.7. Strain

gauges G1 through G4 were used for Ties 2 and 16; strain gauges G1 and G2, only, were used for Ties 1 and 7. We also had a displacement transducer but the signal proved to be erratic.

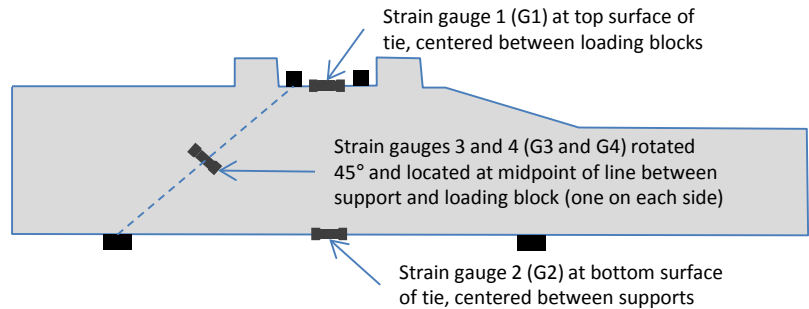


Figure 5.7. Diagrams of instrumentation used in tie positive rail seat moment tests.

Table 5.3 lists the ties we tested; ties were selected to reflect a range of cracked conditions. Three of these ties are the same ties from which core samples were removed for the petrography and other mechanical tests. The first two, Ties 1 and 2, were relatively uncracked; that is, we were unable to detect any cracks. Tie 7 showed a clear horizontal crack near the tested end of the tie. These three ties were made according to the pre-2003 specifications. Tie 16 was made to the post-2003 specifications and showed no signs of cracking.

Table 5.3. Ties for the positive rail seat moment test.

Tie No.	Date of Manufacture	Fastener Type	Notes
Pre-2003 NEC, uncracked or minor cracking			
1	1999	Fast Clips	Pre-2003 design; initially uncracked
2	1993	E-Clips	Pre-2003 design; initially uncracked
Pre-2003 NEC, cracked			
7	1998	Fast Clips	Pre-2003 design; horizontal crack running parallel to top strand from front face to rail seat
Post-2003 NEC			
16	2008	Fast Clips	Post-2003 design; initially uncracked

All ties were loaded at a constant loading rate between 3 and 10 kips per minute. Once the load reached 52 kips, we held the load constant for approximately 3 minutes while we performed an inspection to determine if structural cracking had occurred. We sprayed isopropyl alcohol on the ties' surfaces to aid in this process. After the inspection, we continued loading the tie at a

constant rate between 3 and 10 kips per minute until the maximum load was reached, while noting the load and location when significant events (e.g., onset of structural cracking, prestressing strand slipping) occurred.

Figure 5.8 is a plot of load versus time for the four tests. (Time is used on the x-axis, because the displacement measurements were erratic and, therefore, do not provide a good means for making plots. In addition, all plots were made to coincide in time at a load of 20 kips.) The maximum loads and some other parameters are listed in Table 5.4.

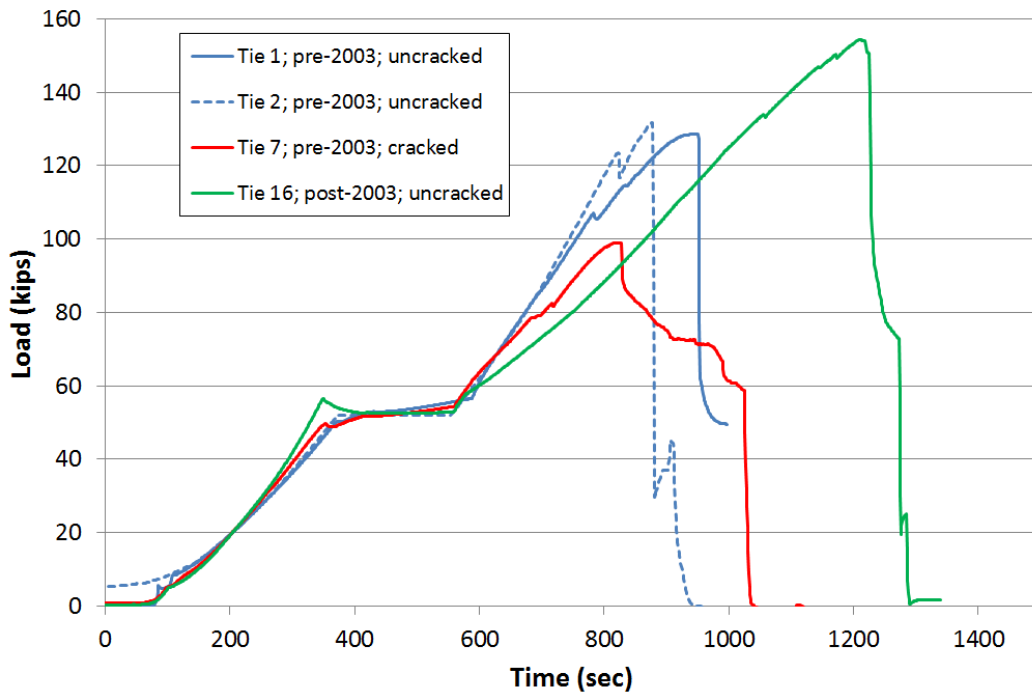


Figure 5.8. The load plots for flexural strength testing of some of the case study ties.

Table 5.4. Results from the positive rail seat moment test.

Tie	Maximum Load (kips)	Maximum Rail Seat Moment (in-kip)	Top Strain – G1 at 52 kips ($\mu\epsilon$)	Bottom Strain – G2 at 52 kips ($\mu\epsilon$)
1	128.7	753	-240	+317
2	130.2	765	-260	+257
7	98.8	580	Strain gage failed	+510
16	153.6	902	-210	+346

The general response of all ties was similar. Examination of the ties during the hold time at 52 kips did not reveal any cracking; the exception was Tie 7, which was already cracked but did not show additional cracking at 52 kips. With continued loading, the tie eventually developed a flexural crack, an example of which is shown in Figure 5.9. This flexural crack preceded attainment of the maximum load, presumably as the reinforcing strands picked up load. Eventually the maximum load was reached, after which there was a sudden drop in load; the exception was Tie 7, the tie with the pre-existing crack, which showed a gradual drop in load after the maximum load. Significant strand slip and a degree of vertical cracking occurred during the final stages of the test; Figure 5.10 shows an example. The exception was the post-2003 tie, Tie 16, which did not show strand slip, indicating a stronger bond capacity, at least in the tested condition, than the pre-2003 ties. We did not observe the initiation or further propagation of the horizontal cracks of the predominant type observed in the field.

The ultimate flexural strength of the nominally uncracked ties was about 760 in-kip, which exceeds the calculated strength value (from ACI 318) of 627 in-kip. (There is not a required ultimate strength value in the AREMA manual or tie specifications.) The ultimate flexural strength of the substantially cracked tie 7 was 580 in-kip.

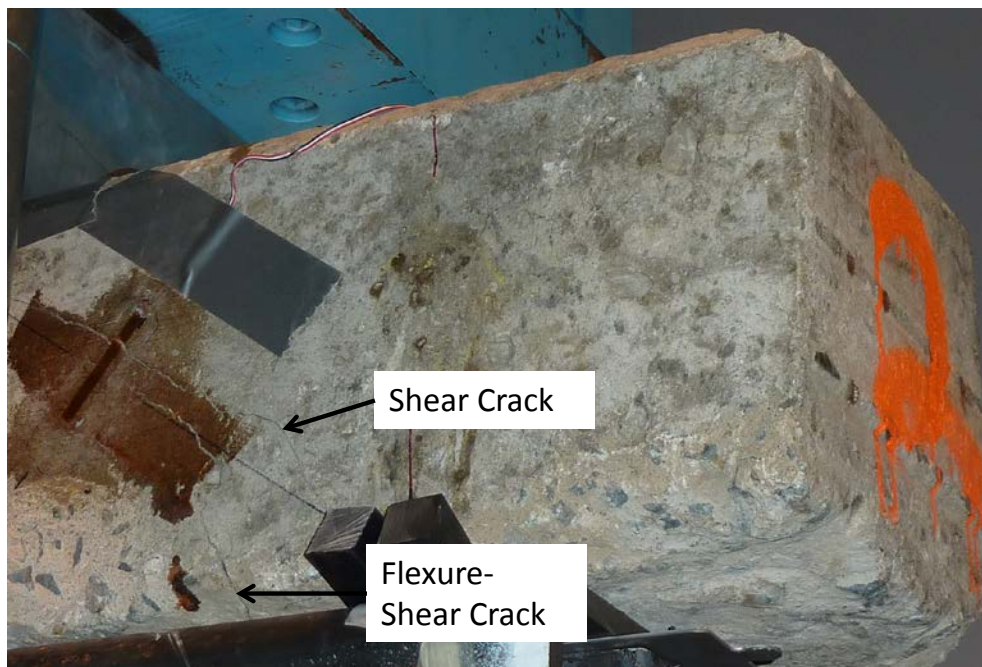


Figure 5.9. An example of the type of flexural crack that occurred in each of the ties from the positive rail seat moment test.

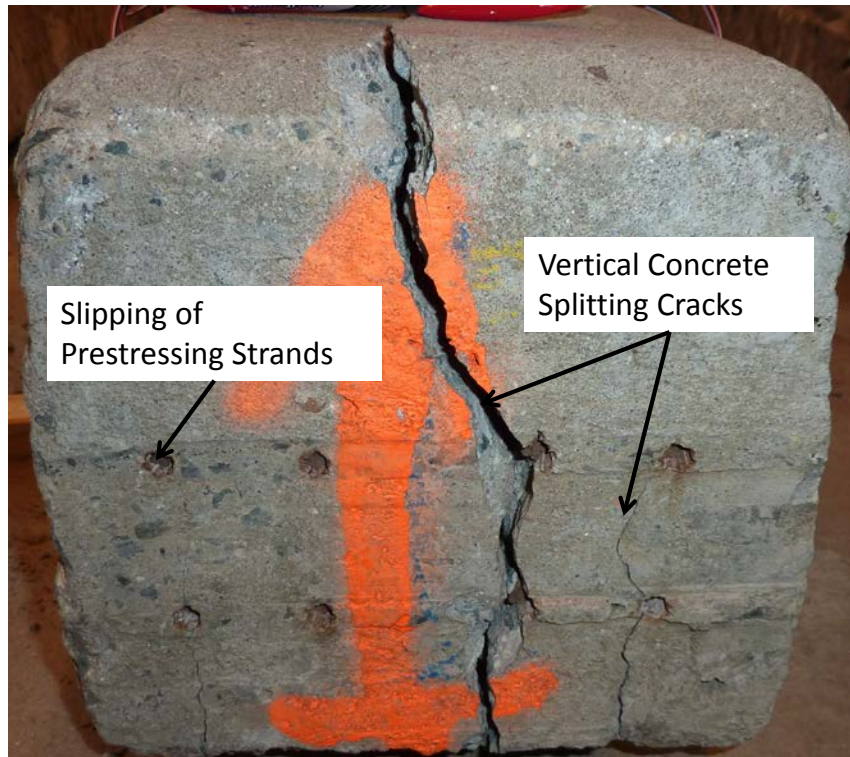


Figure 5.10. An example of the type of strand slip and vertical cracking that occurred in the final stages in each of the pre-2003 ties from the positive rail seat moment test.

All four ties met the Amtrak specification requirement that they show no (flexural) structural cracking when subjected to a positive rail seat moment test with an applied load of 52 kips. Most interesting is the observation that the horizontal cracking mode most prevalent among the ties of the NEC does not seem to prevent the tie from reaching the 52-kip load without flexural cracking.

The measured strains in the concrete tie compare favorably with those predicted by finite element analysis, as discussed in Section 7.4.1 of this report.

6. Loads

This section provides a description of the work we conducted in the project to assess the loads on the concrete ties. The primary task was a field test, in which we measured the loads at which concrete ties had cracked on a section of track on the NEC. We used this same test to also measure some other parameters, including concrete tie strains and accelerations. All measurements were made for two sets of tie pads, one softer than the other. The purpose of the field test was to investigate whether unusual wheel loads—vertical or lateral—or tie motions (e.g., vibrations) are associated with and possibly the cause of cracking. However, the results do not reveal anything that could explain the cracks. We also examined another source of information, wheel impact detector data, to determine the magnitude and form that loads could take on the system.

We note that the nominal wheel loads for the types of vehicles that run on the NEC are as shown in Table 6.1. We note that the AREMA Manual, with which the Amtrak tie specifications are consistent (see Section 7.1), uses a design wheel load of 100 kips, inclusive of dynamic effects.

Table 6.1. Rail vehicles that passed the test site during field test measurements.

Vehicle Type	Nominal Wheel Load (kips)
Acela power car	25
Acela coach car	15.8
Amfleet coach	13.8
AEM-7 locomotive	25.9
Freight locomotive	35
Freight car	26

6.1 Field Test

6.1.1 Overview

The objective of the field test was to measure loads, strains, and accelerations in the ties for a section of concrete tie track on Amtrak’s NEC. An additional objective was to determine the effect of using a different rail pad on the measured parameters.

We conducted the test on a location of track selected with Amtrak that included high speed, tangent operation. The test site was located on the NEC at MP 168.7 on Track 2 between the Davisville and Malcom interlockings, geographically located near Kingston, RI. The site

contains concrete ties manufactured around 1994. We instrumented three ties and the rails between them to measure the following parameters:

- Vertical wheel-rail load
- Lateral wheel-rail load
- Vertical load on the tie
- Tie strains
- Tie accelerations

Using a proven method in which the load is derived from calibrated strain gage bridges installed on the web and base of the rail, we measured the vertical and lateral wheel-rail loads and the loads on the ties [6.1]. We bonded strain gages to the side of the ties to measure strains under load. Finally, we attached accelerometers to one of the ties to determine the primary modes of tie vibration under the action of the moving train wheel loads.

Figure 6.1 shows the overall layout of the instrumentation, and Figure 6.2 shows a photograph of the installation. We collected data for several weeks that included operation of different types of trains, including conventional electric trains, the Acela high-speed electric train, diesel trains, and freight trains. We collected data for two track conditions: with existing components and after replacing the tie pads with softer units on the instrumented and adjacent ties. Data were collected with an unattended data collection system.

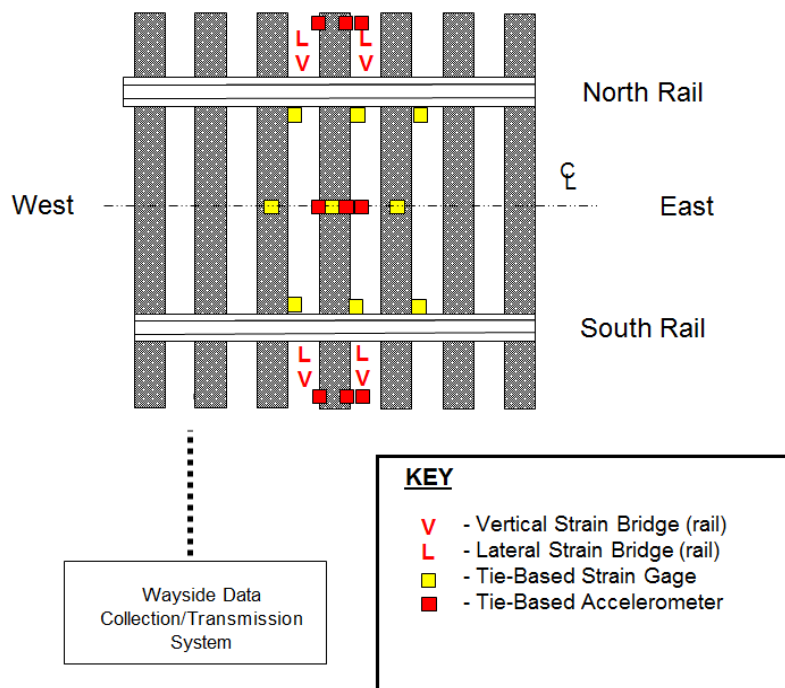


Figure 6.1. Layout of the field test instrumentation.



Figure 6.2. View of the test site from an overpass (Track 1 is at the bottom).

6.1.2 Track Condition

The section of track we instrumented had the following components:

Concrete ties: date code 1994, indicating they were manufactured to the Amtrak 1992 specification

Rail: 132 RE

Tie pads: Elvax 460/660 (measured hardness 89 Shore A)

Clips: Pandrol e-clips

Insulators: not determined

All of the ties in the test section had some degree of cracking. The cracks were always located on one side or both at the ends of the tie and with the same form as we have seen throughout the program. We selected three consecutive ties with the smallest cracks we could find. The condition of these ties and several in the vicinity were described in Section 3.2.1.

As stated, we conducted the first set of data collection using the tie pads that were in place when we arrived at the site. We changed the tie pads on several of the ties in the vicinity of the instrumented ties after approximately 1 week of data collection. We installed new, softer pads on the three instrumented ties and on one tie on each side of these three ties. We also replaced the pads on four ties beyond these five with new pads of the same material as the original pads.

The new pads had the characteristics shown in Table 6.2 together with estimated modulus. We resumed collecting data for approximately 11 days after the tie pads were changed.

Table 6.2. Tie pad properties.

Pad Material	Measured Hardness (Shore A)	Estimated Modulus (ksi)
Elvax 460/660 (existing pads)	89	6.3
Santoprene 101-80	85	4.0

6.1.3 Instrumentation and Data Acquisition

Figure 6.3 shows the vertical and lateral wheel-rail load strain gages after they were welded to the rail and before the weatherproofing was applied. The two strain gages on the web of the rail are for the vertical wheel-rail load, and the two strain gages on the base are for the lateral wheel-rail load. We applied this configuration at four locations: the two cribs between the three ties on each side of the track. An identical configuration of strain gages for the tie vertical load was applied over each of the three ties on each side of the track.



Figure 6.3. Vertical and lateral wheel-rail load strain gages.

We mounted three linear-axis strain gages on each of three ties; all gages were oriented along the axis of the tie. One strain gage was mounted in the center of the tie on the top surface. The other two strain gages were mounted underneath each rail on one side of the tie. Figure 6.4 shows a sketch of the locations. The strain gage at the top center was mounted slightly to the edge of the tie, but centered between the rails because of the stamp (indentation) on the top center of the tie.

We used a concrete epoxy filler to ensure a smooth surface for bonding of the strain gages. Figure 6.5 shows one of concrete strain gages bonded to the center of the tie.

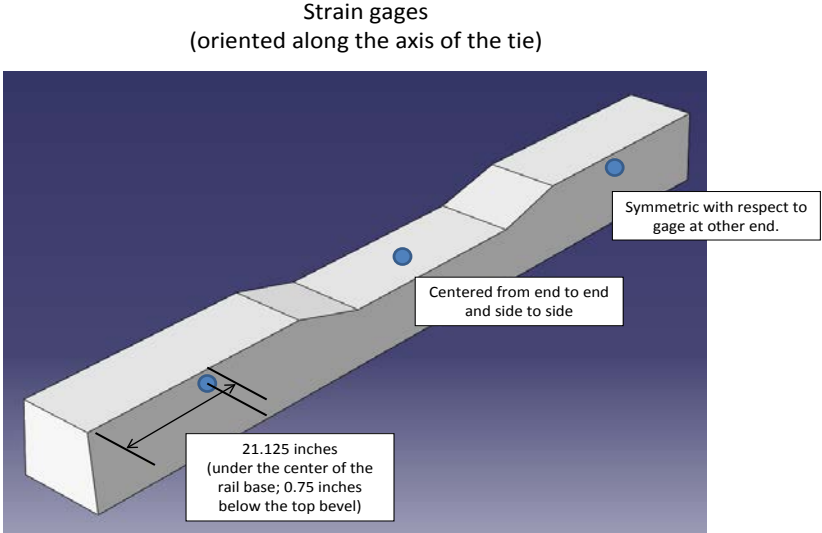


Figure 6.4. Field test strain gage locations on the concrete ties (sketch)



Figure 6.5. Concrete strain gage mounted to the center of a tie

We mounted nine single-axis accelerometers to the center tie only. Acceleration was measured perpendicular to the mounting surface. Figure 6.6 shows a sketch of the locations. We used a concrete epoxy to bond the mounting blocks to the concrete. Figure 6.7 shows three accelerometers mounted to one end of the tie.

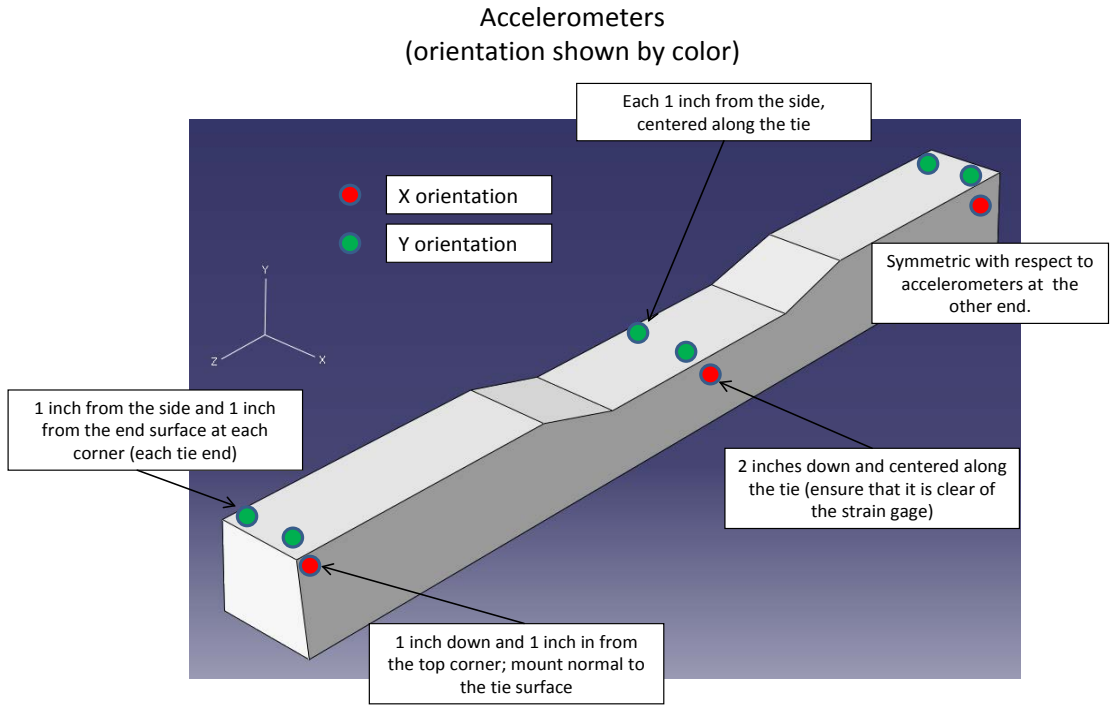


Figure 6.6. Field test accelerometer locations on the center tie (sketch).



Figure 6.7. Three accelerometers mounted to one end of the tie.

Data was gathered from strain gage triggers we installed on one rail approximately 200 feet in both directions from the three instrumented ties. These triggers were half of the normal vertical strain gage bridges and were used to start and stop the data collection for the autonomous system. Data were collected at a rate of 5 kHz whenever a train passed the wayside site on Track 2. Signal conditioning filters were applied to all data channels. Strain gages were filtered at 1 kHz (a low pass filter), string pots were filtered at 2 kHz, and accelerations were filtered at 2.5 kHz.

An Automated Equipment Identification (AEI) tag reader was used to identify the specific vehicles that passed the test site as the autonomous data were collected. Constraints at the installation site resulted in having to place the tag reader at a distance from the track greater than the ideal in order to reliably read all vehicle tags; it was, fortunately, able to read many of them.

The wayside signal conditioning and data acquisition equipment were mounted on three poles which were installed into concrete in the ground. The system is run from a battery pack inside the enclosure. Solar panels were used to charge the batteries during the day. Additional power required for powered filters was provided by a nearby signaling shed.

The collected data were saved to a binary data file with the AEI tag data in a separate text file. Post-processing was used to convert the binary data file to a text data file. Due to the data file size, physical access to the computer enclosure was needed in order to retrieve all of the data. This was performed twice: when the tie pads were changed out and when the equipment was removed at the end of the testing.

6.1.4 Results

Vertical Wheel Loads

An example of the vertical wheel-rail forces for the passing of an Acela train is shown in Figure 6.8. We note that the peak load in this trace is consistent with the expected wheel load of a power car, which is 25 kips (Table 6.1).

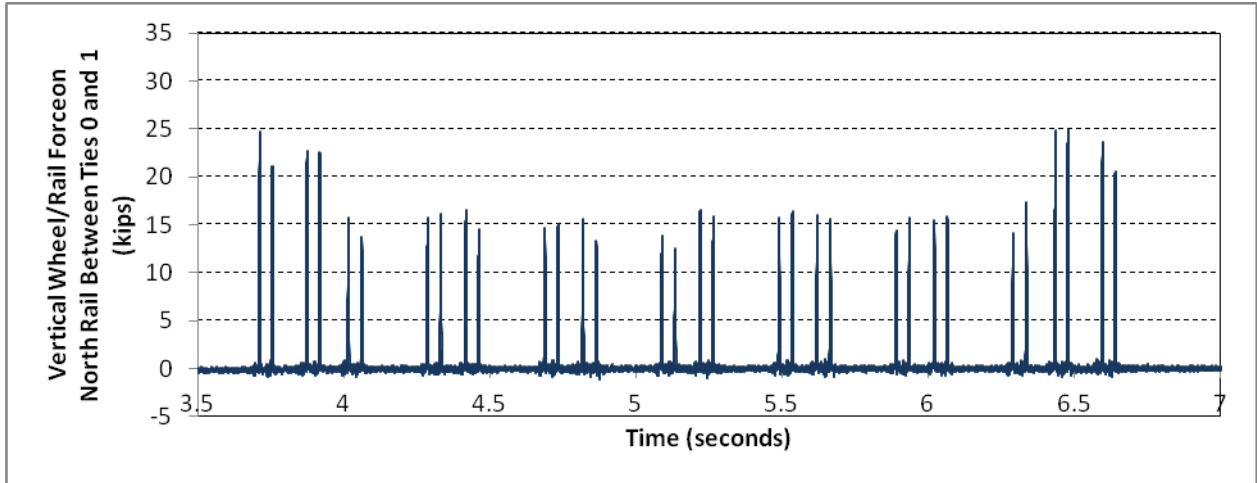


Figure 6.8. Vertical wheel-rail force on north rail between Ties 0 and 1 for an Acela train.

An example of the measured vertical load over a tie is shown in Figure 6.9. Recall that this is a load that essentially corresponds to the load carried by the rail over the tie. We used the following procedure to calculate the load into a tie: the load in tie i = measured load at tie i minus the average of the measured loads in the two cribs on each side of the center tie (after accounting for offsets in time). Figure 6.10 shows an example of the results of this calculation for the passing of two wheels, and Figure 6.11 shows an example for the passing of an entire Acela train.

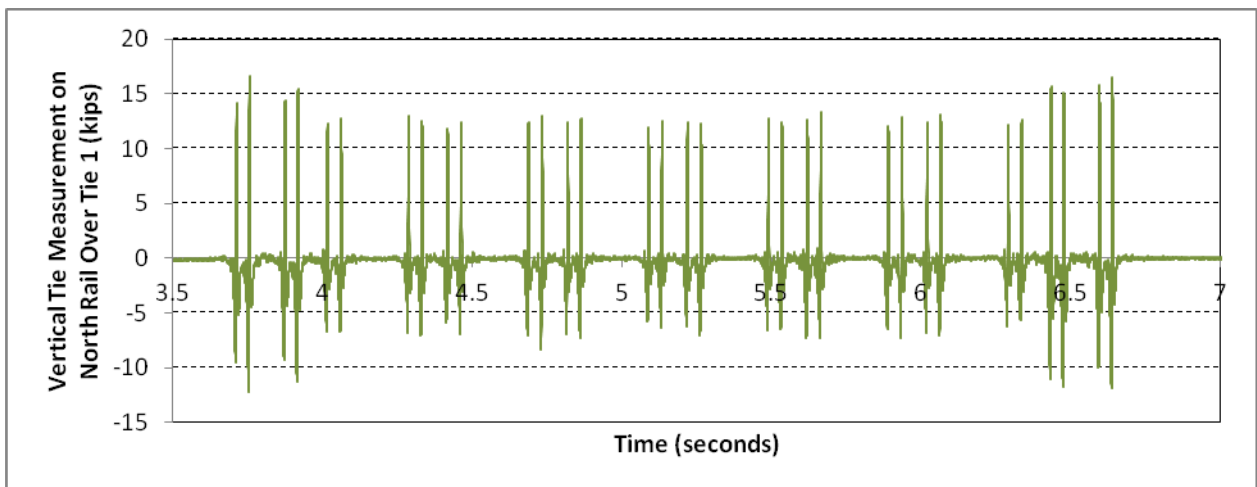


Figure 6.9. Vertical tie measurements on the north rail over Tie 1 for an Acela train.

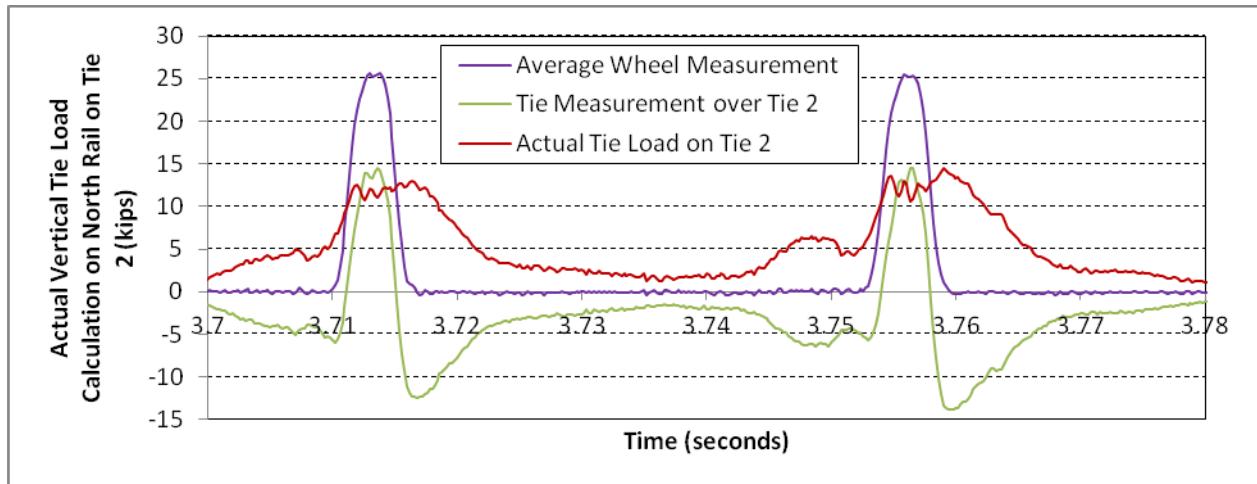


Figure 6.10. Calculation of the actual tie load for Tie 2.

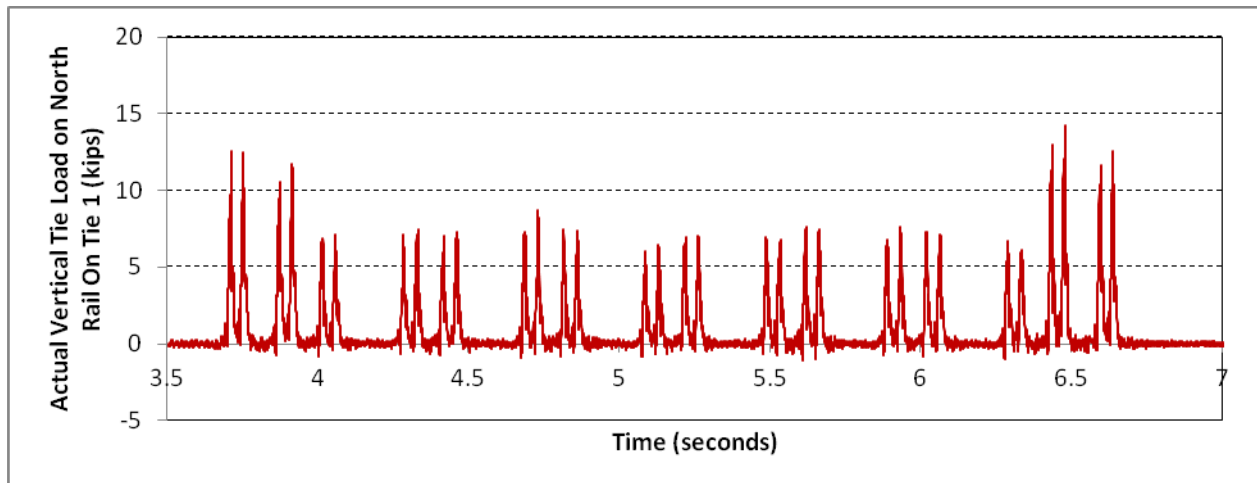


Figure 6.11. Actual vertical tie load for Tie 1 under the north rail.

We compiled the vertical wheel-rail load results for the data corresponding to both the original and new tie pads. These data included 162 recorded train passes and a total tonnage of 91,740 T for the original tie pads. Figure 6.12 shows the distributions of peak loads for every passing wheel as measured by each crib. The peaks in the distribution correspond generally to the dynamic wheel-rail loads from the Amtrak conventional passenger car at around 15 to 17 kips, the Acela coach car at around 18 to 21 kips, and the Acela, AEM-7, and HHP locomotives at around 27 to 30 kips. Of the 162 recorded train passes with the original pads installed, 77 were Acela trainsets (48%).

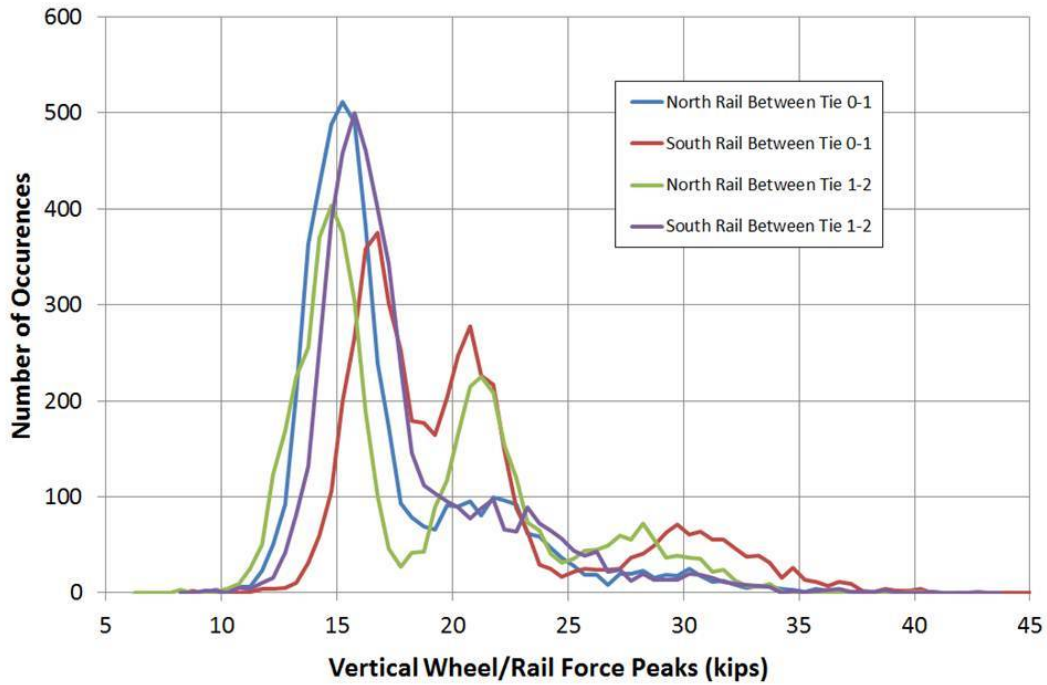


Figure 6.12. Vertical wheel-rail force histogram with original tie pads.

The distribution of vertical wheel-rail loads for the new pad installation included 190 recorded train passes and an approximate total tonnage of 115,470 T. Figure 6.13 shows a comparison of the data for the two pad types in terms of the percentage distribution of vertical wheel-rail loads for every passing wheel over every crib. Of the 190 recorded train passes with the new pads installed, 83 were Acela trainsets (44%).

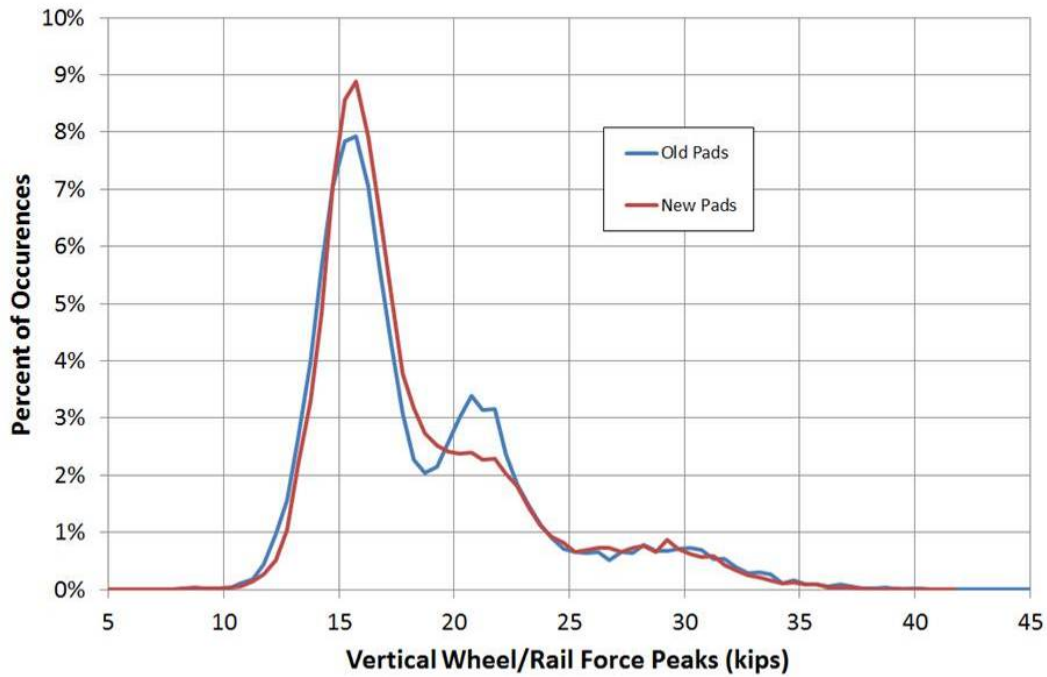


Figure 6.13. Vertical wheel-rail load histogram comparing old and new tie pads.

We made a similar examination of the vertical loads experienced by each of the three test ties and a summary of these results is shown in Figure 6.14. In general, the distribution of the actual vertical loads imparted to each tie is centered approximately at a value equal to 35 percent of the vertical wheel-rail load. We note that the tie load distribution shifted to a lower value by about 0.8 to 1 kips after the new tie pads were installed.

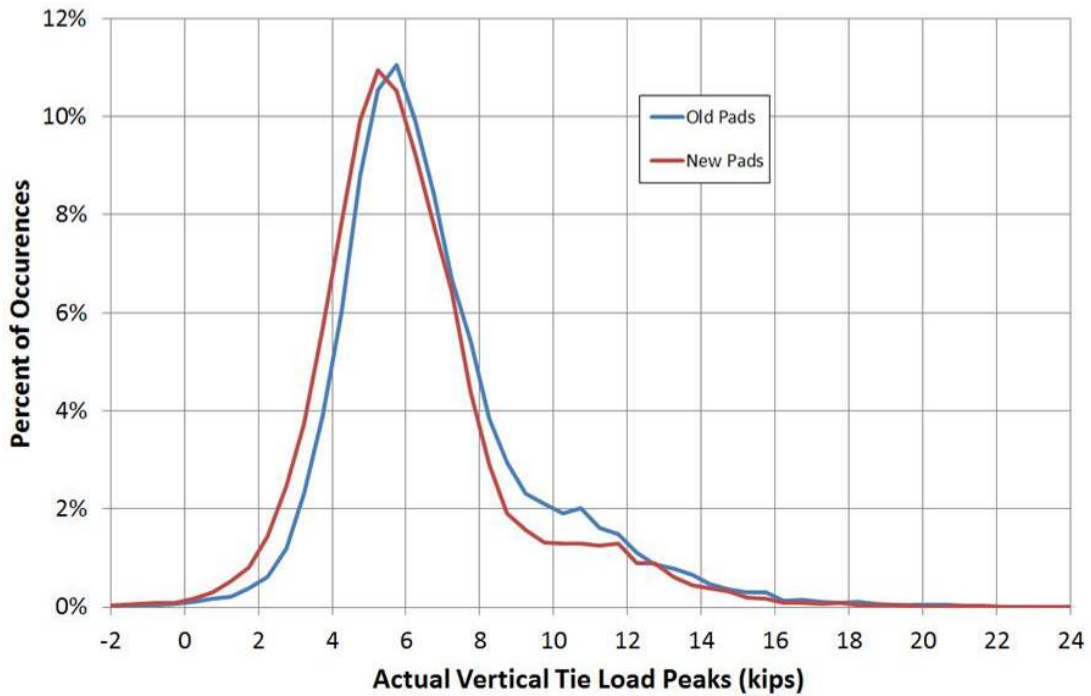


Figure 6.14. Actual vertical tie load histogram comparing old and new tie pads.

Lateral Wheel Loads

Figure 6.15 shows an example of the measured lateral wheel-rail forces at one location for an Acela trainset; a positive load represents a load toward the field side. As expected, the lateral forces are relatively small since the test site is located in a tangent section of track. Figure 6.16 shows the distribution of lateral peak loads with the original tie pads, and Figure 6.17 shows the percentage distribution of the lateral wheel-rail loads for two tie pad installations.

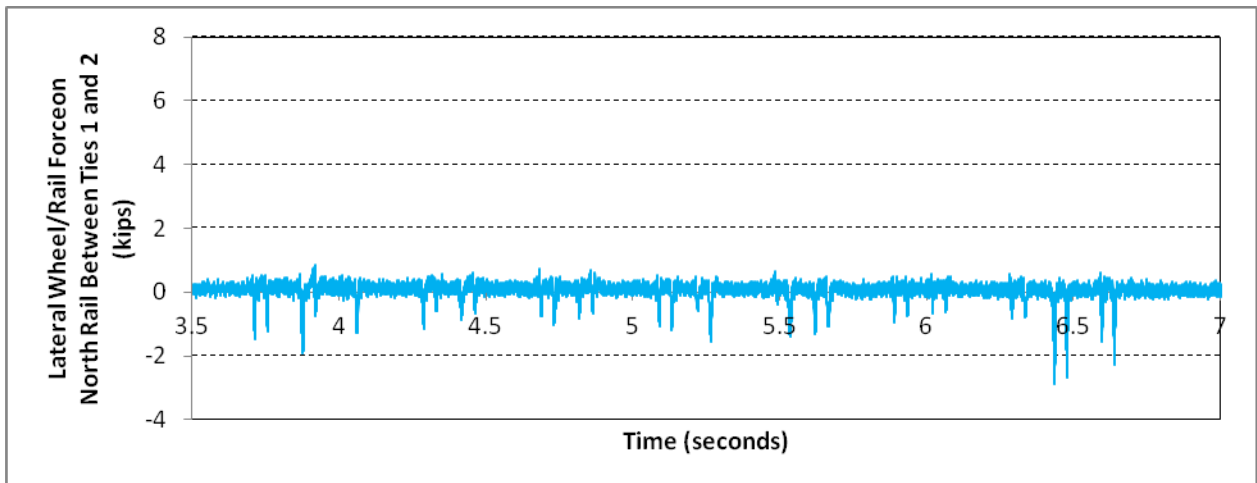


Figure 6.15 Lateral wheel-rail force on the north rail between Ties 1 and 2.

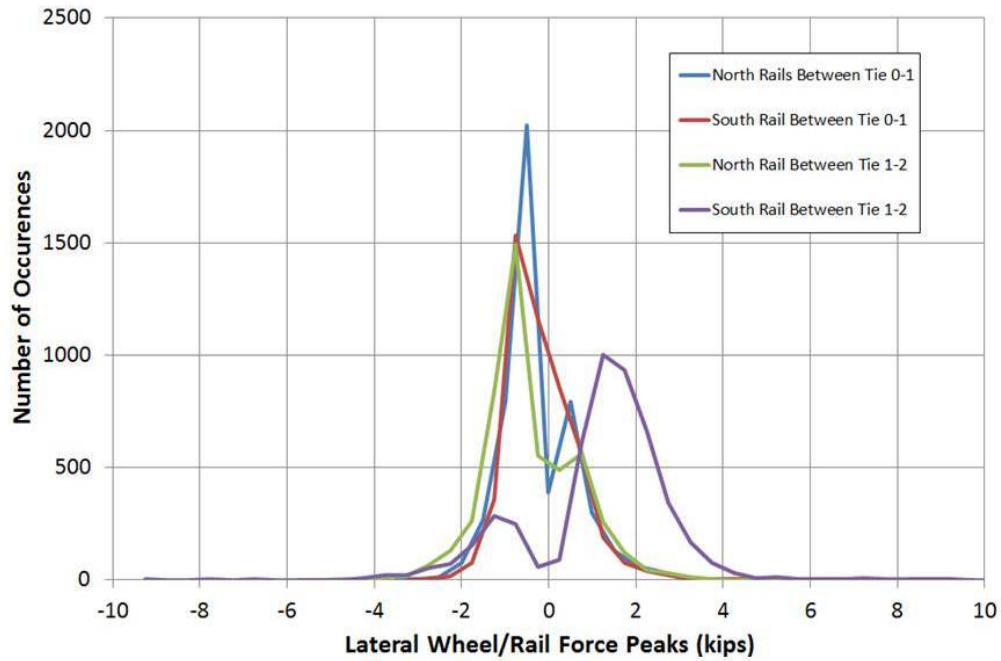


Figure 6.16. Lateral wheel-rail force histogram with old tie pads.

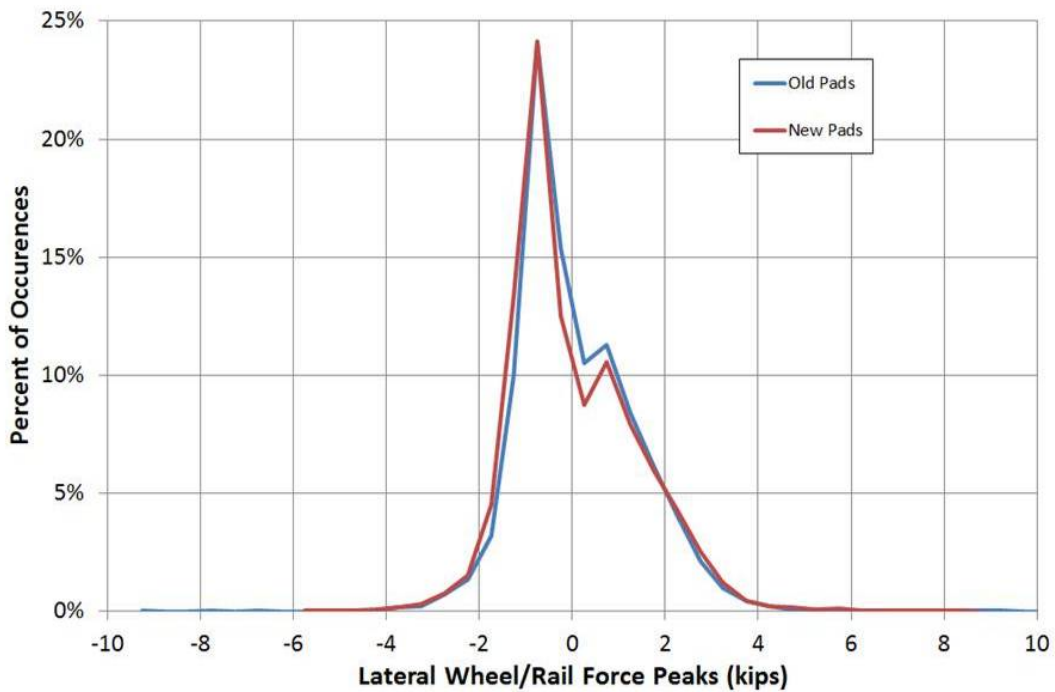


Figure 6.17. Lateral wheel-rail force histogram comparing original and new tie pads.

Concrete Tie Strains

The measured concrete strains were relatively low, as expected. Figure 6.18 shows an example for the center gage of one of the ties during the passage of an Acela trainset. The overall strain data show greater scatter than the load data and it is difficult to select true maxima. (Note: We do not know the reason for the negative peaks in Figure 6.18, but we suspect it is a noise issue.)

Table 6.3 lists typical values of strain for the strain gages corresponding to the heavier Acela power car wheel loads. The strains are small and, therefore, have a degree of uncertainty. Nevertheless, we can use them to check the consistency of some of the other measurements. The stresses corresponding to these strains are also listed in Table 6.3 using a value for the modulus of 4.7×10^6 psi (the value measured in some of our mechanical tests (Section 5)). The stress values can also be used with the section properties and locations of the gages to calculate the bending moment at the gage locations; these values are shown in Table 6.3. These inferred moments are much lower than the values to which the ties were designed: the design moments are 337 in-kip for the rail seat and 208 in-kip for the center of the tie. The inferred moments are consistent with the difference in measured and design tie loads: 5–10 kips versus 50 kips.

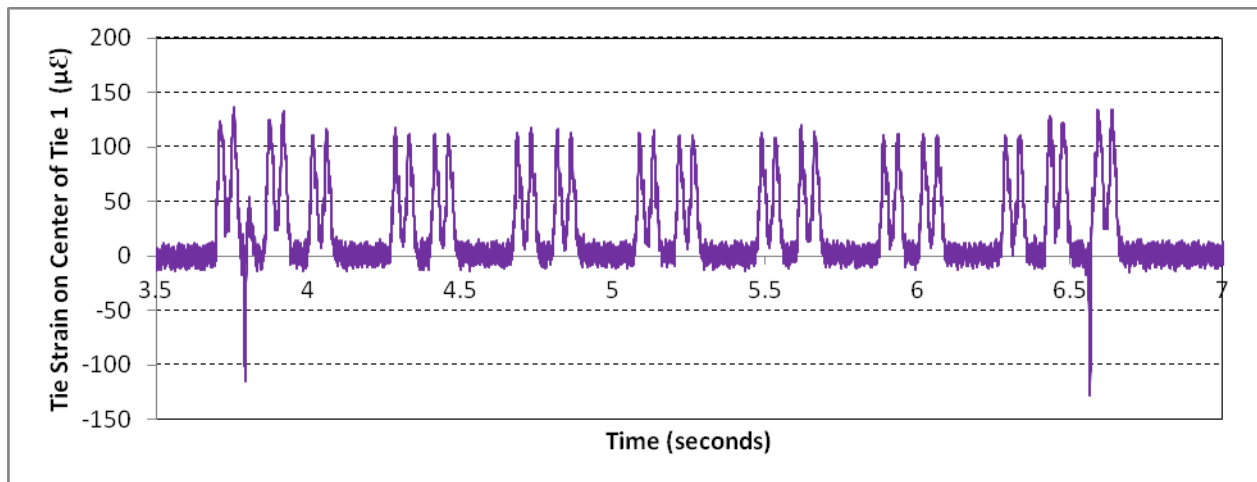


Figure 6.18. Tie strain on the top center of Tie 1.

Table 6.3. Typical concrete tie strains and inferred stresses and moments.

Location	Measured Strain ($\mu\epsilon$)	Calculated Stress* (psi)	Calculated Moment (inch-kip)
Under rail seat	-30	-141	24.3
Top of tie at center	+100	+470	38.7

*Using a modulus of 4.7×10^6 psi.

Tie Accelerations

Examples of the measured accelerations for a vertical sensor and a longitudinal (with respect to the track) sensor are shown in Figures 6.19 and 6.20. Figure 6.21 shows the accelerations from a vertical sensor overlaid with measured vertical wheel loads, indicating that peaks occur together. We analyzed the acceleration-time histories for the passage of a set of wheels to extract natural frequencies and mode shapes. The results for the primary modes about the longitudinal axis with respect to the track are provided in Table 6.4; we only include those modes for which the mode shapes were clear from the results. We note that the first four modes have a rigid body character and are associated with the frequency of wheel passage; for example, at 125 to 150 mph, the frequency of wheel passage for the end trucks of two coupled cars is approximately 20 Hz. We note that the first mode of true deformation, mode 7, is the mode corresponding to bending about an axis along the track. As shown in the stress analysis section (Section 7), this is the first mode determined using finite element analysis for which the natural frequency is about 100 Hz, close to the measured 110 Hz value. We acknowledge that the use of nine accelerometers limits the number of modes that can be detected. Nevertheless, these results do not suggest any unusual vibration in the ties for this location and the loading to which they were subjected during the test.

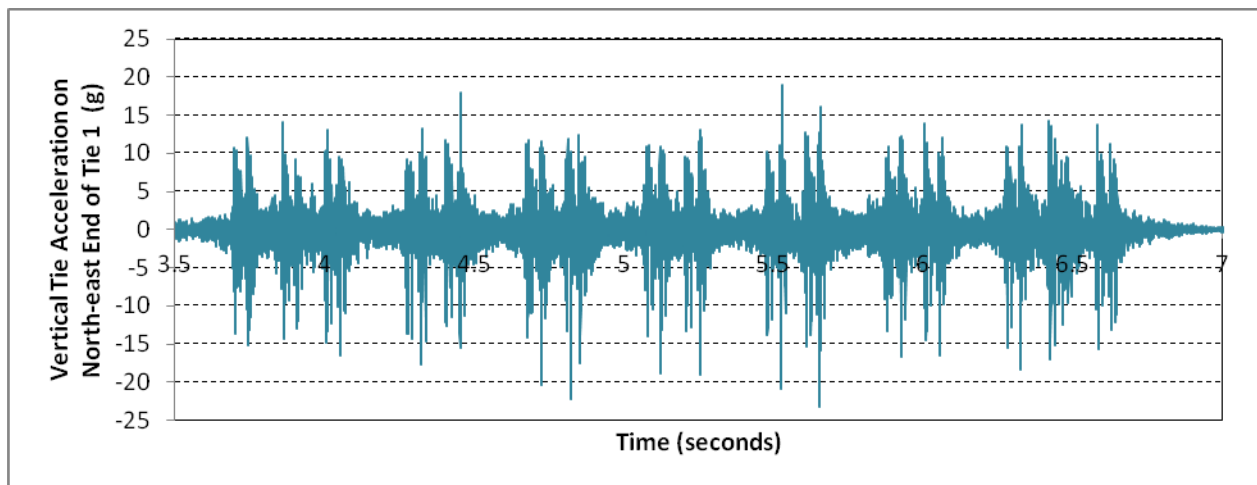


Figure 6.19. Vertical acceleration on the northeast end of Tie 1.

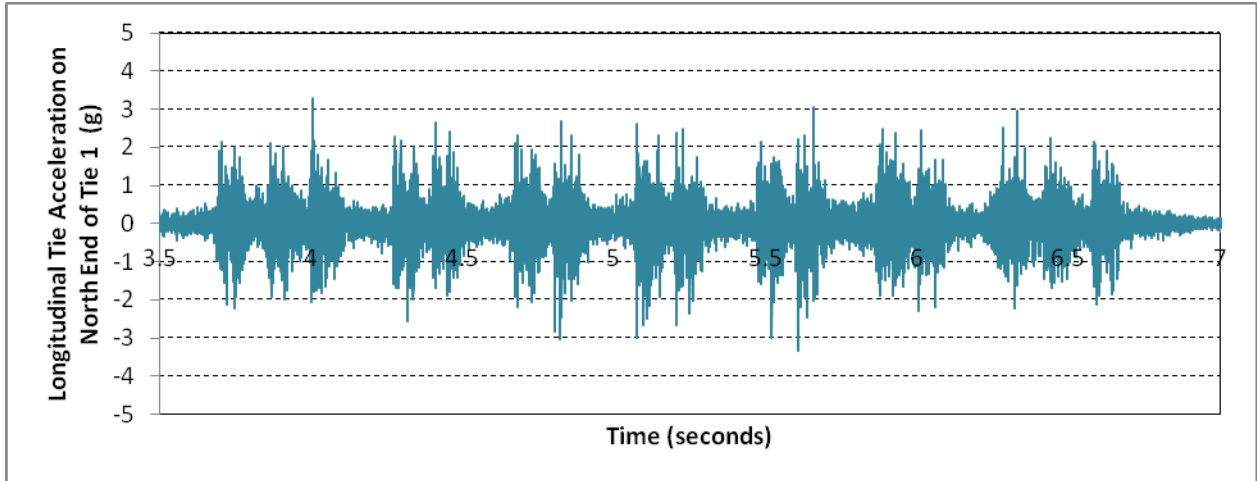


Figure 6.20. Longitudinal acceleration on the north end of Tie 1.

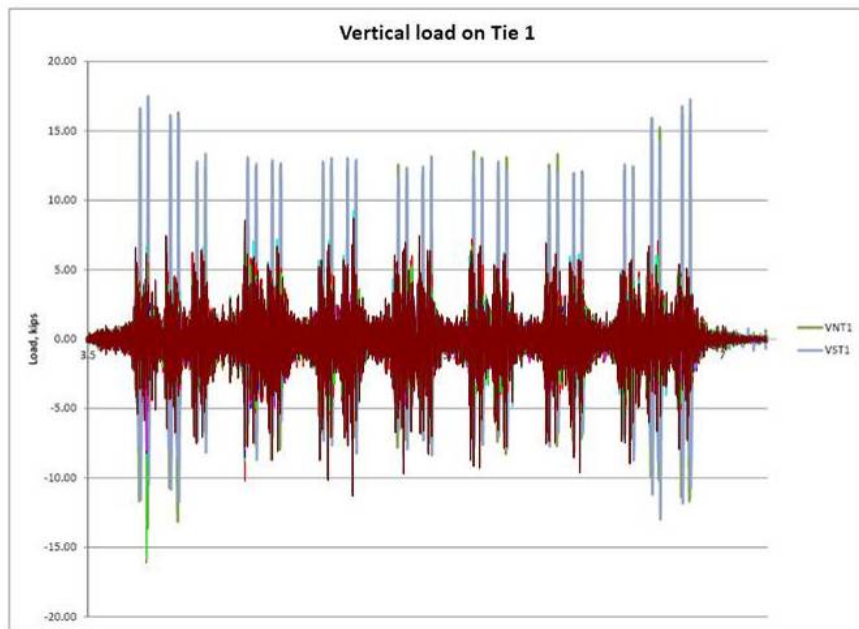


Figure 6.21. An overlay of vertical accelerations and wheel loads on the north end of Tie 1.

Table 6.4. The natural frequencies and corresponding mode shapes determined from the field test data.

Mode Number	Frequency (Hz)	Mode Shape
1	16.5	Vertical displacement (a rigid body mode)
2	38.2	Rocking about a longitudinal axis with respect to the track (a rigid body mode)
3	45.2	Vertical displacement (a rigid body mode)
4	66.3	Rocking about a longitudinal axis with respect to the track (a rigid body mode)
7	110	Bending about a longitudinal axis with respect to the track
8	126	A combination of bending about a longitudinal axis with respect to the track and vertical displacement

6.1.5 Discussion of Field Test Results

We conducted the field test to obtain information about the load environment and response of concrete ties that have cracked on the NEC. If loading is an important factor determining (poor) performance, then our measurements in this test should be relevant.

We did not observe any extreme vertical loads. Rather, the peak wheel load was only about 40 kips and this likely corresponds to a locomotive. The peak load on an individual tie (one side) was about 20 kips. This is substantially less than the load for which the tie is designed: about 50 kips. This implies that the design basis used by AREMA is conservative for the NEC section we evaluated. We also did not measure any unusual lateral loads. It is, of course, possible that loads from wheel flats occur only occasionally, and we did not detect any during our approximately 4 weeks of testing.

We also did not measure unusual tie vibration modes. We discuss in Section 7.4.3 the stresses induced by the modes we did detect in the field test and these do not appear to induce substantial stresses that could explain the common mode of cracking.

6.2 Other Load Data

Amtrak has conducted measurements for some time on the peak loads experienced by their track on the NEC. Figure 6.22 shows an example from Staplin [6.2]. We note that the loads that occur with the highest frequency are similar to those we measured. However, the highest loads for the trains relevant to the section we examined, the Acela and Amfleet trains, are higher (though not as frequent) than what we measured in our study. For example, the highest load corresponding to the Amfleet equipment is more than 70 kips, and this is likely due to a wheel

anomaly which would give rise to an impact load. Thus, we cannot rule out that each of the ties has experienced a wheel defect impact in its life.

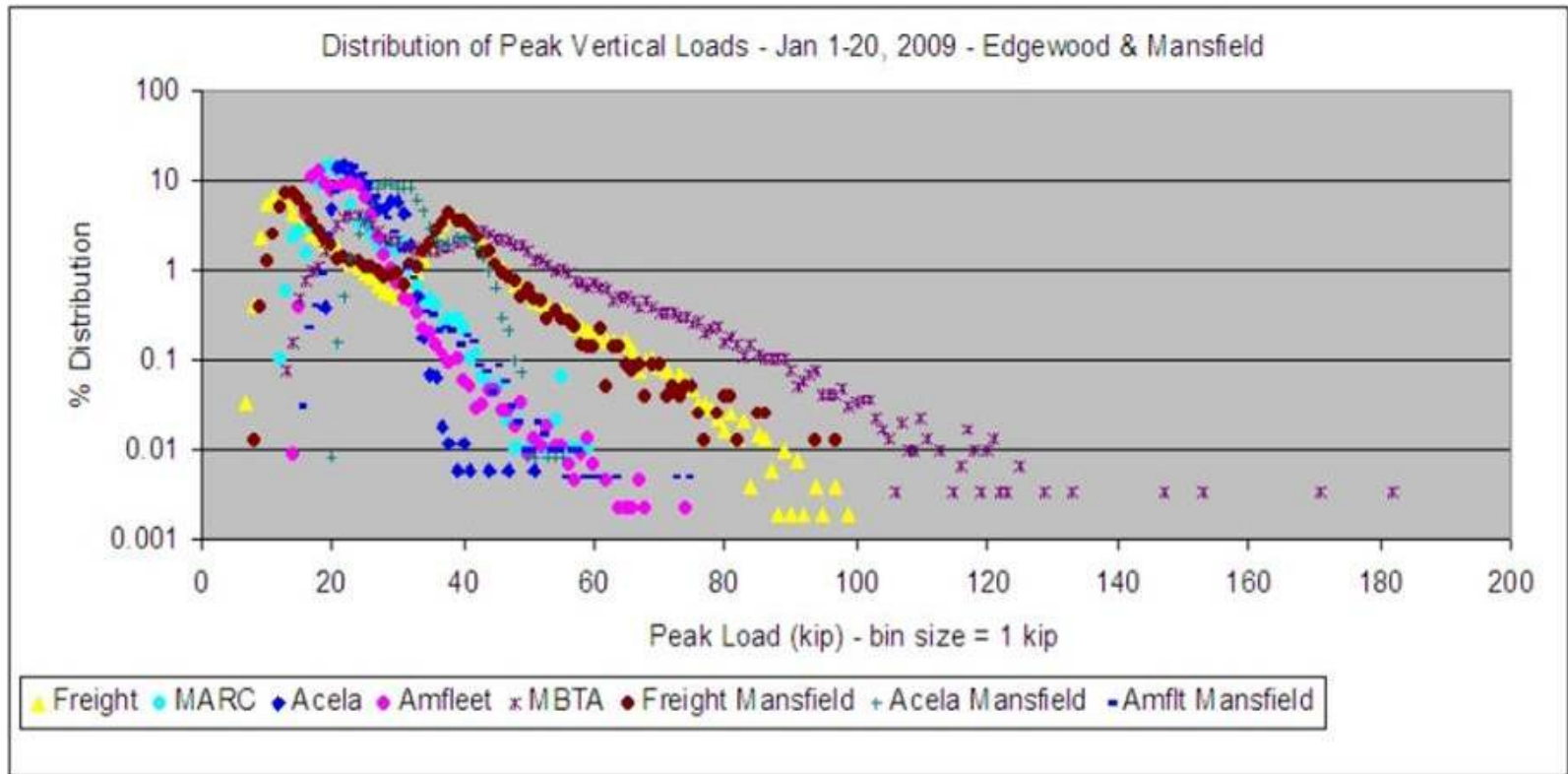


Figure 6.22. Peak loads measured by Amtrak on the NEC (from Staplin [6.2]).

7. Stresses in Concrete Ties

This section provides the results of various analyses we conducted to determine the stresses in the case study concrete ties and to better understand the conditions under which the observed horizontal cracks may have initiated. We are particularly interested in the parameters that can cause significant tensile stresses perpendicular to a horizontal plane because these are the types of stresses that can cause the type of cracking most commonly observed in the failed concrete ties. We first review the design basis for the ties and then consider stresses from several sources, particularly for the pre-2003 tie design. Our analysis focuses on the factors that could contribute to the observed horizontal cracking. We also examine the stress state in the post-2003 ties to determine whether the driving force for cracking is different than in the pre-2003 ties.

7.1 Concrete Tie Design

The concrete tie has the function of supporting the rails under a variety of loadings. The tie is essentially designed against flexural loading; loads are applied to it at the rail seats, and it is supported at its base by the track ballast. The region under most tension is generally on the bottom surface under the rail seat. However, depending on the support conditions provided by the ballast and the location and stress level in prestressing strands, the surface of greatest tension can also be on the top surface in the center of the tie, or even the bottom surface of the center of the tie. (See also [7.1].) Our evaluation of the Amtrak ties, which includes analysis and strength testing, indicates that the ties are properly designed against flexural failure.

Table 7.1 lists the required flexural strengths from the specifications for the case study concrete ties. The failure criterion for these loads, with the exception of the repeated load test, is that no structural cracking shall occur (i.e., it is not an ultimate strength criterion). The requirements are identical for the pre-2003 and San-Vel ties (as well as the MBTA tie). The requirements for rail seat positive moment and tie center negative moment are the same for the pre- and post-2003 ties. On the other hand, the post-2003 tie specification requires substantially greater negative rail seat and center positive flexural strengths, which is achieved, we believe, by higher prestressing forces.

Table 7.1. The flexural strength (to initial cracking) requirements for the Amtrak ties from the various specifications.

Parameter	Moment (in-kips)		
	Pre-2003	Post-2003	San-Vel
Rail seat positive moment	306	306	306
Rail seat negative moment	118	162	118
Tie center negative moment	208	208	208
Tie center positive moment	111	144	111
Rail seat repeated load	235 (positive moment) to -88 (negative moment)	336 to 24*	235 to -88

* The post-2003 repeated load requirement is a test carried out after a crack is created in the rail seat positive moment test. Note that the moment is always positive in this test.

The AREMA manual [7.2], which is used for design purposes, provides a design vertical wheel load of 100 kips on track with concrete ties. (It also provides lateral and longitudinal design loads.) Only a portion of the wheel load is carried by an individual tie, and that percentage is given in the AREMA manual as 0.50 for a 24 in tie-to-tie spacing, the predominant value of the NEC. This results in a design tie load of 50 kips (0.5x100). Our own load measurements on a section of the NEC, Section 6, provided a maximum wheel load of slightly more than 40 kips and a maximum tie load of a little more than 20 kips.

The AREMA manual also states (Section 4.4.1.2 of the manual) that the following factored moment should be used for the rail seat positive moment:

$$M = BVT$$

where:

B = 300 in-kips (8 ft 6 in long ties; 24 in spacing) (from Figure 30-4-3 of the AREMA manual)

V = 1.2 (speeds of 120 mph and above, from Figure 30-4-4 of the manual)

T = 0.94 (for 50 MGT, from an Amtrak design document, and also from Figure 30-4-4 of the manual.)

This equation provides a value of $M = 338$ in-kips, which is close to but 10 percent higher than the value required in the Amtrak specification (Table 7.1). The AREMA manual also requires the following:

- The maximum pre-compression, from pre-stress alone, should be less than 2,500 psi;

- The minimum pre-compression under the rail seat should be 500 psi.

The concrete ties of the case studies are designed as prestressed concrete members to resist the moments just listed and, as we will show, they appear to be designed with substantial margin of safety against flexural cracking for the NEC. We described the characteristics of the ties in Section 3.1. The pre-2003, San-Vel, and MBTA ties utilize eight seven-wire strands and a total preload of about 135 kips to achieve the desired prestress. The post-2003 ties use 24 single-wire strands and a total preload of about 155 kips for this purpose. The prestress, when combined with flexural stress from wheel loads, prevents the concrete from experiencing significant tension and cracking. The concrete stresses resulting from transfer of the prestress force to the ties, calculated according to the PCI Design Handbook [7.3], and using values from the tie drawings are listed in Table 7.2. We have assumed in these calculations that initial prestressing losses due to elastic shortening and strand end slippage are 15, 7, and 15 percent for the pre-2003 tie, the post-2003 tie, and the San-Vel tie, respectively. (End slip from our finite element analysis of these ties is less for the post-2003 ties.) The table shows that the post-2003 tie is designed to have higher initial compressive stresses than the other ties.

Table 7.2. The stresses due to prestress transfer in ties calculated using PCI methods [7.2].

Location	Outer fiber stress* (psi)		
	Pre-2003	Post-2003	San-Vel
Bottom, below the rails seat	-1730	-2320	-1770
Top, at rail seat	-772	-797	-648
Bottom, tie center	-815	-1310	-973
Top, tie center	-2570	-2900**	-2300

* Negative stresses are compressive;

** If a 15% prestress loss is used, this value is -2500 psi.

We can estimate the loads (moments) required to cause cracking and ultimate failure using American Concrete Institute (ACI) calculation methods [5.3]. Table 7.3 shows the results. Measured values of ultimate moment (Section 5) exceed the calculated values. The results in Table 7.3 show that the ties are designed against the required moments with significant margin, especially in the case of the post-2003 tie. The margin of safety against actual moments measured in track (Section 6) is substantial.

Table 7.3. The initial flexural cracking and ultimate moments for the case study ties calculated using PCI methods [5.3].

Parameter	Pre-2003	Post-2003	San-Vel
Calculated initial cracking moment	359	449	356
Design moment (no cracking)	306	306	306
Calculated ultimate moment	627	725	656
Measured ultimate moment	759	902	NA

We note that the Amtrak specifications do not require the use of vertical stirrups anywhere in the tie. The San-Vel tie drawings did include stirrups just outboard of the rail seat, but it does not appear these were required. (In fact, we did not find stirrups in the San-Vel ties we sectioned.) Modern design guidelines (e.g., AASHTO [7.4]) require the use of transverse reinforcement at the ends of prestressed concrete members to protect against bursting (splitting) cracks. This point is discussed further below.

7.2 Finite Element Analysis of Prestressing Loads

The first step in the analysis of the ties is to determine the state of stress induced by the prestressing wires/strands. This is the state to which stresses from other sources, such as flexural loading, loads from inserts, and impact loads, are added. The state of stress from prestressing is also very important because, as mentioned in the previous section, prestressed concrete structures are at risk of horizontal cracking (splitting) from the prestresses that develop at the ends of post-tensioned or pre-tensioned members at prestress transfer. There is substantial literature on this subject (e.g., [7.5-7.7]) and, as described earlier, recommendations are provided in industry standards (e.g., AASHTO [7.4] and the PCI Design Handbook [7.3]) to prevent such horizontal cracking. The terms “bursting” and “splitting” are frequently used interchangeably; however, in this section bursting stresses will refer to the vertical stresses that develop at the surface of prestressed member ends, and splitting stresses will refer to the vertical stresses that develop adjacent to the surface of the prestressing strands.

7.2.1 General Analysis Approach

We developed a finite element model to determine the state of stress in the ties with particular attention to the region observed to crack in the pre-2003 tie designs. The model was set up for a variety of loads, including prestressing, which is described in this section of the report. We used the computer program Abaqus Standard for this purpose. Some of the conditions of the model are as follows:

- One-quarter of the tie is modeled because of symmetry. The exception to this is for some dynamic simulations, for which asymmetric modes of deformation must be captured.

- The strands are modeled as cylindrical with a constant cross section, the diameter of which is selected to give the same cross-sectional area of the actual strand. Thus, a diameter of 0.328 in is used to simulate a nominal 0.375 in diameter seven-wire strand.
- Solid, eight-node elements are used for all components except for vertical stirrups, which are simulated using beam elements.
- The analysis is with uniform, isotropic, elastic properties. For concrete: elastic modulus, 4.77×10^6 lb/in²; Poisson's ratio, 0.17. For steel: elastic modulus, 29×10^6 lb/in²; Poisson's ratio, 0.3. We conducted some calculations using a lower concrete modulus.
- We did not simulate the effects of concrete creep or strand stress relaxation. (The implications of these idealizations are discussed below.)

The simulation of prestressing consists of the following steps, as illustrated in Figure 7.1 for the pre-2003 ties:

- a) Prestress the steel strands to the desired prestress level by applying a load to their ends.
- b) Model the tie with longitudinal holes of circular cross section in the locations of the prestressing strands. Make the diameter of the holes equal to the effective diameter of the steel strands in their prestressed condition. (Note that the prestressed strands reduce in diameter because of Poisson's contraction.) Include the steel strands, modeled as solid, also with a circular cross section even for seven-wire strands, in the holes in the tie. In this state, there is no stress transfer, neither radial nor longitudinal, between the strands and the ties.
- c) Unload the strands and allow contact and longitudinal slip to occur between the outer surfaces of the strands and the inner surfaces of the holes in the concrete tie. Utilize Coulomb friction with the desired coefficient of friction, generally 0.5.

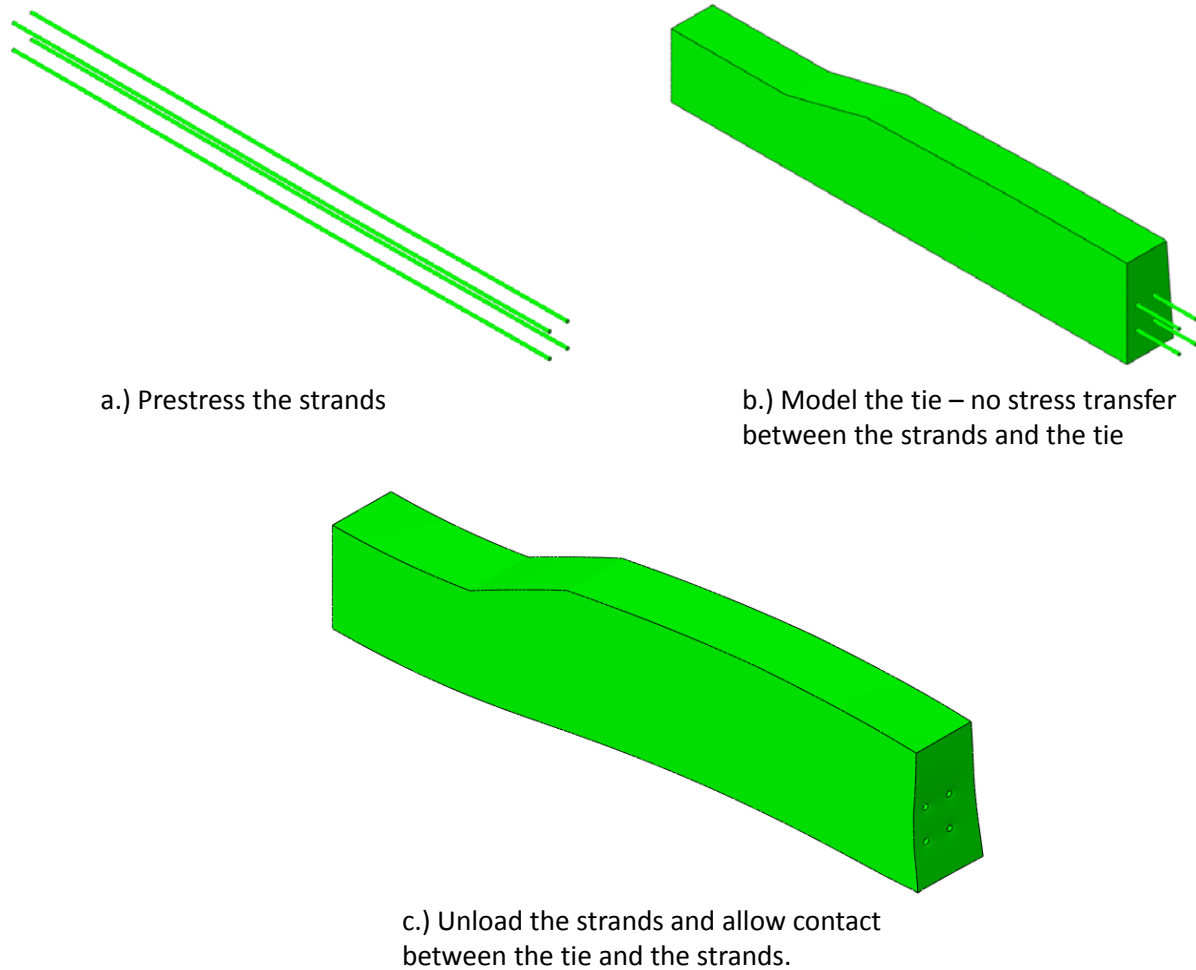


Figure 7.1. An illustration of the analysis steps used to simulate concrete tie prestressing.

This set of steps is similar to the steps in the actual tie production process in which strands are prestressed, concrete is poured around the strands and allowed to cure to some strength level, and then the strands are unloaded, releasing the original prestress load. Our simulation approach, as in actual production, results in a transfer of load from the strands to the concrete through friction over a certain length, referred to as the transfer length, at the strand ends.

We selected this simulation approach and 0.5 as the value for coefficient of friction by using results from a technical paper in which transfer length was accurately measured [7.8]. Figure 7.2 shows a comparison between the strand stress calculated using the methodology just described with measured values for the test sample geometry of that paper—a 2x2x72 in member with a 0.197 in diameter strand located at the center of the cross section.

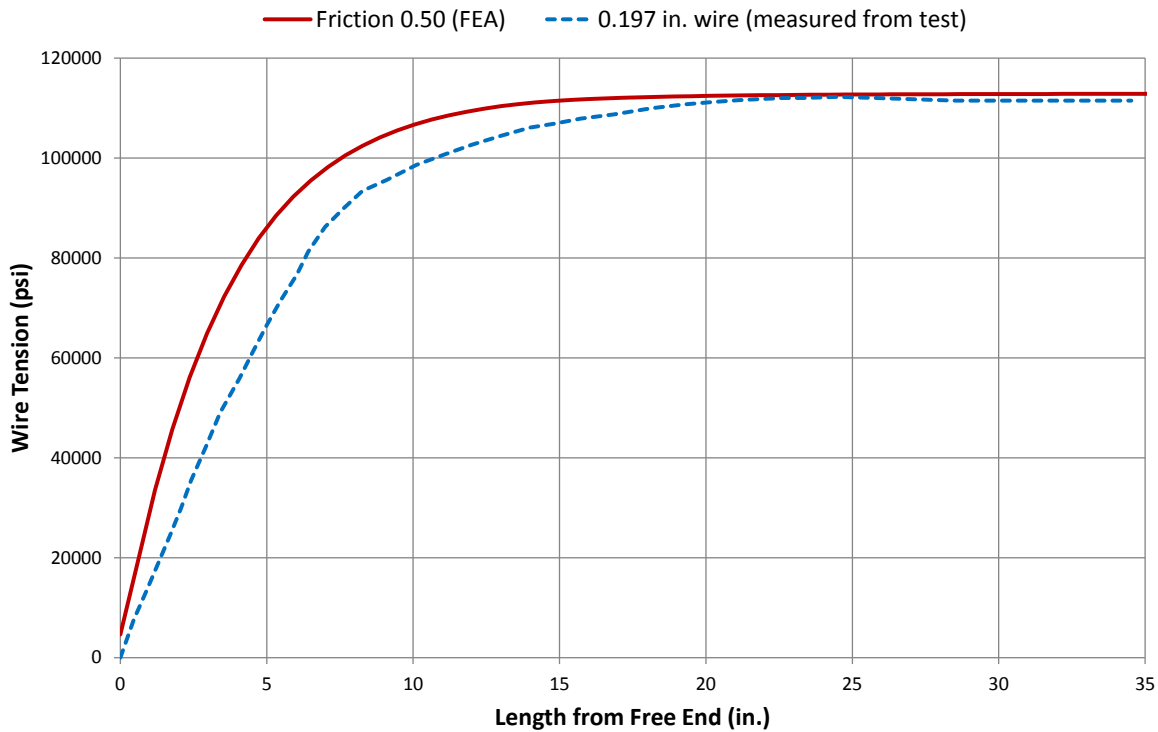


Figure 7.2. Comparison between the calculated and measured distributions of stress along the prestressing strand for a test beam [7.8].

We note that the mechanism of transfer in the model can only be through friction on a smooth surface, while in an actual concrete member it can be a combination of friction, adhesion, and mechanical interlocking. There is a very large volume of work on the mechanisms of bond transfer which we will not cover in this report. The transfer mechanisms for multiwire strands are more complex than for individual wires. Interlocking of cement paste with “cusps” between adjacent wires, shortening of pitch between wires at prestress release, and “unwinding torque” of strands at prestress release may all contribute to increased friction between strands and concrete [7.9]. Our use of a simple, Coulomb friction model is intended to capture frictional sliding, adhesion, and mechanical interlocking in a single parameter.

7.2.2 Prestresses in Pre-2003 Ties

Figure 7.3 shows the stress along a simulated seven-wire strand for the pre-2003 tie geometry, an initial prestress of 210 ksi (78% of the nominal, 270 ksi tensile strength of the strands), and a coefficient of friction equal to 0.5. The results indicate a transfer length, defined here as the distance from the free end of the strand to the point at which the stress reaches 95 percent of the center, plateau level, equal to approximately 14 in. (The total tie length is 102 in and the distance from the end of the tie to the center of the rail seat is approximately 21 in.)

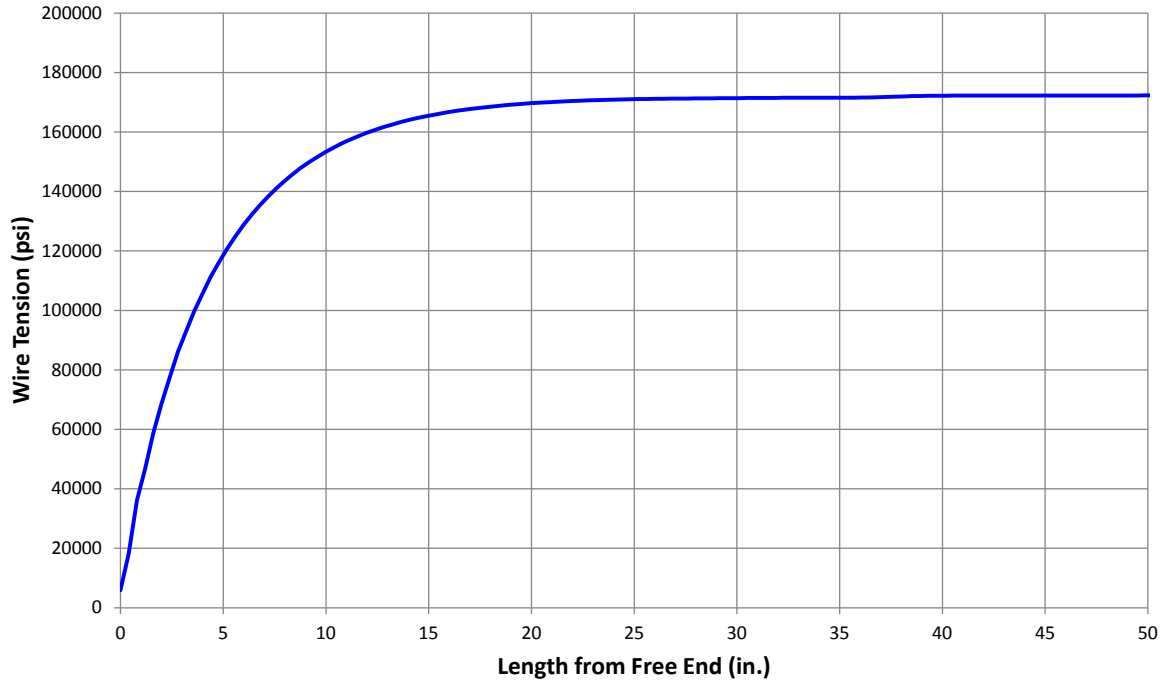


Figure 7.3. The calculated stress along the top, center prestressing strand in the pre-2003 concrete tie.

The calculated longitudinal stresses in the tie induced from prestressing are shown as a contour plot in Figure 7.4. The maximum precompression stress is about 2800 psi (but only at a very small region at the transition between the center horizontal surface and the sloping surface at the top of the tie.) The compressive stress below the rail seat is between 600 and 950 psi.

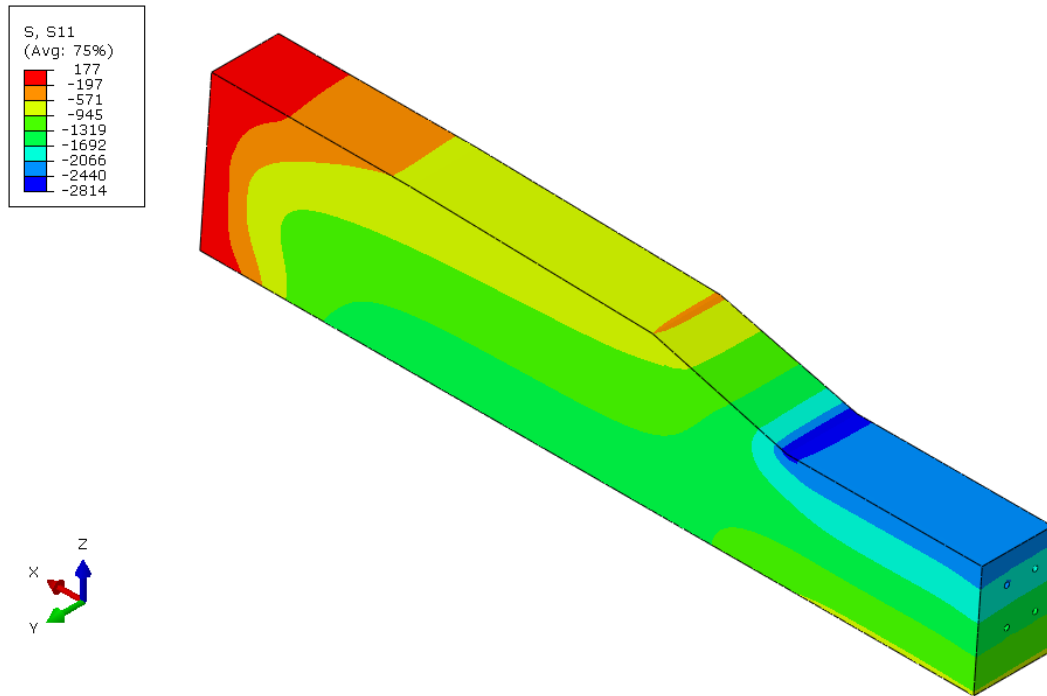


Figure 7.4. The longitudinal stresses calculated by finite element analysis for prestressing-only in the pre-2003 ties.

The calculated stresses induced around the strands in the concrete for the pre-2003 tie design at a few longitudinal sections are shown as contour plots in Figure 7.5. Vertical tensile stresses, the type of stresses that would explain the form of cracking observed in the Amtrak ties, are significant near the ends of the tie. (Note that these vertical stresses also coincide with the maximum principal stresses in the tie from prestressing.) Figure 7.6 shows a plot of the vertical tensile stress along a line that passes laterally through the top row of strands and which is 4.3 in from the tie end; this is the location at which these vertical stresses from prestressing are highest for this configuration.

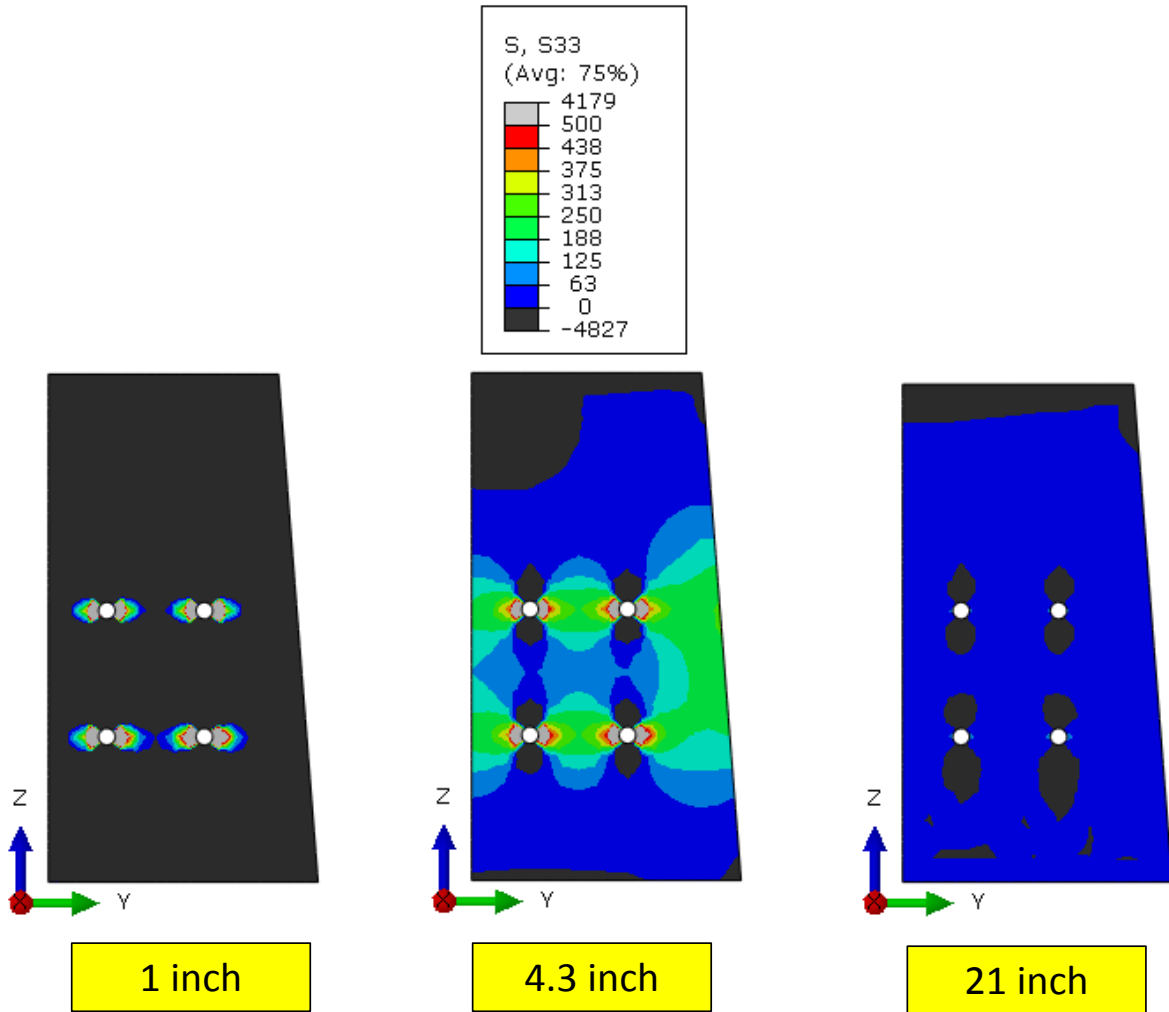


Figure 7.5. The calculated vertical stresses, due to prestress-only, in the pre-2003 tie at longitudinal sections 1 in, 4.3 in, and 21 in from the tie end. (Regions that are black are in compression. Regions that are gray have tensile stresses greater than 500 psi.)

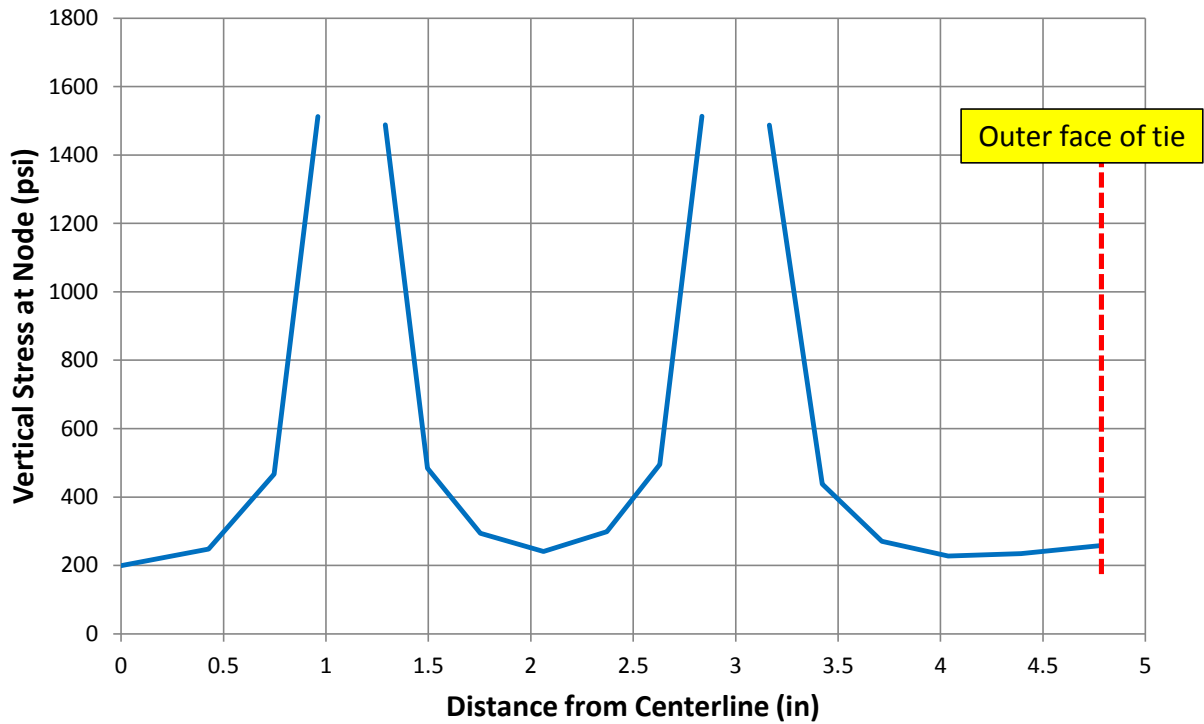


Figure 7.6. The calculated vertical stresses along a path through the top row of strands due to prestress-only in the pre-2003 ties at a section 4.3 in from the tie end.

The large vertical tensile stresses adjacent to the prestressing strands (i.e., splitting stresses) result from a mechanism known as the Hoyer Effect. As the prestressing force is transferred from the bed to the strands during the cutting operation, the diameter of the strand increases and the strand exerts a radial pressure on the surrounding concrete; this pressure is what allows longitudinal friction forces to be generated between strand and concrete in the model. This pressure causes tensile splitting stresses to develop in the concrete adjacent to the strand. While designers, prestressing manufacturers, and practitioners have developed ways to account for these forces in practice, the internal mechanisms through which they occur are not well understood and are thought to be highly nonlinear.

For example, note that the tensile strength of the concrete after complete hydration is less than or equal to 1000 psi (see Section 5). At prestress transfer, we would expect the tensile strength of the concrete to be less than 1000 psi. Therefore, it is unlikely that the concrete could sustain the very high splitting stresses adjacent to the strands indicated by modeling; rather it seems likely that the concrete experiences localized nonlinear deformation due to a mechanism such as microcracking [7.9]. This belief is reinforced by the general lack of observed cracking in our detailed examinations, up to 10x magnification, of sections of nominally uncracked ties (note that microcracks would not be visible at this level of magnification) and our observations at thin sections near the prestressing strands, as described in Section 4.5.

The vertical tensile stresses that occur at the outer face of the tie (i.e., bursting stresses) result from the redistribution of longitudinal stresses. To visualize this, it is helpful to use the strut-and-tie model (in this case a “tie” is a tension-only element and is not related to a railroad tie) illustrated in Figure 7.7. Prestressing forces are applied to member ends as concentrated loads; these concentrated loads tend to become uniformly distributed along the depth of the member (i.e., they will tend to spread out). Bursting forces (represented by the “tie” in Figure 7.7) develop to balance the vertical redistribution of longitudinal forces.

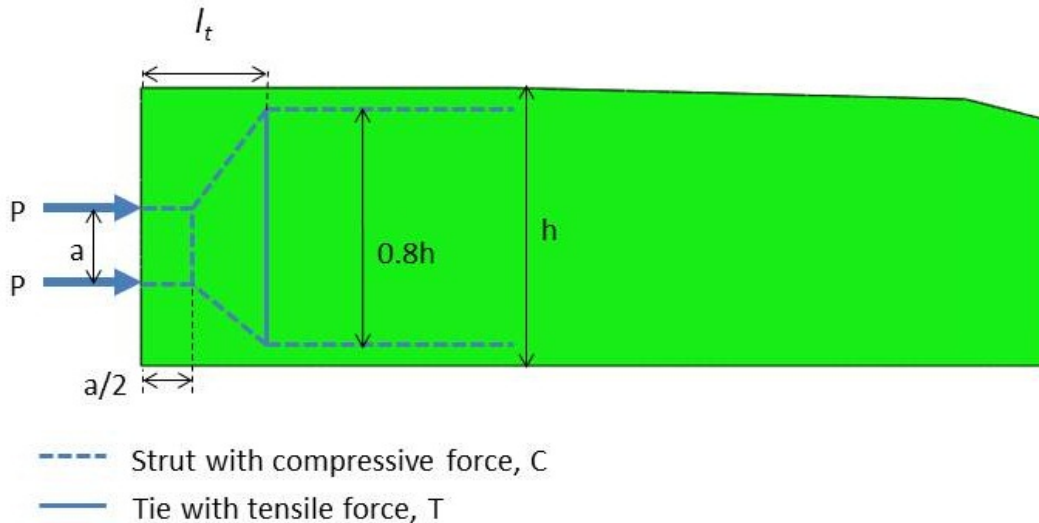


Figure 7.7. The strut-and-tie model for visualizing stresses near the transfer point of prestressing strands in the pre-2003 tie design.

The vertical tensile force (the bursting force) that occurs near the end of the prestressing or post-tensioned strands is given approximately by the formula [7.4]:

$$T = \alpha \frac{P_o h}{l_t}$$

where:

α = proportionality factor

P_o = total prestressing force

h = member height

l_t = transfer length.

This equation indicates that the vertical bursting force is greater for higher prestressing loads, shorter transfer lengths, and deeper members. Our finite element analyses support these relationships as will be shown below.

There are some phenomena occurring in the prestressed concrete tie that we are not explicitly simulating, but which could have an effect on the resulting stress state. The actual strand induces an additional, effective pressure to the hole in the concrete by virtue of its nonuniform shape moving along the concrete hole. This is not captured in the model because the strands are modeled as having a constant cross section. The wire includes indents or deformations (see Section 4) so that as the nonindented part of the wire slides into the concrete ‘key’ corresponding to the original wire indentation, it causes the concrete to either be sheared or pushed outward. This action is illustrated in Figure 7.8. The effect of such strand features in promoting splitting is the subject of many papers (e.g., [7.6]). It becomes more important near the point of flexural failure of a beam when the strands begin to slip substantially. Under normal operational loads and in the absence of significant cracking, the slip is evidently limited to what occurs just after release of prestress in the manufacturing process. In this case, the greatest slip is at the very end, approximately 0.080 to 0.100 in [7.10], suggesting an average slip of 0.040 to 0.050 in over the transfer length. The spacing between indents on the strands in the pre-2003 Amtrak ties is approximately 0.22 in, and the length of the indent is approximately 0.1 in for the pre-2003 tie design. Thus, there is probably some wedging action in the ties. The geometry of the wire indentations differs for the various case study ties (see Section 4) and this could lead to different effective friction values and transfer lengths. For example, the strands in the San-Vel ties have shallower, smaller, and more widely spaced indentations than in the pre-2003 and post-2003 ties.

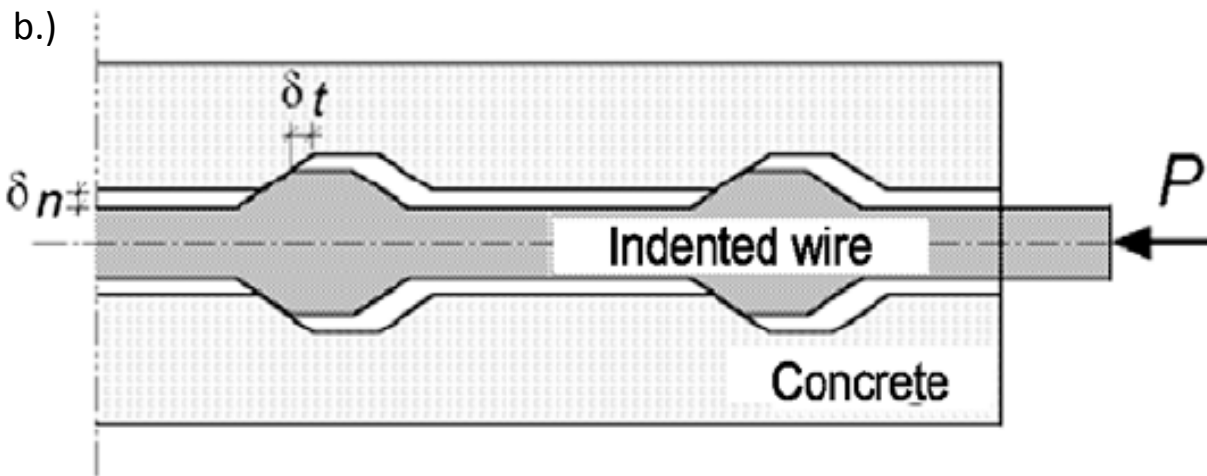


Figure 7.8. Illustration of the outward pressure exerted by an indented strand during slippage.

The strands also experience some stress relaxation after the prestressing operation. It became common in the early 1980s to use low-relaxation prestressing strands, the properties of which are achieved by selection of the steel and processing conditions. The difference in final prestress load between regular and low-relaxation strands can be substantial. For example, the PCI Design Handbook methodology provides an estimated decrease in prestressing stress of 19 ksi with regular strands and only 3 ksi for low-relaxation strands. We suspect, but have not

demonstrated, that the prestressing strands used for the San-Vel ties, which were produced in the late 1970s, were regular strands and therefore had lower prestressing forces. This would result in lower vertical bursting stresses.

Creep also occurs in concrete and has the effect of reducing the prestressing loads. Again, we have not accounted for this phenomenon, but we believe it is not a substantial effect.

We note that there are also significant prestress-induced tensile stresses in the horizontal direction resulting from both the Hoyer and the strut-and-tie effects. These stresses could potentially induce vertical cracks. However, these stresses are lower magnitude than the vertical stresses, as shown in Figure 7.9 (compare with Figure 7.6).

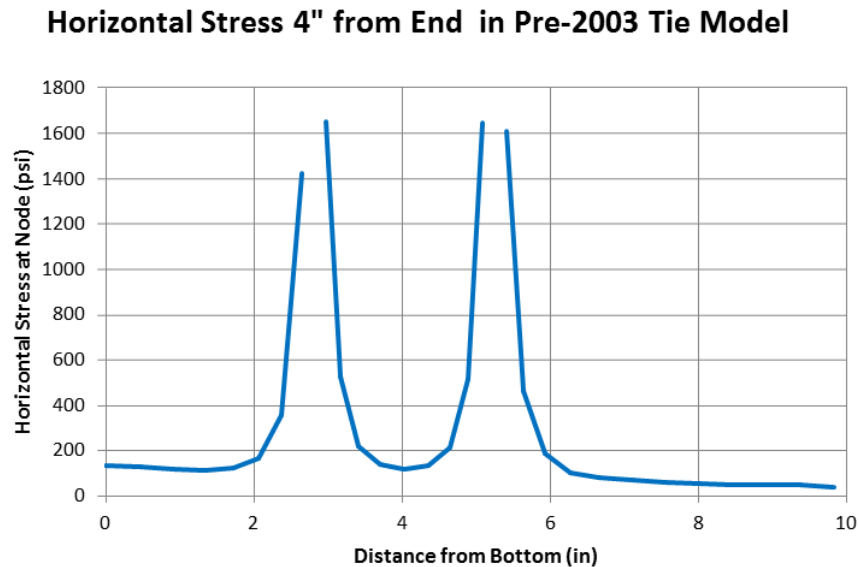


Figure 7.9. The calculated horizontal stresses along a path through the outermost two strands due to prestress-only in the pre-2003 ties at a section 4.3 in from the tie end.

7.2.3 Prestresses in Post-2003 Ties

We conducted finite element calculations for the prestresses induced in the post-2003 ties using the same methodology described above. The configuration of reinforcement for these ties was shown in Figure 3.1. There are 24 single wire strands (compared with the eight seven-wire strands of the pre-2003 ties), each with a diameter of 0.21 in. The prestressing force for these strands is, according to the drawing, 6,550 lb, for a total prestressing force of 157.2 kips. This force is approximately 14 percent greater than the prestressing force for the pre-2003 ties: 137.7 kips. Figure 7.10 shows contours of vertical stress around the strands at a cross section 4.2 in from the tie end, the location at which these stresses are highest. Figure 7.11 shows the vertical stresses along a transverse path through the row of strands second from the top in comparison with the stresses for the top row of strands in the pre-2003 ties; the highest stresses in the post-

2003 ties occur in the second row. (Note that we have changed the vertical scale on this and subsequent similar figures to better show the variation of stress near the surface of the tie; the very high calculated stresses adjacent to the strand are less accurate.) We note that the calculated vertical stresses from prestressing in the post-2003 ties are generally comparable to the stresses in the pre-2003 ties, but are higher at the outer face of the tie, consistent with the strut and tie model (higher prestress load).

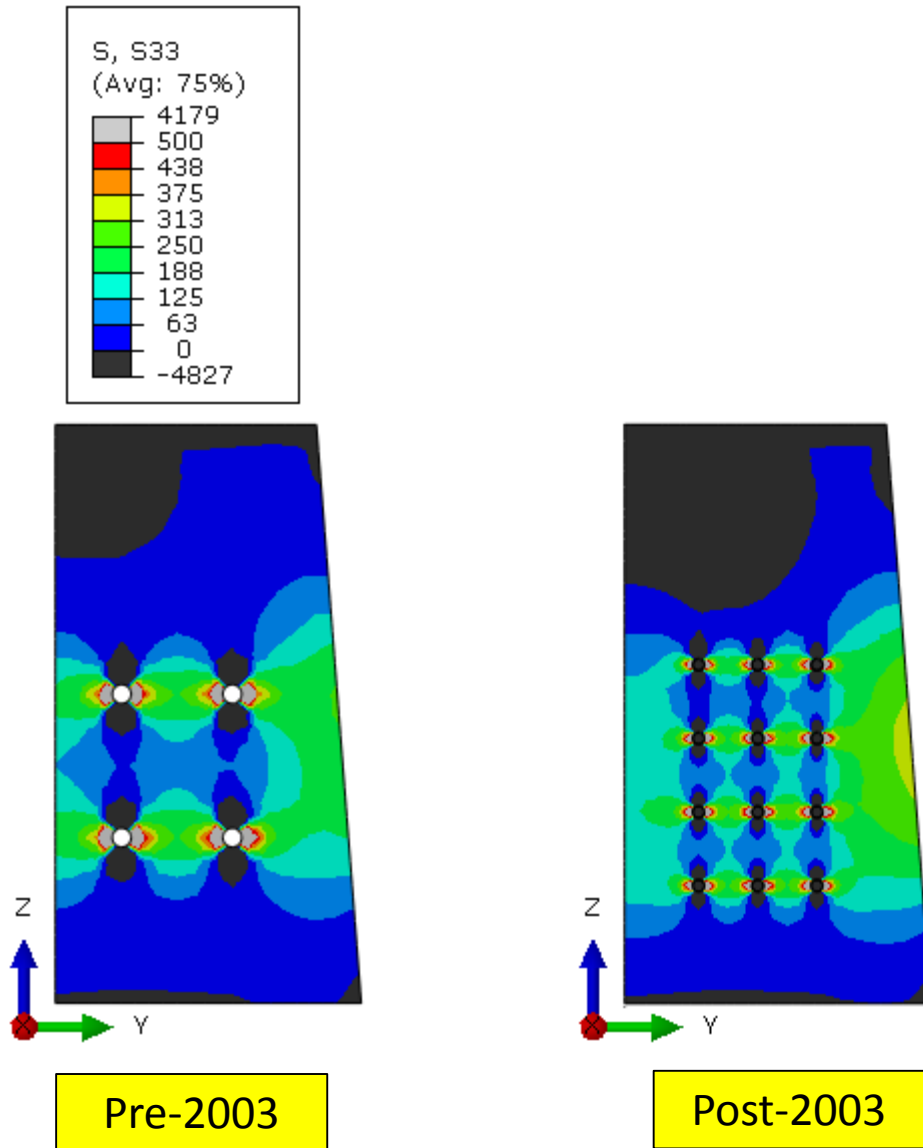


Figure 7.10. The calculated vertical stresses due to prestress-only in the pre- and post-2003 ties at a longitudinal section 4.2 in from the tie end. (Regions that are black are in compression. Regions that are gray have tensile stresses greater than 500 psi.)

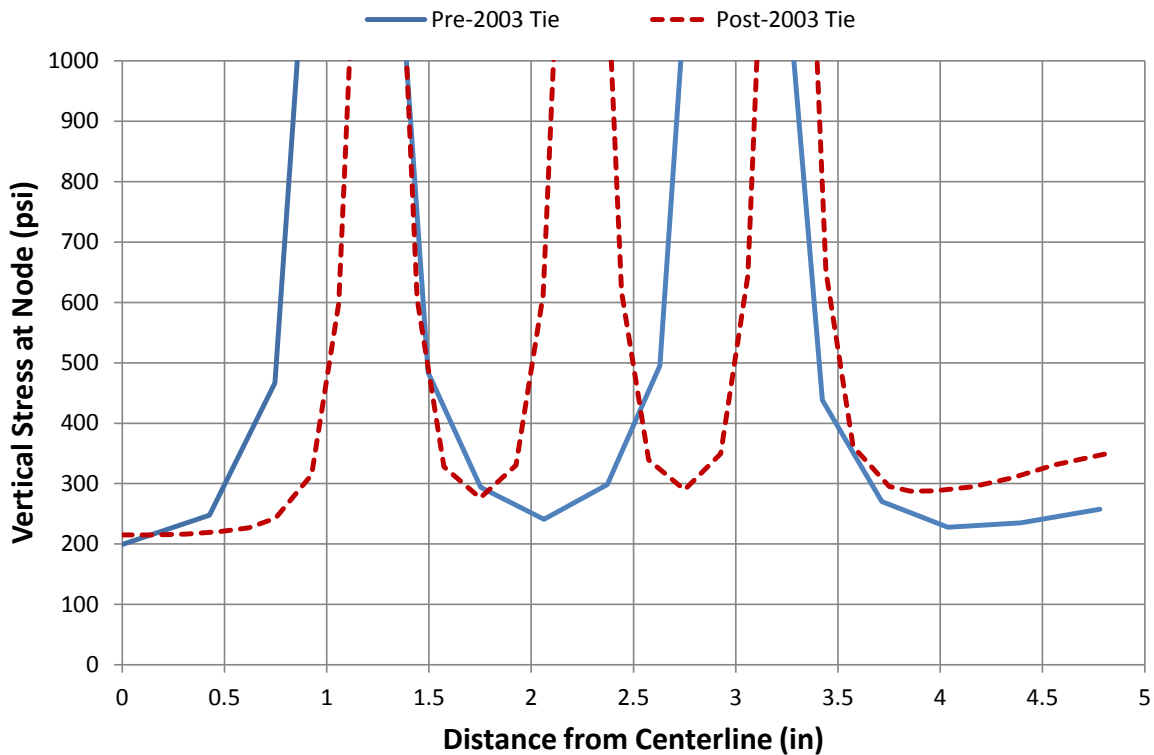


Figure 7.11. The calculated vertical stresses along a path through a row of strands (top row for pre-2003 and second row for post-2003) due to prestress-only in the pre- and post-2003 ties at a section 4.2 in from the tie end.

7.2.4 Prestresses in San-Vel Ties

We conducted similar finite element analyses for the San-Vel ties. We also used a quarter-model for this tie simulation with the following conditions (see also Figure 3.2):

- The individual strand preload was 16.68 kips (per the drawing; no relaxation is assumed).
- The friction coefficient was 0.5.
- The stirrup was simulated using beam elements with assigned cross-sectional area corresponding to a No. 3 bar: 0.11 in².
- The fastener insert was also included. (Results on the effects of the fastener on tie stresses are discussed in a later section.)

Figure 7.12 shows a plot of vertical stress through the top row of strands for the San-Vel and pre-2003 tie designs. We note that the vertical stress is lower by about 25 percent on the outer surface of the San-Vel tie, consistent with the strut-and-tie model (smaller depth and lower prestress load). The distribution of vertical stress along the path through the strands does not otherwise differ appreciably between the two tie configurations.

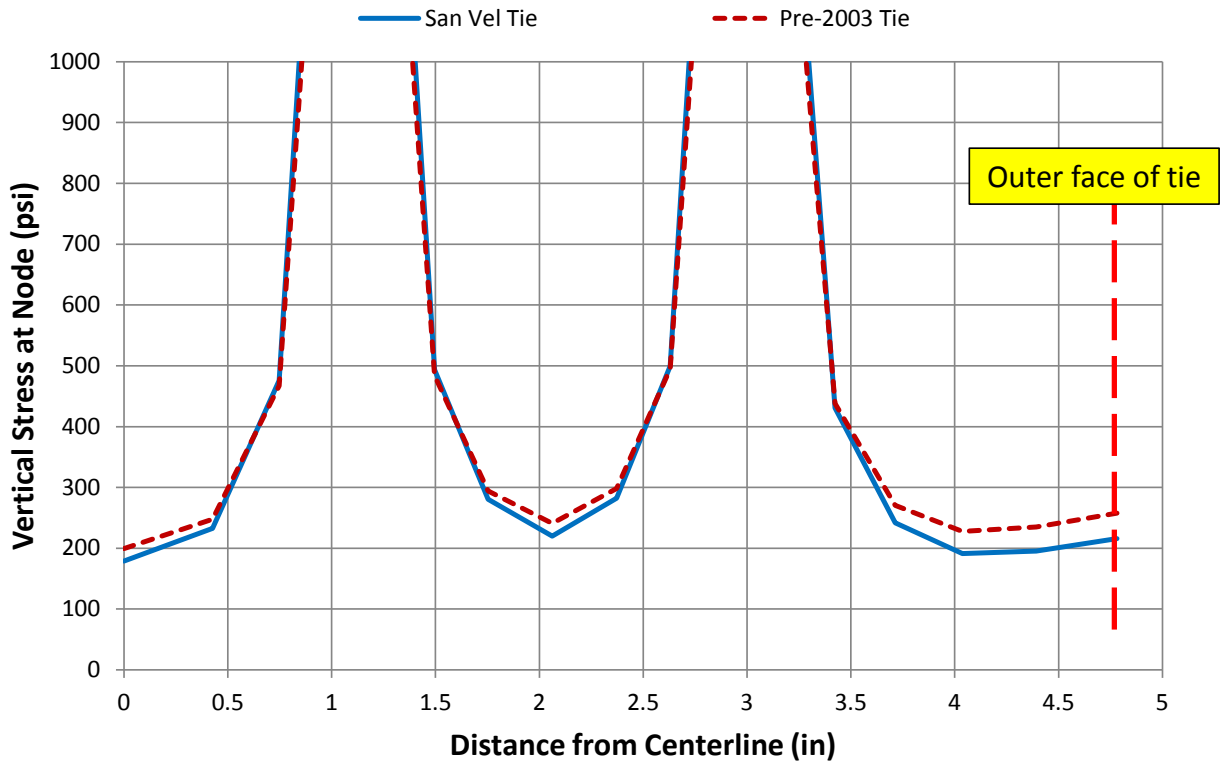


Figure 7.12. Comparison of vertical stress along a path through the top strands at the location of maximum vertical stress for the pre-2003 and San-Vel ties for prestress loading only.

The stress in the vertical stirrup is relatively low at only 300 psi. This is consistent with the location of the stirrup, which is just outboard of the rail seat, approximately 19 in from the tie end compared with the location of maximum calculated vertical stress, which is approximately 4 in from the end. (Note that stirrups were not present in the San-Vel ties we examined in our lab, even though they were indicated on the drawing.)

7.3 Some Parametric Analyses for the Prestress Condition

We carried out some calculations to assess the effects of various parameters on stress from prestressing, paying particular attention to the vertical stress in the vicinity of the reinforcing strands. We first examined the effect of increasing the coefficient of friction between the strand and the concrete for the pre-2003 tie. Higher friction is meant to represent a better bond between strand and concrete, which could result, for example, from larger, deeper dimples in the strands. Higher friction has the effect of decreasing the transfer length and increasing the vertical bursting stress, as shown in Figures 7.13 and 7.14, respectively.

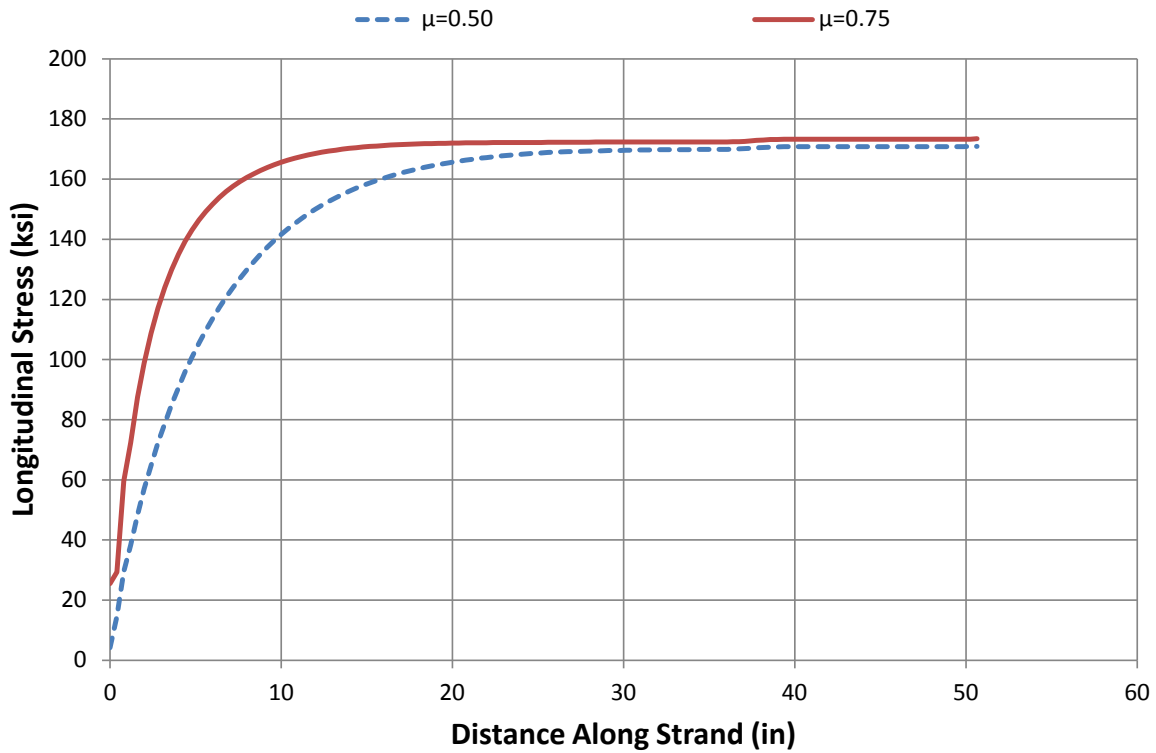


Figure 7.13. The calculated stress along a prestressing strand in a pre-2003 tie for two values of coefficient of friction between strand and concrete.

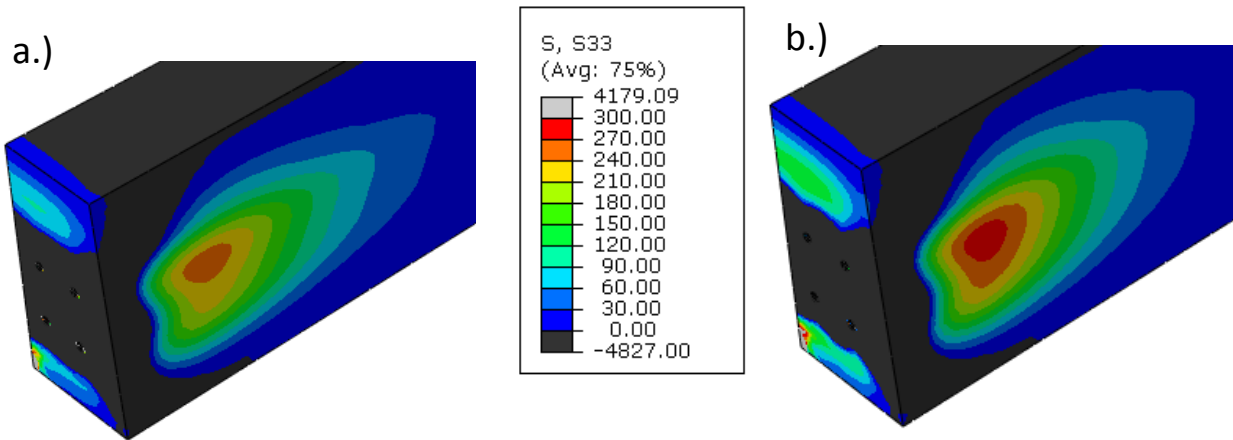


Figure 7.14. The vertical stress contours (prestress-only) in a pre-2003 tie for two values of coefficient of friction between strand and concrete: (a) $\mu = 0.5$; (b) $\mu = 0.75$.

We also conducted some calculations in which we simulated a variation in transfer length by applying different distributions of strand shear forces to the concrete holes of the pre-2003 tie model. These analyses do not include the effects of the strand expansion (Hoyer effect). The

distributions were selected to give different transfer lengths while maintaining a constant prestressing force. Figure 7.15 shows the resulting strand force for the different transfer lengths compared with the curve for a strand in the pre-2003 tie. The resulting plot of maximum vertical bursting stress, in this case at the tie outer surface at the top row of strands, is shown in Figure 7.16, and a plot of the location at which this maximum surface stress occurs is shown in Figure 7.17.

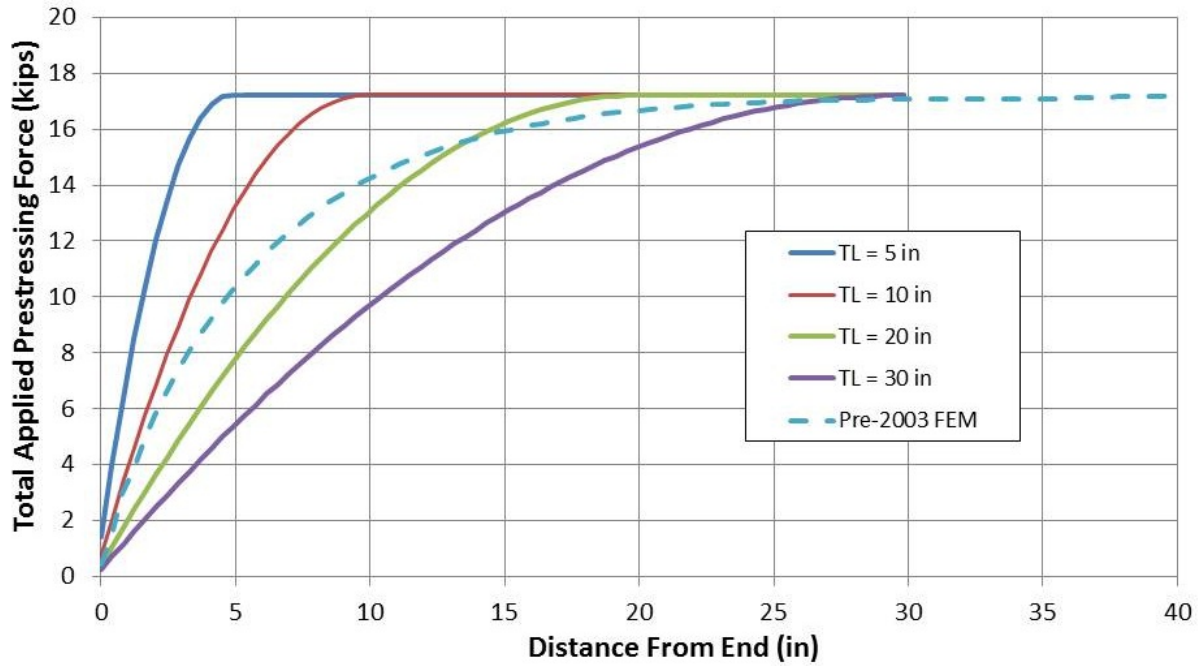


Figure 7.15. The prestress force variation along the strand used in the transfer length (TL) study.

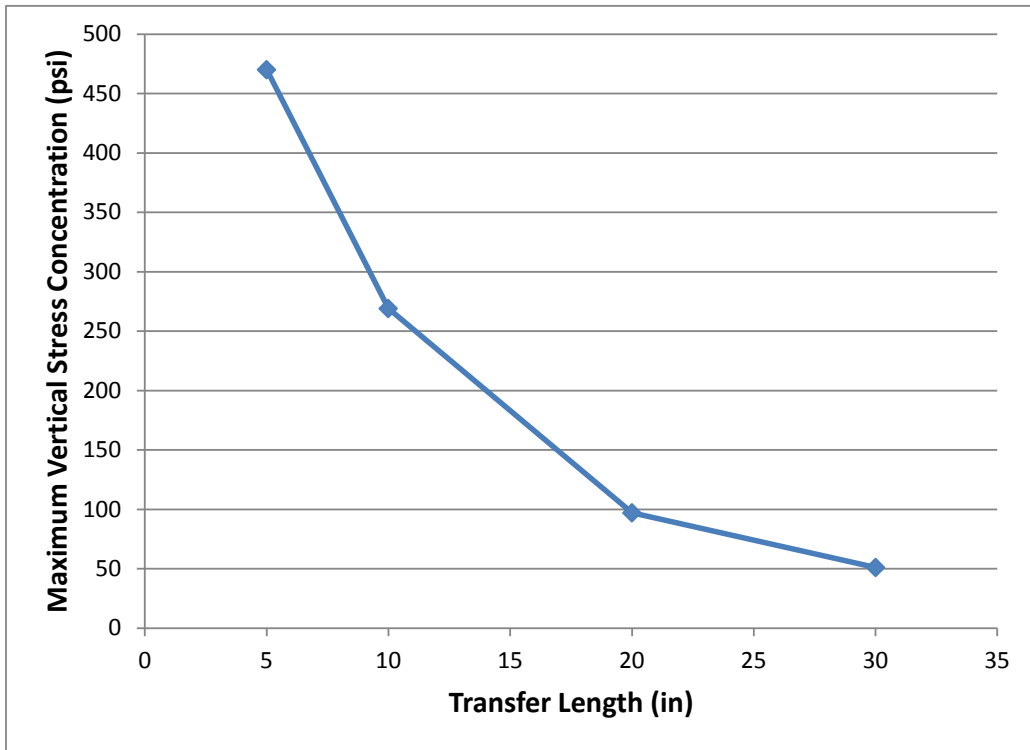


Figure 7.16. The calculated variation in vertical bursting stress vs. transfer length.

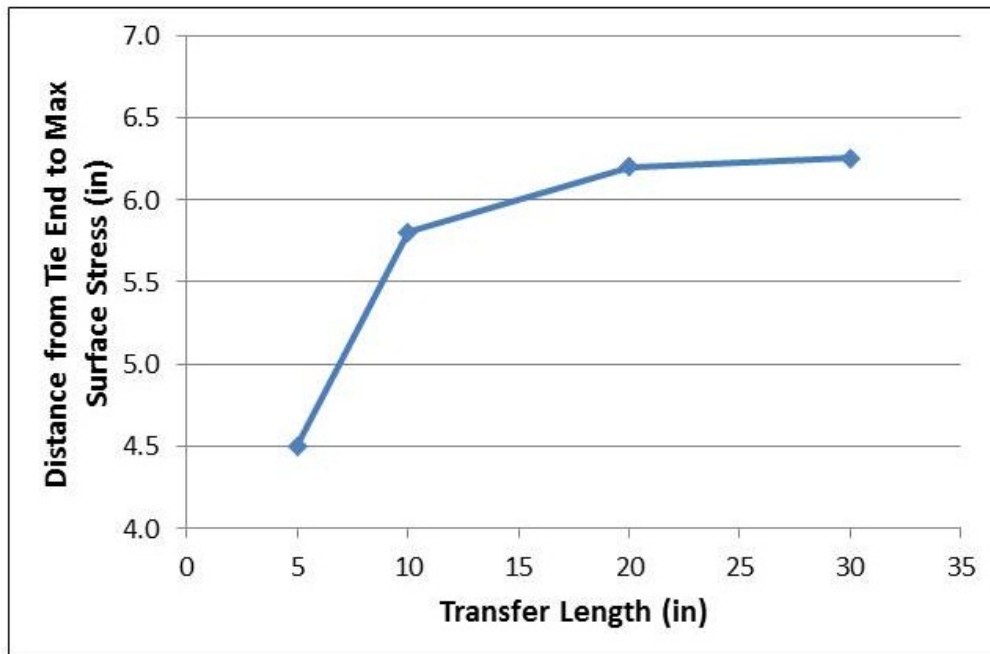


Figure 7.17. The location of calculated vertical bursting stress vs. transfer length.

A condition of shorter transfer length is of interest because it can cause the bursting stresses to increase substantially. One hypothesis put forward to explain horizontal cracking in the ties is that the transfer of prestressing force in the manufacturing process occurs after the concrete has reached a relatively high strength, substantially more than the specified minimum 4,250 psi, thereby increasing bond strength between strand and concrete and decreasing the transfer length. It has been reported that delayed cracking sometimes occurs in prestressed members if too much time is allowed to elapse before cutting the prestressing strands [7.11] and this may be related to a decrease in transfer length. We have no direct evidence that this is the case for the Amtrak pre-2003 ties. We also note that the indentations in the pre-2003 tie strands are deeper and more closely spaced than in the San-Vel ties, indicating that the transfer length is shorter in the former ties. We did not have the opportunity to measure actual transfer lengths in the ties to test these hypotheses.

Figures 7.18 and 7.19 show results of an analysis on the post-2003 tie in which the elastic modulus of the concrete was reduced by 25 percent; the effect is the same for the pre-2003 tie. We note that the transfer length is greater and the vertical stress at the outer surface of the tie is lower for the lower modulus, but these effects are not large.

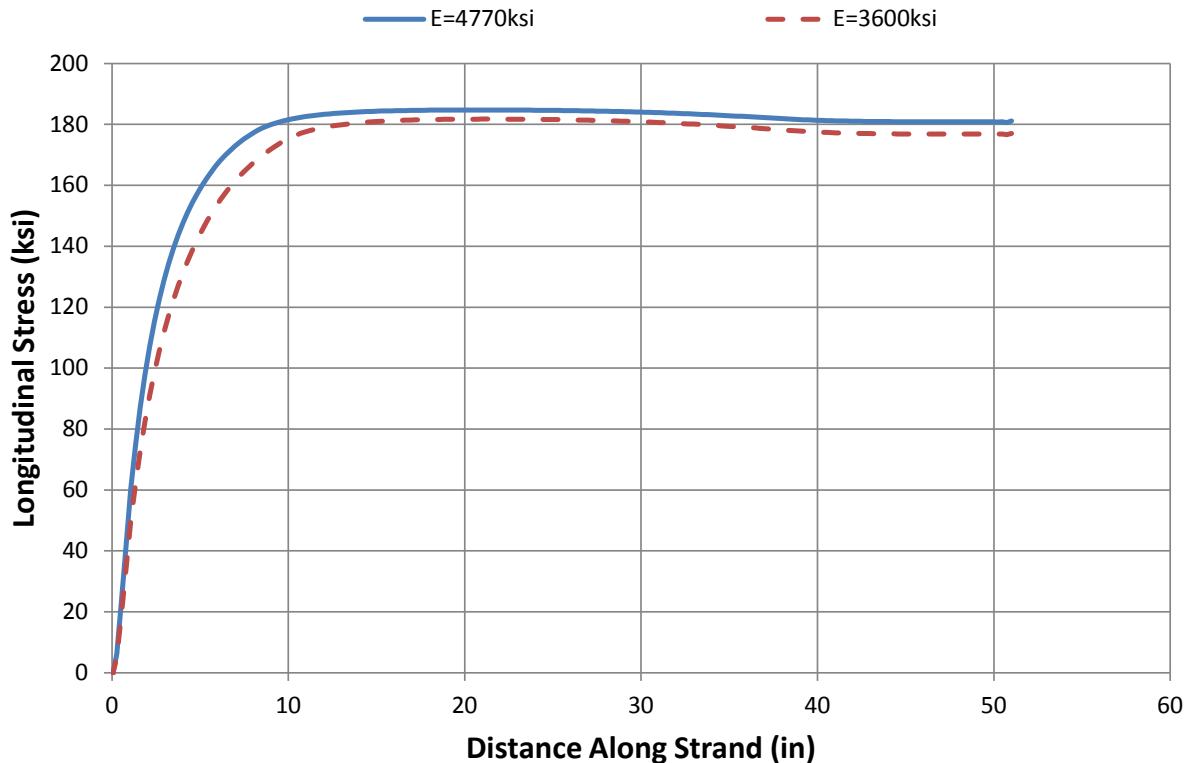


Figure 7.18. The calculated stress along a prestressing strand in a post-2003 tie for two values of concrete modulus.

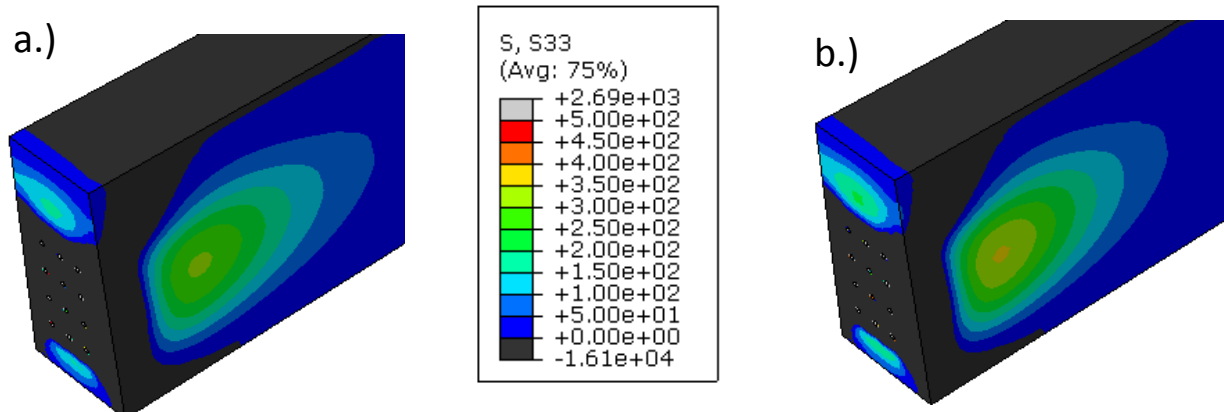


Figure 7.19. Calculated vertical stress contours from prestressing only in a post-2003 tie for two values of concrete modulus: (a) $E = 3,600$ ksi; (b) $E = 4,770$ ksi.

7.4 Stresses from Other Loads

We next examined the stresses induced from some operational loads in the ties:

- Vertical wheel load,
- Vertical load applied to the shoulder insert, and
- Impact and vibration loads.

We conducted these calculations with the pre-2003 tie model.

7.4.1 Nominal Stresses from Vertical Wheel Loads

As stated earlier, the tie is primarily designed to carry the flexural loads from the nominal and extreme vertical wheel loads. Here we focused our calculations on the 52 kip positive rail seat moment qualification load of the specification for comparison with tests conducted in this program (Section 5.3) and as a basis from which to estimate stresses from actual vertical service loads. These calculations included the prestress condition.

Figure 7.20 shows the longitudinal stresses in the tie with the addition of the 52 kip vertical load at the rail seat applied at two points separated by 4.5 in. The tie is supported at two points at its base corresponding to the 28-inch separation in the specification test. The maximum tensile stress, which occurs immediately below the rail seat on the bottom of the tie, is about 100 psi, which is below the tensile strength of the concrete (see Section 7.5 below). Figure 7.21 shows the shear stress distribution in the tie. We note that the highest shear stresses occur in the vicinity of the top row of strands, but closer to the rail seat than the location of maximum vertical stress from prestress alone.

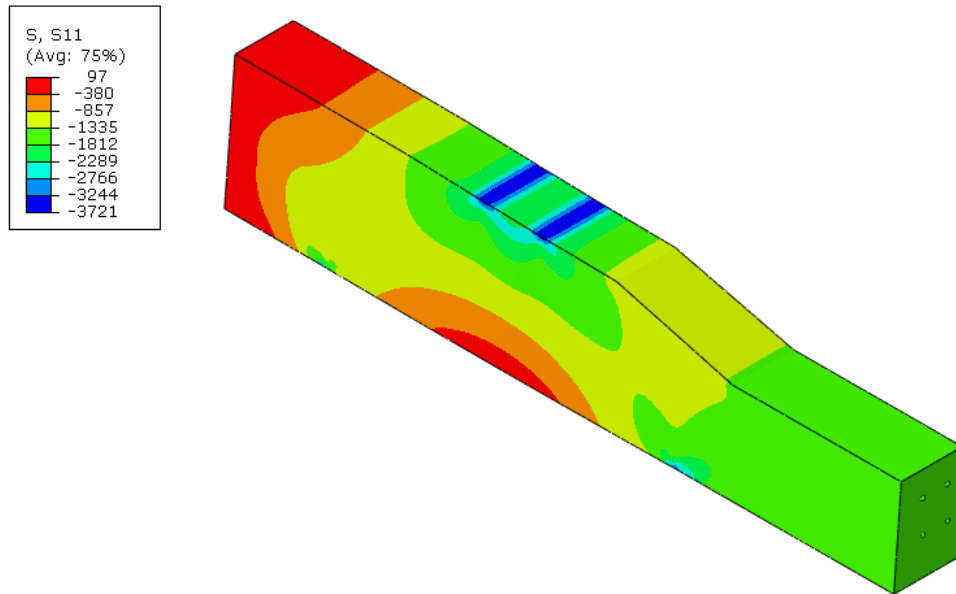


Figure 7.20. Longitudinal stresses in the pre-2003 tie from a 52 kip positive rail seat moment test, including prestress.

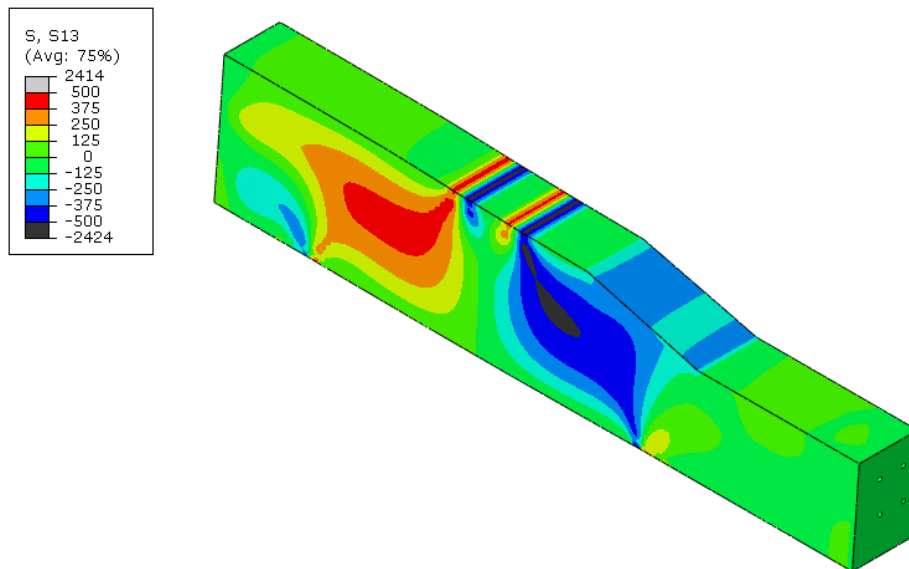


Figure 7.21. Shear stresses in the pre-2003 tie from a 52 kip positive rail seat moment test, including the prestress. The S13 stress acts along horizontal planes through the tie.

The calculated strain increment (due to the addition of the 52 kip load) below the rail seat adjacent to the bottom of the tie is $362 \mu\epsilon$, which is about 25 percent greater than the average value of $287 \mu\epsilon$ measured in our own laboratory tests (see Section 5).

Figure 7.22 shows the change in calculated stress along one of the top, center strands for the addition of the positive rail seat moment. Figure 7.23 shows the change in vertical stress along a transverse path through the top row of strands 4.3 in from the tie end; the same location at which the vertical stresses are at a maximum for the prestressing load only. Both Figures 7.22 and 7.23 show little change in stress with the addition of the substantial vertical load, indicating that the bursting stresses are not significantly affected. In fact, the vertical bursting stress decreases. The actual magnitude of vertical load on the ties is typically between 10 and 20 kips (Section 6), so that the vertical stress change in a tie in track is even less than that shown in Figures 7.22 and 7.23.

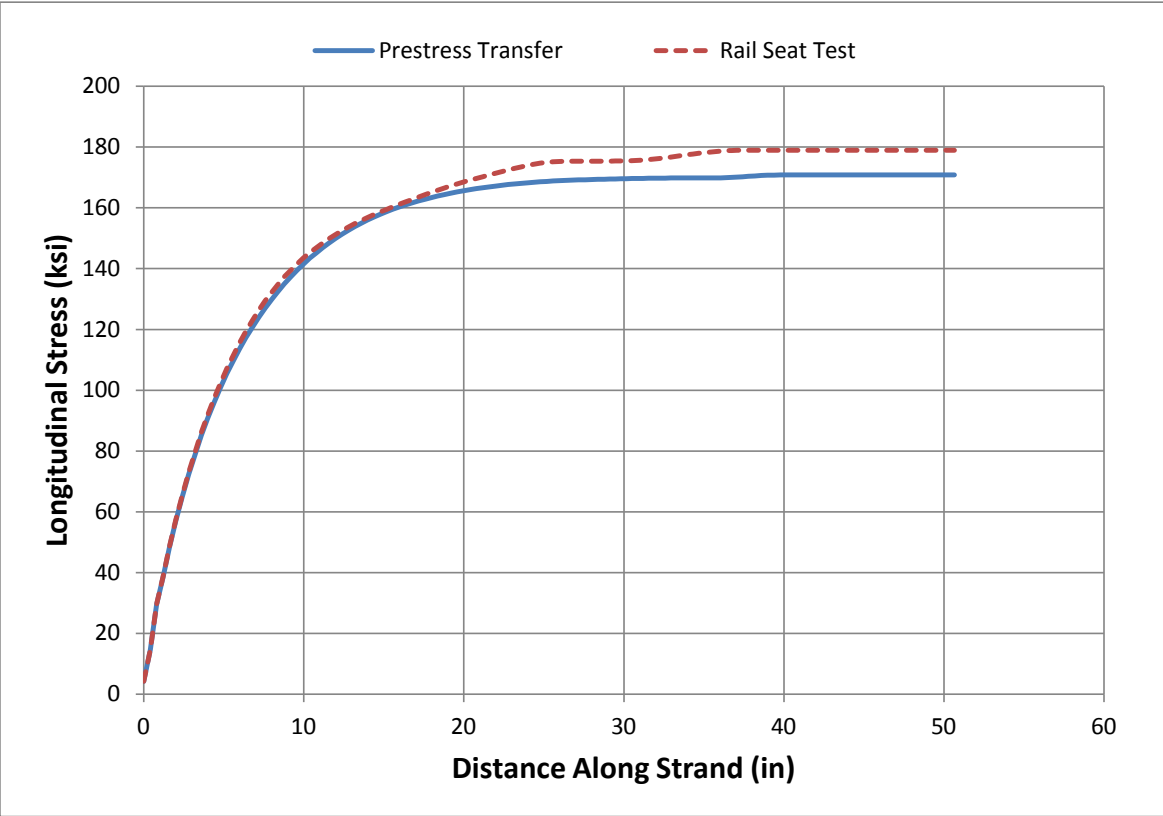


Figure 7.22. Longitudinal stresses in a top, center strand for both the prestress and the prestress plus positive rail seat moment loading.

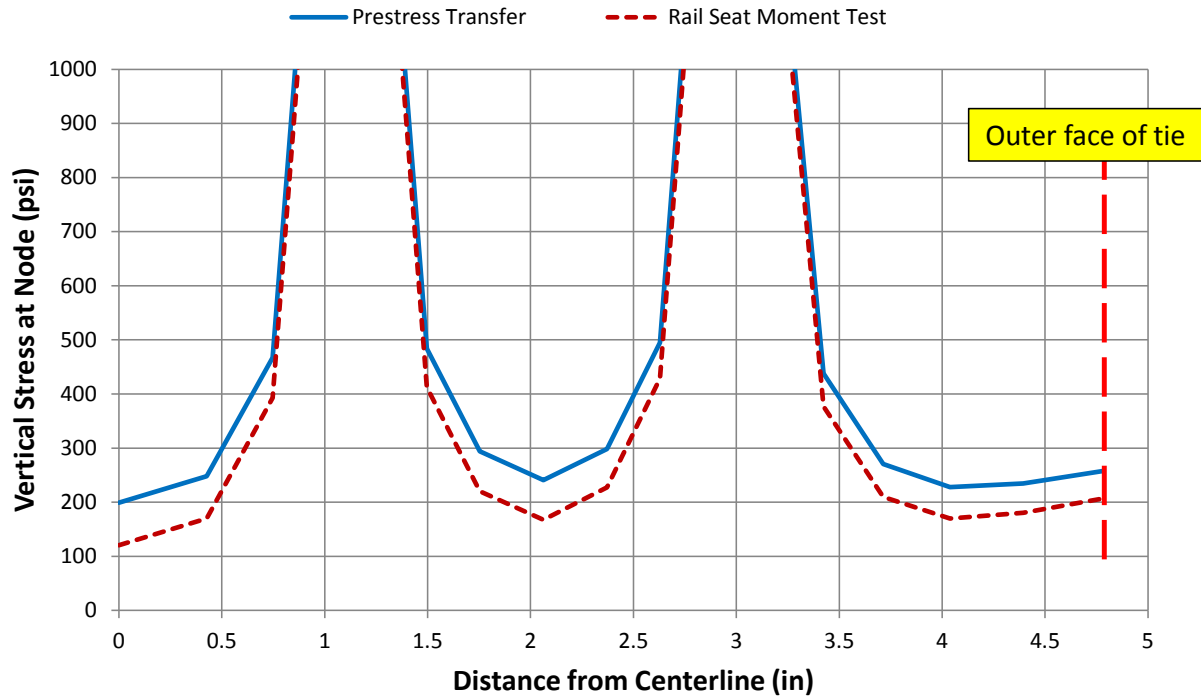


Figure 7.23. Vertical stresses along a transverse path through the top strands of a pre-2003 tie for both the prestress and prestress plus positive rail seat moment loading.

There is a substantial change in shear stress with applied vertical load depending on the location along the tie. Figure 7.24 shows a plot of shear stress acting on the plane corresponding to the top row of strands in the direction of the strands at a location 4.3 in from the tie end and at the location at which the shear stresses in the top row of strands is at maximum—15 in from the tie end. We see that the cyclic component of this shear stress is substantial, but only in the vicinity of the rail seat. Again, the actual shear stress magnitude will be less in track.

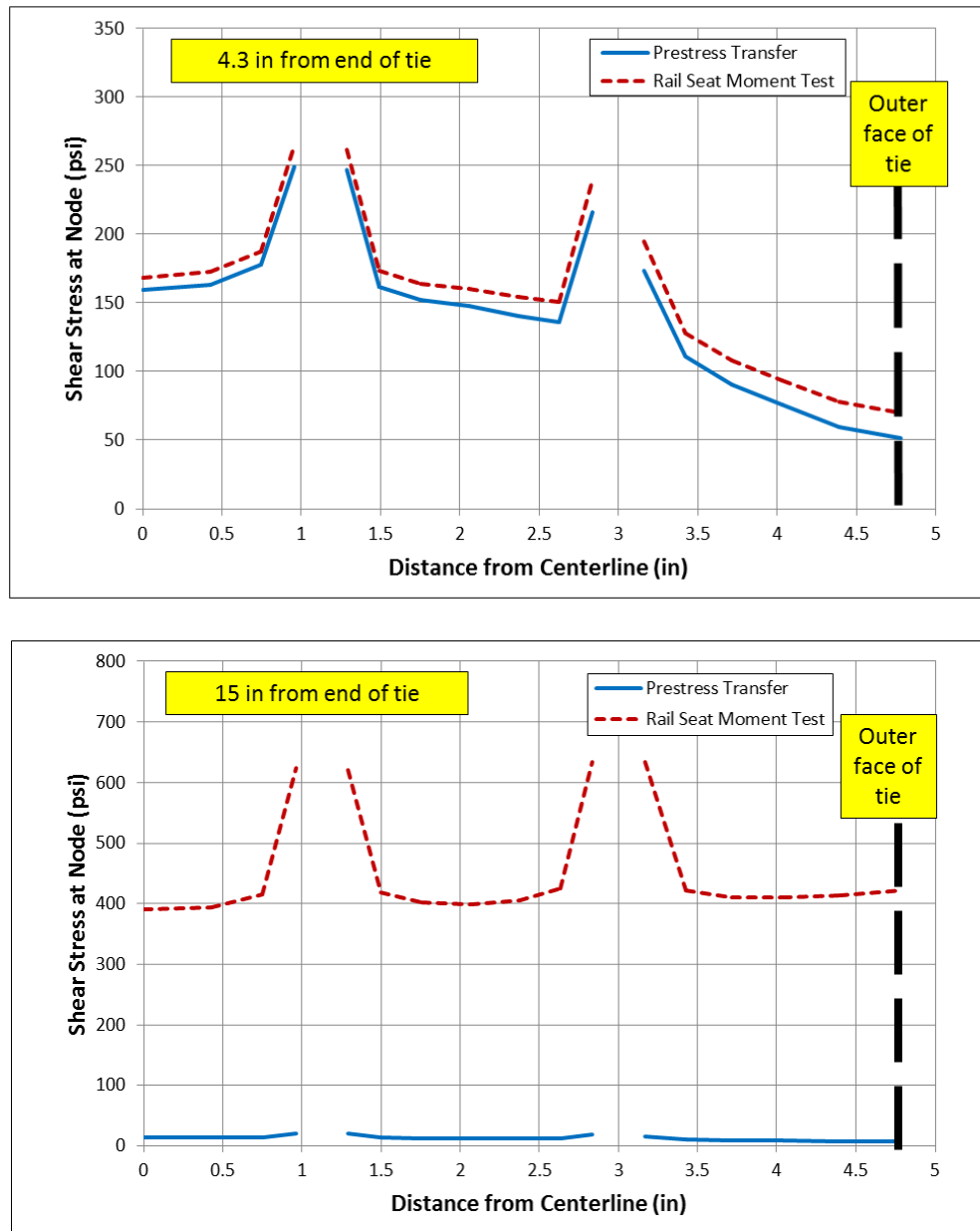


Figure 7.24. The calculated shear stress distribution along a path through the top row of strands for the application of a 52 kip vertical load at the rail seat: (top plot) at 4.3 in from the tie end; (bottom plot) at 15 in from the tie end.

7.4.2 Stresses from the Shoulder Inserts

We also calculated the stresses induced by a load through the rail clip shoulder insert. Such loads arise from the as-installed load, lateral load on the rail, or, under extreme dynamic conditions, from inertia if the tie is moving downward relative to the rail. The shoulder insert is relatively close to the strands inside the tie and there was concern that stress concentrations from the insert could promote cracking near the strands. Figure 7.25 shows the finite element model

we used for this study. We used a symmetric model that was derived from the model used to calculate prestress and flexural stresses. The model for the insert and the concrete surrounding it had a finer mesh and we used constraints to join the two meshes. The geometry of the insert is idealized from the pre-2003 drawing that fits an e-clip fastener. The insert was assigned the elastic properties of steel and was assumed to be bonded to the concrete at all points at which the two make contact. We modeled only the shoulder insert closest to the tie end for simplicity. The distance from the tie end to the center of this insert is approximately 17 in.

Figure 7.26 shows a transverse cross section through the insert and the reinforcing strands to highlight the proximity of the insert to the strands for the pre-2003 tie design. The nominal, minimum distance between the insert and a strand—the upper, central strand—is 0.66 in.

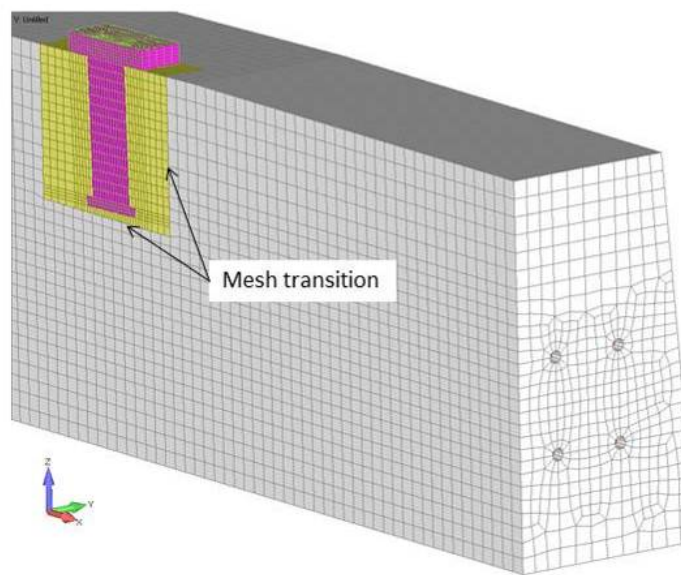


Figure 7.25. The finite element mesh for the pre-2003 concrete tie-shoulder insert analysis.

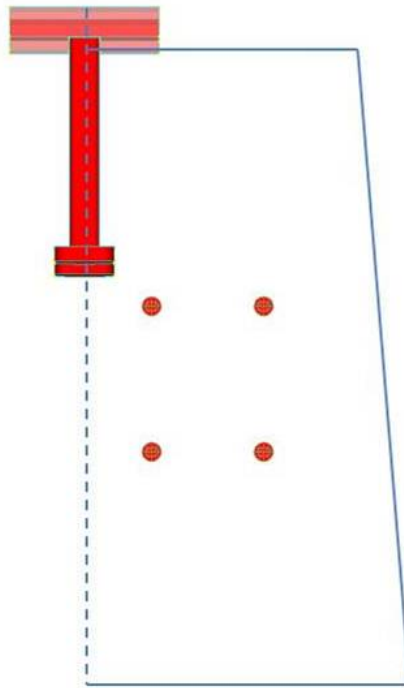


Figure 7.26. A cross-section through the pre-2003 concrete tie model showing the proximity of the shoulder insert to the reinforcing strands.

We present results for two cases:

1. Pre-stress with a 2,750 rail clip load, meant to represent the preload of the clip, and a 52 kip positive rail seat moment load.
2. The same as case 1, but with the addition of a 5 kip, upward vertical load on the insert meant to represent the load from a lateral rail force.

The stresses around the strands are not changed substantially by the presence of the insert. Figure 7.27 shows the distribution of shear stresses in the pre-2003 tie for load case 1. The cross section in the figure shows some slight stress concentrations in the concrete adjacent to the top row of strands; note this cross section is 12 in from the location of the maximum vertical tensile bursting stresses. Figure 7.28 shows the distribution of vertical tensile stresses with the addition of a 5 kip upward load (case 2). The cross section in the figure shows that vertical tensile stresses are transferred from the bottom of the shoulder insert to the top row of prestressing strands. The maximum vertical tensile stress in line with the strands is 250 psi. We simulated the bottom of the insert as being bonded to the concrete. In reality this interface could probably not carry significant tension and so the details of the stress distribution would change, but the overall stress field would be similar. These latter results suggest that under the action of a substantial lateral load the vertical tensile stresses near the strands can be elevated, but only locally.

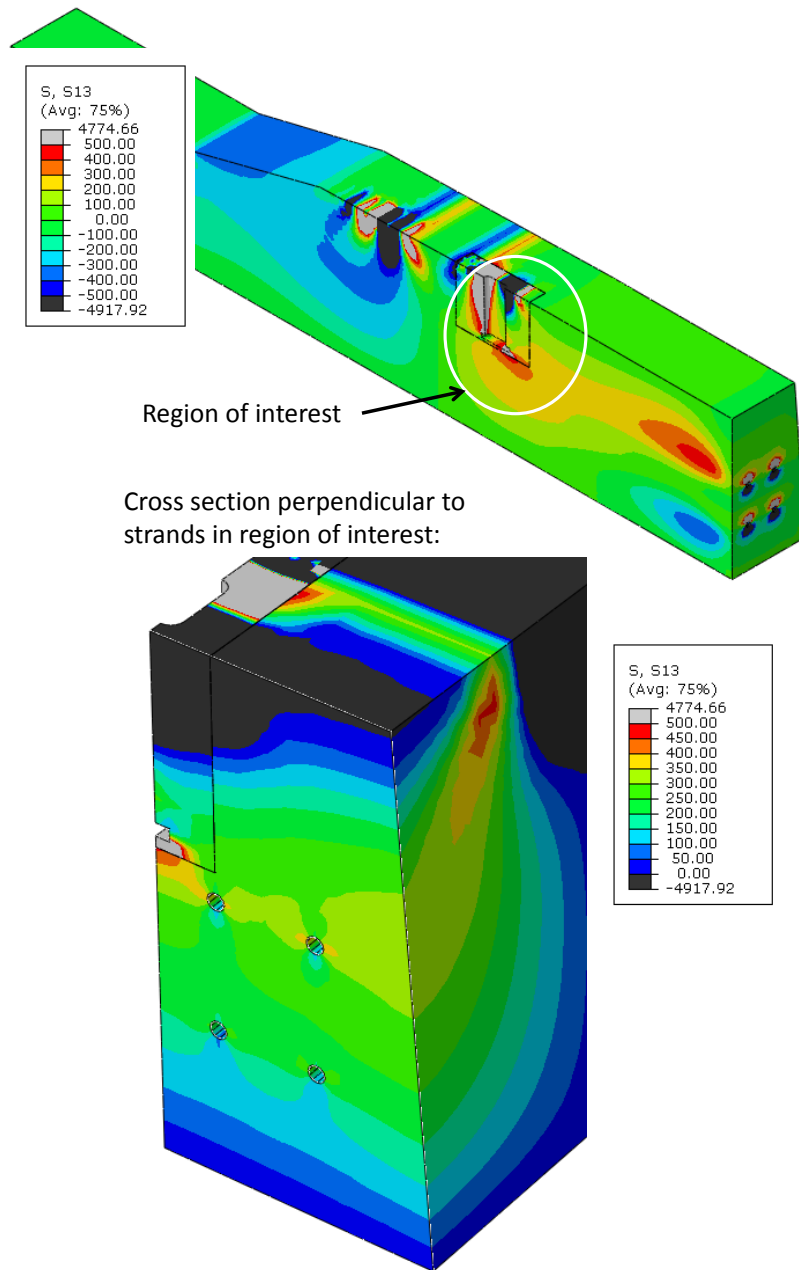


Figure 7.27. Shear stress distribution in the pre-2003 tie with shoulder insert subjected to a 52 kip downward load at rail seat and supported on ballast.

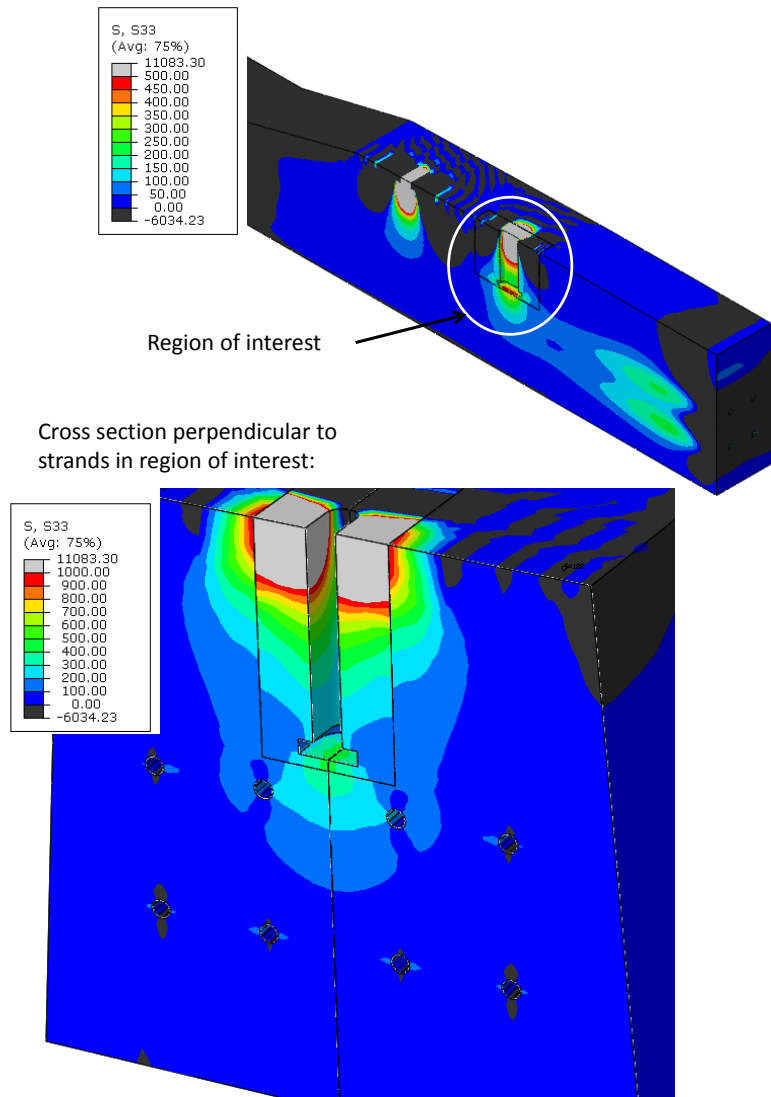


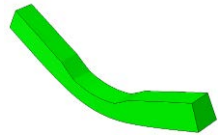









Figure 7.28. Vertical tensile stress distribution in the pre-2003 tie with shoulder insert subjected to a 5 kip upward load at rail seat and supported on ballast.

7.4.3 Vibration and Dynamic Loading Analyses

Another possible source of stress, one that is cyclic and, therefore, could cause fatigue, is vibration of the ties. Our field tests (Section 6) show that the tie does vibrate in service and predominantly in the bending modes. We conducted finite element calculations to determine the first ten vibration modes and the type of stresses induced by these modes. We also conducted some calculations to simulate impact loads.

We first modeled the tie as completely unrestrained to calculate natural frequencies. We included the reinforcing strands in this model (bonded to the concrete along their entire length in this case for simplicity) and the elastic properties of the concrete were: $E = 4.77 \times 10^6 \text{ lb/in}^2$; Poisson's ratio = 0.17. Table 7.4 lists the first ten natural frequencies and corresponding modes.

Table 7.4. Calculated natural frequencies for the concrete tie.

Mode	Frequency (Hz)	Mode Shape	
1	100	Simple bending about a transverse axis in the center of the tie	
2	131	Simple bending about a vertical axis in the center of the tie	
3	309	Asymmetric bending (S shape)	
4	346	Torsion	
5	357	Torsion	
6	598	Double vertical bending	
7	658	Double lateral bending	
8	678	Combined bending and axial	
9	897	Double torsion	
10	925	Asymmetric, double vertical bending	

The addition of track components will change these natural frequencies, but not substantially. The weight of the tie is approximately 800 lb and that of the pad, insulators, and clips is less than 10 lb together. The rail weighs 136 lb/yd or 180 lb per tie when both rails and the tie spacing are considered. The modes and natural frequencies of the ties as determined by our field test were described in Section 6. We note that there is good agreement between the natural frequency of the first mode of true deformation in the field test and the model from the finite element analysis: 110 versus 100 Hz.

We also examined the type of stresses associated with the calculated modes of vibration and none of these modes induce significant vertical tensile stresses in the region at which cracks have been observed in the Amtrak ties.

We conducted finite element analysis to simulate a drop weight test of the type used to study pad attenuation properties. We used this as a surrogate to investigate the extent to which vertical tensile stresses are generated from an impact load. Figure 7.29 shows the geometric model used for this purpose; it has one plane of symmetry. We conducted our analysis using the same pre-2003 tie described earlier with the properties of a 136 lb/yd rail and a 0.25 inch-thick EVA pad ($E = 9300$ psi; $\nu = 0.48$). A 115-pound weight is dropped from a height of 12 in onto the short section of rail that is fastened to a concrete tie with simulated clips. The peak impact load we calculated from these analyses is 5,200 lb. This corresponds to a dynamic factor of about 1.2 for a wheel load of 25 kips, the nominal wheel load for the Acela power car. Figure 7.30 shows contours of vertical stress at a time at which they are close to maximum and Figure 7.31 shows a time-history plot of vertical stresses adjacent to one of the upper strands at the end of the tie. The maximum additional vertical tensile stress in vicinity of the strand is about 200 psi. This is not an insignificant stress. It will be greater for higher impact forces and could explain the occurrence of horizontal cracks in locations at which such impact forces occur. Comparable calculated stresses occur both for the bottom row of strands below the impactor and for both rows at the nonimpacted end. The occurrence of such stresses at the nonimpacted end is consistent with test observations [7.12] which showed that a horizontal crack was generated in such an impact test.

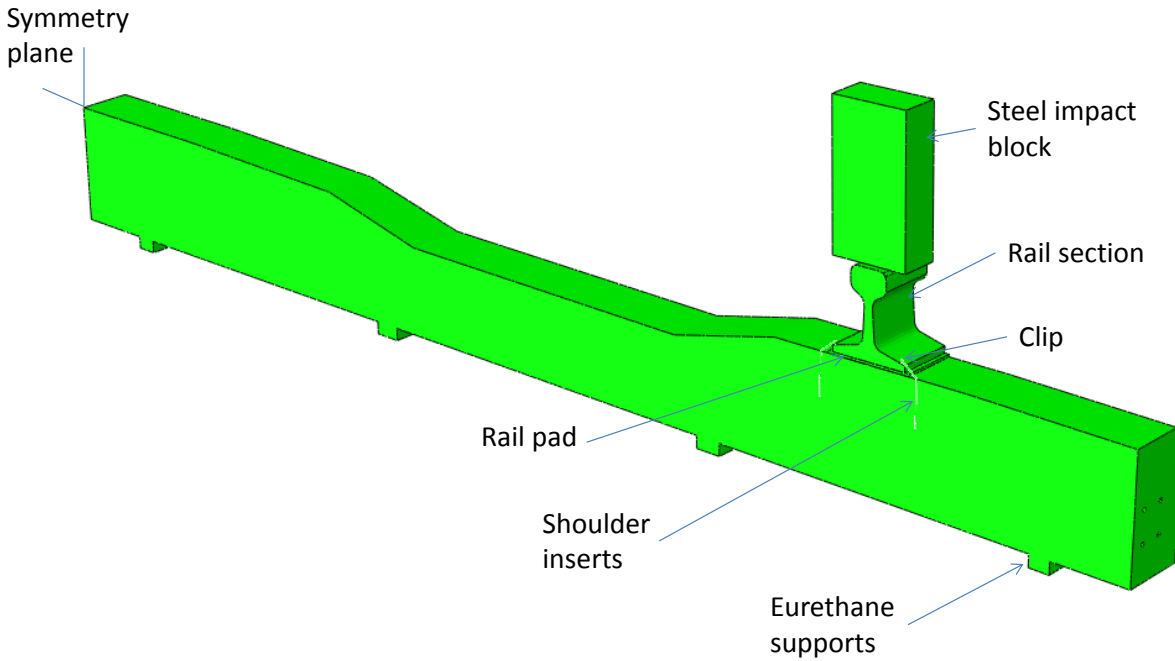


Figure 7.29. The finite element model used for dynamic impact analysis.

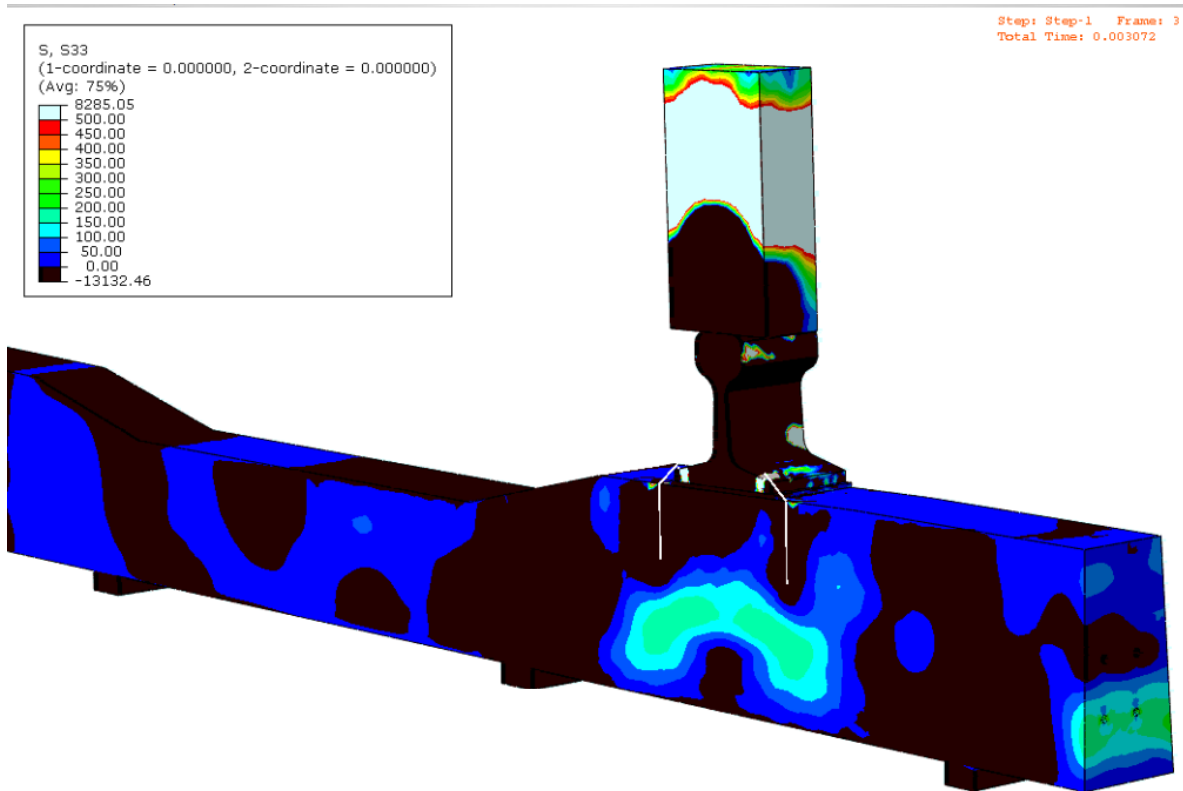


Figure 7.30. Vertical stress distribution at the center of the tie shortly after impact ($t = 3$ ms).

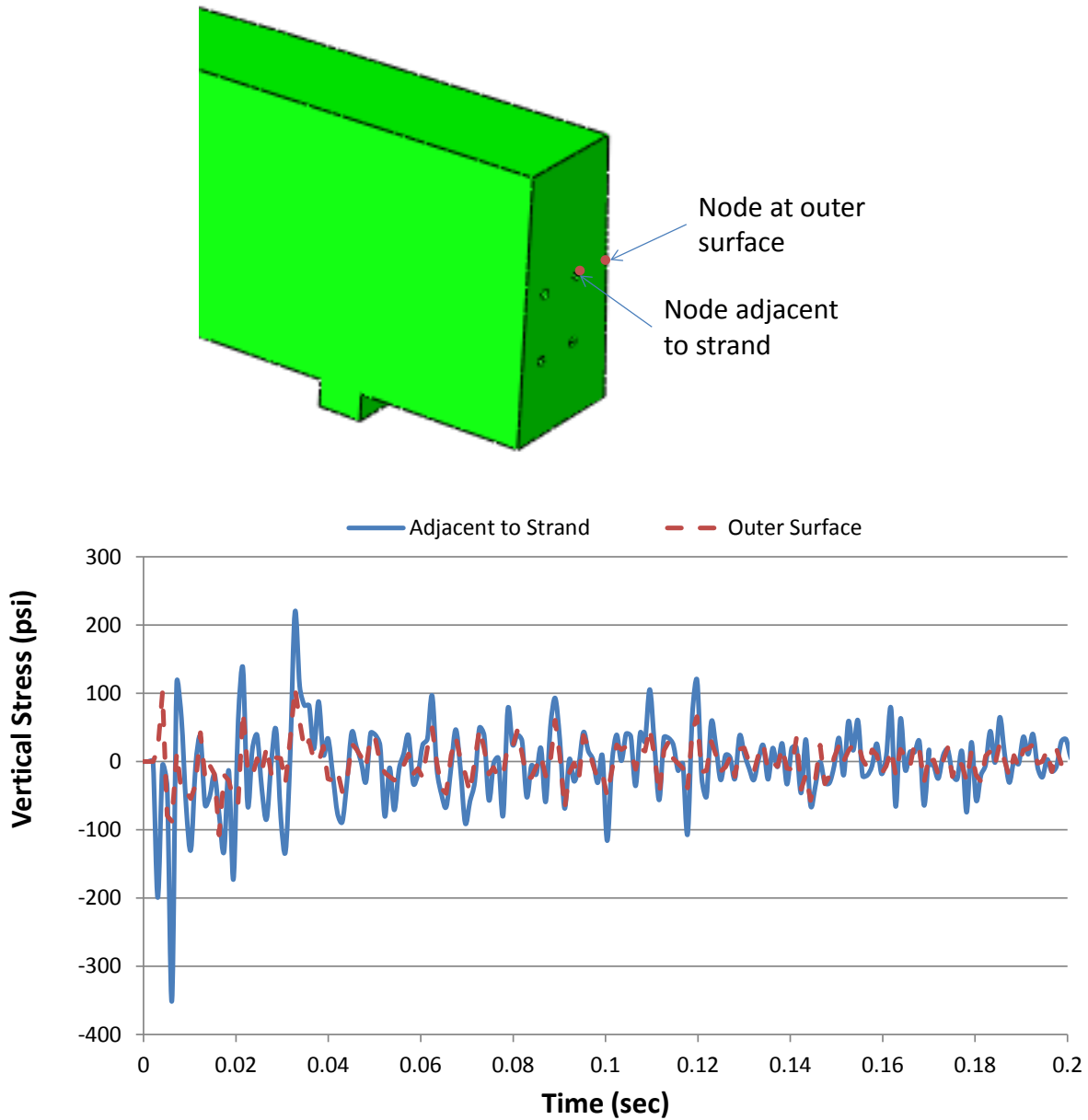


Figure 7.31. Time history of vertical stress in the concrete tie adjacent to a top strand and at the outer surface; tension is positive.

7.5 Strength Considerations

The finite element analysis results just described suggest that substantial vertical tensile stresses are generated adjacent to the strands immediately after release of the prestressing force. This is the direction of stress that would promote the type of cracking observed in the pre-2003 Amtrak ties. We have pointed out how horizontal (and vertical) cracks are sometimes observed at the ends of prestressed concrete members from splitting and bursting stresses (c.f. [7.5]). We now examine whether these stresses are sufficient to initiate a crack from material strength considerations.

While we have measured splitting tensile strength of concrete removed from the case study ties, we do not know what the tensile strength of the concrete was at the time of prestress transfer. We can estimate it by making assumptions about the compressive strength at prestress transfer and using the following relationship:

$$f_t = a\sqrt{f_c'} \quad (\text{Eq. 7.1})$$

where:

a = a factor that depends on the type of tension loading and the purpose of the tensile strength being used, and

f_c' = the compression strength.

A value of $a = 7.5$ is used in the ACI 318 design standard. We note that the value of the parameter 'a' from our own compression and tension splitting tests is as high as 10.3 (Table 7.5.). The required compression strength at the time of prestress transfer is 4,250 psi for the pre-2003 ties. The tensile strength from equation 7.1 is 489 psi, for $a = 7.5$, and 650 psi, for $a = 10$.

Table 7.5. Calculated and measured tensile strengths for the concrete of the Amtrak ties for different times after production.

Case study	Measured compression strength (psi)	Measured splitting tension strength (psi)	Effective parameter 'a' (equation 7.1)
Pre-2003 (ties 1 and 2)	9730	958	9.7
Post-2003 (tie 8)	8740	965	10.3
San-Vel	12190	925	8.4

Ignoring for the moment multiaxial stress effects, comparison of the calculated stresses in the vicinity of the strands in Figure 7.6 with these tensile strength values suggests a chance of cracking adjacent to the strands, but not necessarily across the entire width of the tie.

Multiaxial stresses can significantly reduce the tensile stress at which cracking occurs. There are many theories of concrete fracture, but a consideration of biaxial stresses provides some indication of the magnitude by which the tensile strength can be reduced. Figure 7.32 shows that the tensile stress required to cause failure is reduced as the compressive stress in the transverse direction increases in magnitude relative to the compressive strength of the concrete; σ_c is the uniaxial compressive strength in this plot [7.13].

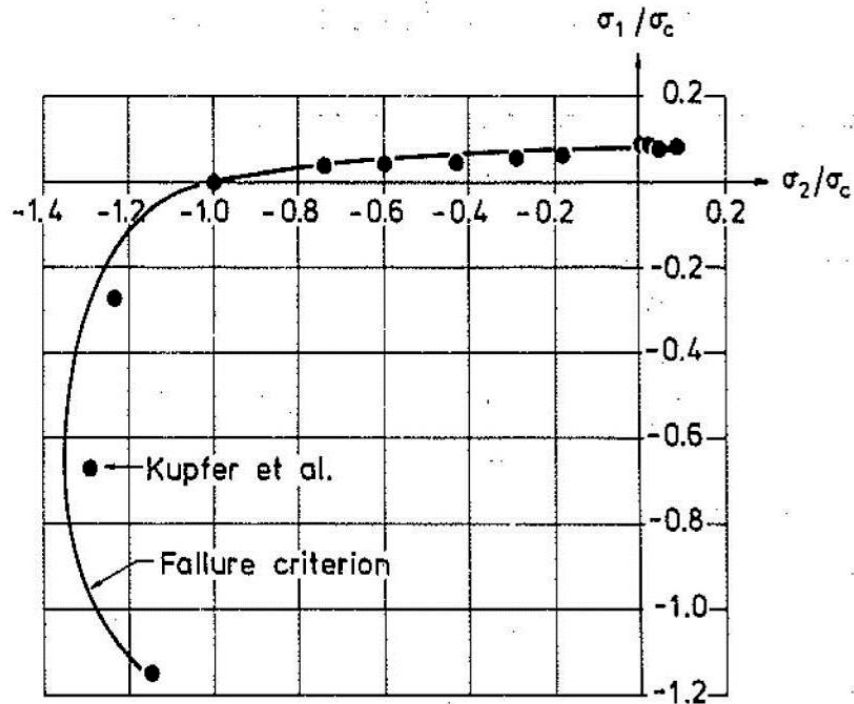


Figure 7.32. Biaxial strength results for an 8,500 psi compression strength concrete (from [7.13]).

At the outer face of the tie where maximum vertical (bursting) tensile stresses occur, the principal stresses at prestress transfer for the pre-2003 tie from our model results are as follows:

- Maximum principal = 260 psi,
- Median principal = -10 psi, and
- Minimum principal = -780 psi.

This point approximates a two-dimensional stress state because the median principal stress is negligible, so that Figure 7.32 is applicable. The ratio of σ_2/σ_c depends on the value used for σ_c . The compression strength at prestress transfer, from Table 7.4, is at least 4,250 psi. With this value, the ordinate σ_2/σ_c is 0.18 indicating a reduction in the tensile strength of around 20 percent. As the strength of the concrete increases, the predicted reduction in tensile strength will be less. A 20 percent reduction in strength is not enough to indicate that bursting cracks will occur immediately, consistent with the observation that cracks in the ties appear after some time. However, the minimum principal stress is approximately the same in the interior of the tie at the top row of strands, and a reduction in tensile strength suggests that internal cracking (splitting) would be more likely.

There is a potential for cyclic stresses to affect the propensity for cracking. The primary cyclic stresses arise from wheel loads. We showed in Figure 7.24 that there can be a relatively high cyclic shear stress, but this is only in the vicinity of the rail seat. There is also a cyclic vertical stress (compressive) arising from the vertical wheel load, but this too is in the vicinity of the rail

seat. It seems likely that if these cyclic stresses play a role, it is in propagating a crack rather than initiating one.

We note that the strength of the tie, at least with respect to the horizontal cracking, changes once cracking initiates. There are two effects to consider. If cracking occurs adjacent to the strands (splitting), then there will be a loss in ability to generate friction or mechanical locking because the force associated with the Poisson expansion will be lower. This should cause the strand to slip, which will affect the transfer length. In effect, the part of the strand over which force transfer occurs will move toward the rail seat, potentially propagating the crack in that direction, but the magnitude of prestressing force will decrease as the overall strand shortens. We expect the prestressing force in the top row to be lost entirely with substantial cracking. It is interesting to note that the calculated initial flexural cracking strength and the ultimate flexural strength of a tie in which only the bottom strands have prestress are only 16 and 18 percent lower than those for which the top row is also prestressed.

Even though we expect the prestressing force to decrease with cracking, we also expect the stresses required to propagate the crack to be lower. Perhaps the initial cracking is driven by the splitting and bursting stresses and subsequent cracking is driven by cyclic stresses from wheel loads as the crack reaches the rail seat area. The field of concrete fracture mechanics is not well developed and we have not pursued its application in this project.

7.6 Discussion on the Vertical Location at which Cracks Occur

We are now in a position to consider possible reasons for why cracks are observed at the top row of strands in the pre-2003 tie design (which also includes the MBTA ties) rather than the bottom row. We discuss three factors here:

- 1) magnitude of the vertical stress,
- 2) amount of concrete cover, and
- 3) magnitude of cyclic stresses.

The vertical tensile (bursting) stresses due to the longitudinal strand loads in the pre-2003 tie are greatest at the outer tie face adjacent to the top row of strands. Figure 7.33 shows the distribution of vertical tensile stresses at a cross section of the pre-2003 tie taken perpendicular to the strands at the location of maximum bursting stresses (about 4 in from the tie end); the maximum bursting stress is 35 percent greater adjacent to the top row than at the bottom row. Figure 7.33 also shows the distribution of splitting stresses in concrete adjacent to the strands due to the Hoyer effect. Recall from Section 7.2.2 that we expect the magnitude of splitting stresses in the actual tie to increase due to mechanical interlock between the concrete and the deformed surface of the strands. There is also evidence that resistance to splitting is related to the concrete cover provided to prestressing strands, as demonstrated in [7.6], although no quantitative relationship was given in that reference. Table 7.6 lists the nominal minimum concrete cover for different rows of strands in the case study ties. The amount of concrete cover in the pre-2003

ties (and the other ties) is less for the top row of strands than for the bottom row: 1.59 versus 1.79 in. Therefore, the potential for splitting is greater at the top row of strands.

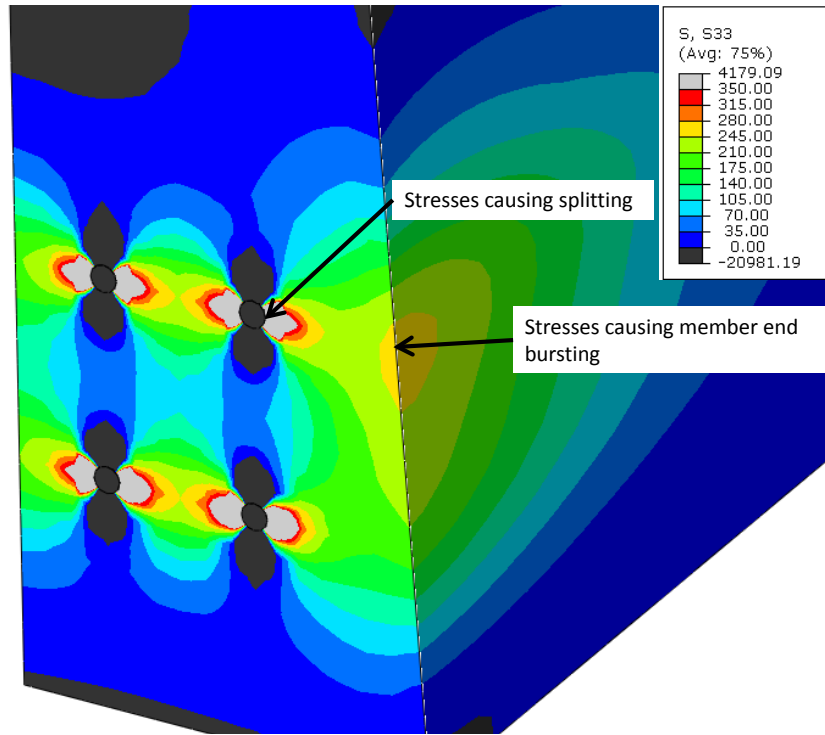


Figure 7.33. Vertical tensile stress distribution at a section of the pre-2003 tie taken perpendicular to the strands at the location of maximum bursting stress.

Table 7.6. Comparison of maximum bursting stresses and clear concrete cover to the tie side for different tie designs.

Tie design	Strand row	Outer surface vertical stress (psi)	Concrete cover to tie side (inches)
Pre-2003 (and MBTA tie)	Top	258	1.59
	Bottom	191	1.79
Post-2003	Row 1 (top)	289	1.39
	Row 2	351	1.49
San-Vel	Top	205	1.61
	Bottom	173	2.01

If horizontal cracking occurred at the top row of strands for the pre-2003 tie because bursting stresses were greater adjacent to the top row and concrete cover to the side surface was less at the

top row, then this has implications for the post-2003 tie design. Figure 7.34 shows the distribution of vertical tensile stresses at a cross section of the post-2003 tie taken perpendicular to the strands at the location of maximum bursting stresses (about 4 in from the tie end). Calculated maximum vertical tensile stress due to member end bursting is 40 percent higher in the post-2003 tie model than in the pre-2003 tie model; splitting stresses captured by the model are similar. Note that maximum bursting stress at the outer tie face does not occur adjacent to the top row of strands; it occurs adjacent to the row of strands second from the top. Maximum bursting stress adjacent to the row second from top is 21 percent greater than the maximum bursting stress adjacent to the top row. Additionally, clear concrete cover provided to the top row is only 7 percent less than the clear cover provided to the row second from top. Based on this, it seems likely that if horizontal cracking were to occur in the post-2003 tie, it would initiate at the row second from top.

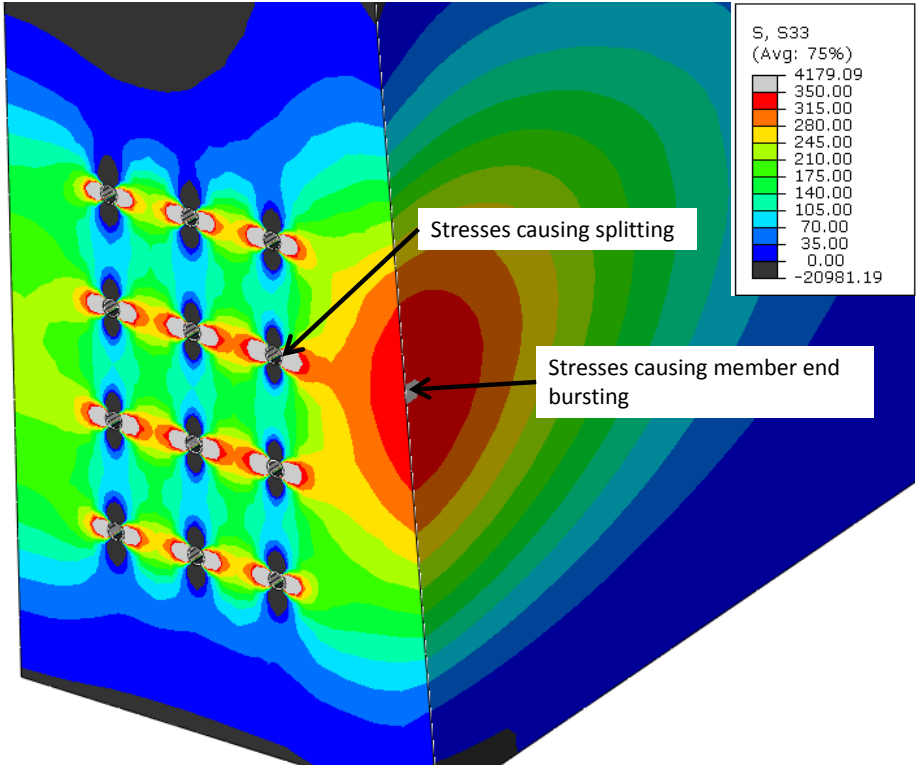


Figure 7.34. Vertical tensile stress distribution at a section of the post-2003 tie taken perpendicular to the strands at the location of maximum bursting stress.

8. Evaluation of Contributing Factors

In this section, we consider the work that we and others have conducted in various technical areas to determine which factors contribute to the performance of the concrete ties in the NEC. By performance, we mean the resistance against cracking and, in particular, against the type of cracking that seems to be most prevalent along the NEC. Although cracking of some form or another can be caused by just about any factor being taken to extreme, for this study we focus on a relatively narrow range of factors pertaining to the nominal pre-2003 tie design. At the end of the section, we incorporate our findings regarding the changes made to the post-2003 ties and assess the effects of the changes on future performance.

8.1 Cracking of pre-2003 Ties

Recall the predominant form of cracking observed in concrete ties on the NEC. It consists of a horizontally oriented crack that intersects some or all of the tendons in the top row. In some cases, this crack extends to the very end of the tie, and in others it extends to the sloping section near the center of the tie. Sometimes it is observed on only one side of the tie and sometimes it appears to extend across the entire width. In its most severe form, the top section of the tie on one end fractures away, as shown in Figure 8.1.



Figure 8.1. A severe example of a tie with the predominant mode of cracking investigated in this study.

The various factors we considered in this project, some in more detail than others, include:

- Material parameters: cement, aggregate, water content, admixtures, air content, reinforcing steel;
- Manufacturing parameters: curing temperature, time, prestress release approach;
- Tie design: reinforcing steel dimensions, number, pattern and pre-stress level;
- Component properties: pad stiffness, clip insert position;
- Loading: vertical, lateral, impact, cyclic; and
- Environmental conditions: temperature, moisture.

As is the case for many failures or incidents, we find that the tie distress was caused by a combination of interacting factors. Based on our investigation, we divide these factors into primary, secondary, and noncontributory factors below.

8.1.1 Primary Factors

We find that the observed cracking is caused primarily by the combination of ASR and the mechanical vulnerability (splitting and bursting stresses in the concrete from the prestressed tendons) of the as-designed and as-manufactured ties to the splitting mode failure. Ties experiencing both of these conditions show the characteristic horizontal splitting, and ties without both of these conditions appear to be performing satisfactorily.

The ASR is implicated by:

- The presence of ASR in the vicinity of the top strands of ties experiencing horizontal cracking, with ties with higher levels of petrographic evidence of ASR exhibiting a higher degree of visible distress.
- The presence of ASR only in the pre-2003 ties and not in the well-performing San-Vel or post-2003 ties.

As discussed previously, we cannot classify the ASR as the sole cause of the cracking because the lack of ASR damage and visible deposits away from the cracked area indicates that the ASR has not progressed to a level at which it would cause cracking on its own.

Discussion of the ability of ASR to contribute to the observed tie failures without causing typical ASR map cracking can be found in the limited available literature describing the mechanism and expansion process of ASR. As previously stated in Section 4.3.4, ASR first causes initial pressures to develop in the concrete; the pressures build to a point where they fracture the concrete and the second stage of ASR (deposition of gel and rapid swelling) occurs. In the pre-2003 ties, we believe that the initial ASR pressures have not yet generated concrete cracking pressures by themselves (as indicated by the lack of widespread characteristic map-pattern

cracking throughout the tie), but have reached a level sufficient to contribute to cracking at the level of the tendons where they are additive to the stresses due to the prestressing.

The mechanical vulnerability of the as-designed and as-manufactured pre-2003 ties to splitting-mode failure is shown by:

- The occurrence of the crack at the same location where our modeling work indicates elevated vertical splitting and bursting stresses occur;
- Evidence that the prestressing forces are relatively high, which promotes higher splitting and bursting stresses; and
- The absence of protection against splitting in concrete tie design, even though such a failure mode is recognized and designed against in the general prestressed concrete member industry.

We cannot classify the mechanical vulnerability of the as-designed and as-manufactured ties as the sole cause of the cracking because the San-Vel and post-2003 ties have similar vulnerabilities but do not exhibit horizontal splitting failures and because our analysis indicates that the splitting stresses are not enough to cause failure by themselves.

We find that the ASR and mechanical vulnerability of the ties combine in the pre-2003 ties in the following manner:

1. The ties were designed for flexure evidently without consideration for splitting and bursting forces, resulting in an emphasis on high prestressing forces and short development lengths. Without a design check or criteria for splitting type failure modes, this led to a tie without stirrups or without a significant safety factor against splitting and bursting, leaving little reserve capacity for this failure mode.
2. Release of the strand forces into the ties during manufacture created a plane of vertical tensile stresses at the level of the prestressing strands through a combination of pressure from the strand expansion (the Hoyer effect) and the relatively concentrated longitudinal forces in the transfer zone.
3. The aggregates thought to be nonreactive due to passing the specified ASTM C227 and C289 during manufacture (tests that are now known to not always detect slowly-reacting aggregates) were in fact reactive, as shown by the observed ASR in all of the petrographic reports on the pre-2003 ties. The initial phase ASR in the ties created additional forces in the concrete that were additive to the existing (mechanical) stresses. Although initial-phase ASR can, in general, develop stresses sufficient to crack concrete on its own (as shown by the formation of cracks in other ASR affected concretes), the stresses in the pre-2003 ties were somewhat less than the full cracking pressures as shown by the lack of ASR-related map cracking elsewhere in the ties.

4. The stresses from the prestressing and the ASR combine to crack the concrete in the vicinity of the strands, where the existing stresses are highest. This is supported by our petrographic observations of cracking only in the vicinity of the strands.

8.1.2 Secondary Factors

Our results indicate that there are secondary factors that contributed to the cracking process. These factors include:

- **Continuing ASR.** Once cracking initiates, it can then propagate through a combination of continued ASR gel formation and expansion within the cracks (as observed in our petrographic observations) and mechanical stresses.
- **Transfer length.** The bond between tendon and concrete is an important secondary factor affecting concrete tie performance because it relates to the degree and distribution of the stresses induced by the prestressing, with higher bond strength leading to shorter transfer lengths which in turn result in greater vertical (bursting) tensile stresses. The bond strength is affected by the deformation features on the prestressing wires, by chemical characteristics of the concrete, and by concrete strength. We did not investigate the effect of wire indentation feature on bond strength directly in this study, but others have (c.f. [7.5]) and find that deeper indentations reduce transfer length. There is a significant difference between the indentations in the pre-2003 ties and in the San-Vel ties: the latter are smaller and should therefore create longer transfer lengths and lower stresses. This is consistent with the observed better performance of the San-Vel ties in service.
- **Tie manufacturing processes.** Our assessment of the factors related to the manufacturing process has been qualitative. The ties are cured by an accelerated process and so the time-temperature history is an important parameter. We suggested in the materials section of this report that the rapid curing of the concrete afforded by this process, though highly desirable from a manufacturing point of view, could lead to higher-than-necessary concrete strengths at the time the prestressing tendons are cut, and this would result in shorter transfer lengths and higher bursting stresses. Similarly, other unquantifiable items could contribute; for example, disturbances due to removal of the end bars and the method of detensioning and cutting the strands.
- **External loading.** The contribution that external loading makes to the driving force for the horizontal cracking varies by loading type. The most frequent type of loading, flexure, actually decreases the vertical stress by approximately 20 percent near the outer surfaces of the pre-2003 tie at its ends, where the vertical prestress stresses are highest. However, flexural loads induce a relatively high cyclic shear stress at the top row of tendons near the rail seat and are likely a source of crack propagation.
- **Time effects.** While it cannot be classified as a cause of the observed distress, time is an important factor in the performance of the ties. The ties currently being replaced in the NEC are of an approximately 1994-1998 vintage. The widespread cracking problem did not reveal itself until approximately 10 years after the ties were installed. While this is partly due to the sensitivity of inspection techniques employed, it also points to the

importance of time-based mechanisms. For example, the occurrence and significant propagation of cracking could be related to the time required for a severe impact loading to occur at that particular location. However, we believe that it is more likely that time is required for the progression of ASR damage and that this damage initiates and contributes to some propagation of cracks.

8.1.3 Non-Contributory Factors

As described in Section 4.5, we did not find evidence of DEF or cyclic freezing and thawing as contributing mechanisms to the most predominant type of cracking. The lack of contribution is confirmed by the work of CTL and LML, which did not find DEF in the ties exhibiting the predominant damage mode and their conclusions that it was a potential cause only in the atypical ties that showed widespread map pattern cracking throughout the tie. Our conclusion regarding the lack of effect of cyclic freezing and thawing is supported by our petrographic observations (which do not reveal any indications of widespread damage characteristic of cyclic freezing and thawing), the results of the ASTM C666 (Resistance of Concrete to Rapid Freezing and Thawing) test data from the original production runs of the pre-2003 ties, which showed acceptable durability factors, and by the findings of CTL and LML in their work.

We also do not find that dynamic loading is a contributing factor. The modes of vibration that occur in track do not appear to raise the stress significantly. On the other hand, vertical impact loading of the type that could be caused by a defective wheel increases the tensile stress significantly, and we expect it could be an important factor in determining where cracking occurs in track. However, we do not have evidence that this type of impact loading has been present at all locations at which ties have cracked (for example, sidings) and, therefore, classify impact and vibration as noncontributing.

Our detailed analysis of the stress state in the vicinity of the clip insert, which at one point is within approximately 0.6 in of a top tendon, indicates that such stresses are also not contributing to the horizontal cracking.

8.2 Expectation of Future Performance of the Post-2003 Ties

The post-2003 revisions to the portions of the concrete specifications related to the manufacturing processes are consistent with good current practice. The specifications have been changed to include new tests that better identify potential ASR and are more conservative in avoiding use of vulnerable aggregates. ASR was a primary contributor to the horizontal cracking in the pre-2003 ties, in combination with the high stresses due to the strand stresses and configuration. The specific measures taken to avoid ASR in the post-2003 tie specification (including improved ASTM standard ASR screening tests to identify reactive aggregate, continued use of low-alkali cement, and inclusion of fly ash to mitigate the reaction) will reduce the likelihood of tie cracking. In addition, the specifications have been updated throughout the 1990s and in 2003 to better avoid other problems that could occur or have occurred in the past, such as DEF and freezing and thawing.

Our investigation shows that while high stresses exist in both the seven-wire configuration used in the pre-2003 and San-Vel ties and in the post-2003 single wire tendon configurations, the calculated vertical stresses in the post-2003 tie 24-wire configuration are actually greater than in the seven-wire strand pre-2003 tie configuration, assuming comparable transfer lengths. This is primarily because the prestressing force is greater in the post-2003 ties. While the stresses due to this prestressing appear insufficient to cause cracking on their own because of the improved concrete ASR resistance, we caution that the revisions to the specifications made in 2003 did not address the tendency for splitting or bursting stresses to develop. The prestressed concrete industry outside of tie manufacturing recognizes this potential problem and includes specific measures, such as vertical stirrups and associated quantitative procedures for stirrup design, to ensure that cracking from this effect does not significantly degrade the condition of the member.

9. Summary and Conclusions

The study reported here was aimed at determining the factors that caused the cracking of concrete ties on the NEC. We investigated several factors including concrete composition, reinforcement characteristics, manufacturing methods, tie design parameters, and types of loading.

The cracking of greatest concern occurred in ties manufactured and installed in the circa 1994–1998 period, which we refer to as the pre-2003 ties because they were made to a set of very similar specifications generated before 2003. The predominant mode of cracking is a horizontal crack that passes through the top row of steel reinforcing strands, generally near one or both ends of a tie. In its most severe condition, the crack eventually turns and intersects the top surface, rendering the tie incapable of fulfilling its function in track.

Our work included several tasks. We examined sets of ties we divided into case studies, each with some distinguishing feature. The case studies were:

- Pre-2003 NEC ties with no externally visible cracking or minor cracking.
- Pre-2003 NEC ties with clear visible cracking.
- Post-2003 NEC ties. These are ties made to the 2003 specification with a very different prestressing tendon configuration and modified concrete material requirements.
- MBTA ties from the Old Colony Line that have a design essentially identical to the pre-2003 NEC ties and which showed the same type of horizontal cracking.
- San-Vel NEC ties from approximately 1978 that have shown virtually no signs of cracking.

We examined these ties in the field and had some sent to our laboratories for more detailed analysis. This analysis included detailed petrographic evaluations of the condition of the ties, the material composition and condition, and mechanical properties of the tie material. We also reviewed petrographic reports on the cracking problem generated by third parties for Amtrak and production test records from pre-2003 and post-2003 ties.

We carried out finite element analysis to investigate the effects of various tie and external loading parameters on the types of stresses potentially influencing the initiation of the predominant mode of cracking observed in the field. This analysis was validated to some degree by results from a field test we conducted on a section of the NEC in Rhode Island. We measured loads into the track as well as the loads, strains, and accelerations of the concrete ties themselves.

We found that that the tie cracking was caused by a combination of factors, none of which would have caused the distress on its own. The primary factors contributing to the distress are:

- A high concentration of tensile stress in the ties at the level of the prestressing steel due to forces associated with the transfer of load from the steel to the concrete during the strand detensioning process. These stresses are greatest at the top row of tendons.
- Stresses within the concrete from the pressure caused by ASR. Although ASR pressures start to build once the reaction has begun and can eventually cause widespread general map cracking solely due to ASR, in the ties, the pressures were additive to the stresses at the level of the tendons due to the prestressing, causing the failure to occur at the level of the strands before the ASR progressed sufficiently to cause typical ASR pattern cracking elsewhere in the ties where forces from the prestressing were not present.

After the cracking occurred at the zone of highest stress where the ASR and prestressing stresses combined at the upper prestressing tendon level, it was then easier for it to propagate there rather than form at new locations. Our work shows that this propagation was assisted by the following secondary factors, which were not initial causes of the distress:

- Continued ASR, with additional pressures created by the rapid swelling of gel deposited within the cracks formed by the combination of ASR pressures and the stresses due to the prestressing forces.
- A likely shorter length over which stresses are transferred from the prestressing strands to the concrete because of more distinct strand indentations in the pre-2003 ties, as compared with the strand indentations used in the San-Vel ties. This caused higher bursting stresses in the pre-2003 ties.
- External, repeated loading from passing trains.

Lastly, we found that that the tie distress was not caused by the following factors:

- Cyclic freezing and thawing,
- DEF, or
- Stresses from other mechanical effects, such as from fastener inserts or unusual tie vibrations.

Our assessment of the post-2003 ties, with their different prestressing tendon configuration and alternate material requirements, suggests they will not develop horizontal cracks. Although the stresses appear to be comparable adjacent to the strands and higher on the surface (bursting stresses) than for the pre-2003 ties, the specifications had been improved to reduce or eliminate ASR. This was achieved by better screening tests and improved ASR mitigation measures. In addition, the aggregate used in the post-2003 ties we examined is a carbonate aggregate not susceptible to ASR.

We note that the splitting and bursting failure mode that represents the dominant form of cracking in the NEC ties is known in the general prestressed concrete industry. However, specifications and designs of concrete ties do not explicitly address it. In fact, the changes made

to the mechanical specifications in 2003 increase resistance to flexural failure, perhaps unnecessarily, and increase splitting and bursting stresses without corresponding protection. We believe that the specifications should be changed to protect against this failure mode.

10. References

- 1.1 Coleman, J.W., “Delayed Ettringite Formation versus Alkali-Silica Reaction,” *Concrete International*, July 2011, 76-77.
- 2.1 Amtrak, National Railroad Passenger Corporation Technical Provisions CT10, Concrete Cross Tie and Fastening Assembly, 1992, 1995, 2003.
- 2.2 Ahlbeck, D.R., J.M. Tuten, H.A. Hadden, and H.D. Harrison, “Development of Safety Criteria for Evaluating Concrete Tie Track in the Northeast Corridor,” Volume 1, Remedial Projects Assessment, Report No. FRA/ORD-86/08.1 (June 1986), 105 pp.
- 3.1 Carino, N.J., “The Impact-Echo Method: An Overview,” *Proceedings of 2001 Structures Congress and Exposition*, May 21-23, 2001, Washington, DC, ASCE (2001), 18 pp.
- 4.1 PCI MNL 116 – Manual for Quality Control for Plants and Productions of Precast and Prestressed Concrete Products.
- 4.2 Tracy, S.L., Boyd, S.R., and Connolly, J.D., “Effect of Curing Temperature and Cement Chemistry on the Potential for Concrete Expansion Due to DEF,” *PCI Journal*, January, February 2004.
- 4.3 Dinal, A., “The Determination of Gel Swelling Pressure of Reactive Aggregates by ASGPM Device and a New Reactive-Innocuous Aggregate Decision Chart,” *Construction and Building Materials* 22, Elsevier Publishing, 2008.
- 4.4 American Concrete Institute’s (ACI’s) Committee ACI 221, ACI 221.1R-98 Report on Alkali-Aggregate Reactivity, Manual of Concrete Practice, American Concrete Institute. (Reapproved 2008).
- 4.5 Powers, L.J., “Evaluation of Cracking in Precast Concrete Rail Ties,” CTL Construction Technology Laboratories, Inc., February 9, 2001.
- 4.6 Powers, L.J., “Petrographic Examination of Cores Taken From Concrete Rail Ties, Amtrak,” CTL Construction Technology Laboratories, Inc., October 9, 2001.
- 4.7 Lee, S.Y., “Petrographic Examination of Concrete Rail Ties–Amtrak,” CTL Group, September 23, 2009.
- 4.8 “Test Results of Duggan Tests of Two Concrete Rail Ties Identified as ‘Tie 1362’ and ‘Tie 150,’” CTL Construction Technology Laboratories, Inc., November 14, 2001.
- 4.9 “Petrographic Examination of Concrete Cores Taken From Prestressed Concrete Railroad Ties (VFL Project 22260),” Lankard Materials Laboratory, Inc., January 10, 2001.
- 4.10 “Petrographic Examination of Concrete Cores Taken From Prestressed Concrete Railroad Ties (VFL Project 22467B),” Lankard Materials Laboratory, Inc., October 31, 2001.
- 4.11 “Investigation of Pre-stressed Concrete Railroad Ties,” Valley Force Laboratories, Inc., January 25, 2001.
- 4.12 “Investigation of Pre-stressed Concrete Railroad Ties, Chloride-ion Content of Tie #1205,” Valley Force Laboratories, Inc., February 6, 2001.

- 4.13 Physical Properties Testing, Hanson Aggregates, Project No. CT 13950-400, CTL Thompson Materials Engineers, Inc., 7 August 2007.
- 4.14 Physical Properties Testing, Alkali Aggregate Reactivity, Hanson No. 67 Stone and Sand, Project No. CT 13950-400, CTL Thompson Materials Engineers, Inc., 7 February 2008.
- 4.15 Physical Properties Testing, Hanson No. 67 Stone and Sand, Project No. CT 13950-400, CTL Thompson Materials Engineers, Inc., 8 February 2008.
- 4.16 Hanson Pit Aggregates, Alkali-Silica Reaction Testing, Project No. CT 13950-400, CTL Thompson Materials Engineers, Inc., 29 February 2008.
- 4.17 Rapid Freeze-Thaw Test Results, ASTM C666, Project No. CT 13950-400, CTL Thompson Materials Engineers, Inc., 6 March 2008.
- 4.18 “Report on Petrographic Examination of Stone and Sand from the Hanson Concrete Aggregates Quarry Located in Downingtown, Pennsylvania,” DRP Consulting Inc., 7 December 2007.
- 4.19 “Report on Petrographic Examination of a Railroad Tie from the Rocla Concrete Railroad Tie, Inc. Plant located in Bear, Delaware, Tie Code 4394,” DRP Consulting Inc., 30 November 2007.
- 4.20 “Report on Petrographic Examination of a Railroad Tie from the Rocla Concrete Railroad Tie, Inc. Plant located in Bear, Delaware, Tie Code 3767-05,” DRP Consulting Inc., 18 February 2008.
- 4.21 “Report on Petrographic Examination of a Railroad Tie from the Rocla Concrete Railroad Tie, Inc. Plant located in Bear, Delaware, Tie Code A4446,” DRP Consulting Inc., 11 February 2008.
- 4.22 Lee, S.Y., “Petrographic Examination of Concrete Rail Ties Manufactured During 2003 through 2008 - Amtrak,” CTLGroup, 8 April 2009.
- 4.23 Bulletin 14 # HAP15A14 PA DOT Approved Source, Hanson Aggregates, Fax, 3 March 2008.
- 4.24 Amtrak the Cracking Issues, Investigation Results Corrective Action, Rocla, 21 February 2008.
- 4.25 Barenberg, E.J., et al., “Investigative Study of Concrete Crossties for Amtrak,” Phase 1 Report, Concrete Crosstie Manufacture, UIUC, 4 December 2009.
- 5.1 Nilson, A.H., *Design of Prestressed Concrete*, Second edition, 1987.
- 5.2 Gerwick, B. C., “Construction of Prestressed Concrete Structures, Second Edition,” John Wiley & Sons, Inc., New York, NY, (1993).
- 5.3 ACI318-05/318R-05, Building Code Requirements for Structural Concrete and Commentary, 2005.
- 5.4 Dolen, T.P., “Materials Properties Model of Aging Concrete,” Report DSO-05-05, Bureau of Reclamation (December 2005), 50 pp.

- 5.5 Bazant, Z.P., Kazemi, M.T., Hasegawa, T., and Mazars, J., "Size Effect in Brazilian Split-Cylinder Tests: Measurements and Fracture Analysis," *ACI Materials Journal* (May-June 1991) 325-332.
- 5.6 Tuchscherer, R.G., "Investigation of the Cracking Problem of Short Type IV Girders," M.S. Thesis, The University of Texas at Austin (May 2006) 190 pp.
- 6.1 Harrison, H.D. and D.R. Ahlbeck, "Development and Evaluation of Wayside Wheel/Rail Load Measurement Techniques," U.S. Department of Transportation Research and Special Programs Administration Transportation Systems Center – Publications – DOT TSC UMTA, 1981.
- 6.2 Staplin, D.E., "Future Development of Amtrak," presented at the Austrian Society for Traffic and Transport Science, Berlin, Germany, 10 Sept 2010.
- 7.1 Hay, W.W., *Railroad Engineering*, 2nd edition (John Wiley & Sons; New York) 1982.
- 7.2 AREMA *Manual of Railway Engineering – Volume 1: Track*, 2010.
- 7.3 *PCI Design Handbook*, 6th Edition, 2004.
- 7.4 AASHTO, *AASHTO LRFD Bridge Design Specifications*, 5th Edition, 2010.
- 7.5 Marshall, W.T. and A.H. Mattlock, "Control of Horizontal Cracking in the Ends of Pretensioned Prestressed Concrete Girders," *PCI Journal* (October 1962)56-74.
- 7.6 Galvez, J.C., J.M. Benitez, B. Tork, M.J. Casati, and D.A. Cendon, "Splitting failure of precast prestressed concrete during the release of the prestressing force," *Engineering Failure Analysis* 16 (2009)2618-2634.
- 7.7 Goto, Y., "Cracks Formed in Concrete around Deformed Tension Bars," in *ACI Journal* (April 1971)244-251.
- 7.8 Janney, J.R., "Nature of Bond in Pre-Tensioned Prestressed Concrete," PCA (1954).
- 7.9 Chandler, I.J., "End Zones of Pretensioned Prestressed Concrete Beams," Doctor of Philosophy Thesis, University of Melbourne, 1984.
- 7.10 Gustavson, R., "Bond Behavior of Four Types of Stands in Sleepers during Release of Prestress and Loading," Research Report 02:14, Chalmers Concrete Structures, Gothenberg 2002, 152 pp.
- 7.11 Private communication with Richard Mogel, Ben C. Gerwick, Inc. (August 2011).
- 7.12 Wang, N., *Resistance of Concrete Railroad Ties to Impact Loading*, Ph.D. Thesis, U. British Columbia (May 1996) 229 pp.
- 7.13 Ottosen, N.S., "A Failure Criterion for Concrete," *J. Engr. Mechanics Div., ASCE*, Vol. 103, EM4 (August 1977)527-535.
- A.1 Fogarasi, G.J., J.C. Nijhawan, and M.K. Tadros, "World Overview of Flow Line Pretensioning Method", *PCI Journal* (March-April 1991), 38-46.

Appendix A.1.

Concrete Tie Manufacturing

The Amtrak concrete crosstie is a pretensioned, prestressed concrete member. The tendons are stressed before the concrete is placed into the casting molds and the stressing force is transferred to the concrete after the concrete has cured to a specified strength, called the transfer length. The North American manufacturers of the Amtrak crosstie use the long line method, with fixed pretensioning beds and sliding molds.

The molds are usually gang molds one tie in length and several ties wide. The molds provide the geometry of the tie, the fixtures for securing the rail seat hardware cast into the tie, and end "bars" to separate the molds and to locate and hold in position the stressing tendons. The crossties are cast upside down in the molds. The molds are placed end-to-end in the pretensioning beds, held level, but allowed to slide longitudinally. The tendons run continuous through the molds to the ends of the pretensioning bed, which holds the stressing force. The length of the beds varies, but is usually several hundred feet long, hence, the name long line. The tendons are jacked (stressed) from one end, which is called the jacking end and anchored at the other end, which is called the dead end.

In the fixed bed technology, the beds and molds remain in the same place during the entire production and curing cycle. During production, equipment is brought to the line and moved down the line performing the various production operations. The beds also contain the curing heat piping, which along with an enclosure placed over the casting molds after the concrete has been poured, forms the curing system for accelerated curing.

The production cycle is usually daily, a 24-hour cycle. The following is a typical sequence of operation beginning after the concrete has reached the transfer strength at the conclusion of the accelerated curing cycle:

1. Remove the curing enclosure.
The enclosure is generally an insulated tarp held above and away from the concrete and molds for circulation of heat/steam. It is removed by rolling up and storing at the end of the bed.
2. De-tension the bed and transfer the prestress force to the concrete ties in the molds.
The tendons are all simultaneously released from one end. The release is gradual to prevent any shock loading on the crossties ends. Since the release is from one end (jacking end) the molds will slide slightly longitudinally to the other end (dead end). There is also a slight

narrowing of the gap between the forms due to the tendon shortening as the tendons bond to the concrete.

3. Cut the tendons between the molds.
A diamond/abrasive blade saw is used to cut the tendons in the gap formed by the removal of the end bars. As the tendons are cut, the prestress force is fully transferred to the crossties. The crosstie shortens - about 1/16 in., and provisions are made in the mold fixtures, which secure the hardware, to allow for this movement. This prevents the crossties from locking themselves into the molds and damaging the hardware and concrete.
4. Remove the ties from the molds.
There are several methods of removing the crossties. The crossties can be secured on the top or ends and lifted from the molds, or the molds can be flipped over to dislodge the crossties. In any case the crossties will be turned right side up, inspected, and stored. This is also the step where the loose rail seat hardware will be installed on the crossties, which is the last operation before shipment.
5. Clean and oil the molds.
This is also the time when the molds are inspected for damage and repaired or replaced before the next pour.
6. Place and secure rail seat hardware in the molds
7. Place tendons continuous thru the molds and secure at the stressing apparatus at the bed ends.
8. Place the mold end bars in horizontal rows to locate the tendons in the proper vertical position. Place other fixtures to hold the tendons in horizontal alignment; these fixtures are generally removed just ahead of the concrete placement.
9. Stress the tendons and secure for the duration of the concrete pouring and accelerated curing. The tendons are usually seven-wire stress-relieved strands or individual wires. The tendons are also indented for better bond control, which is important for the limited bond transfer length available from the rail seat to the end of the tie.
10. Pour the concrete, vibrate, and finish.
The concrete is usually placed with automated pouring machines, but can be placed directly from delivery vehicles. The vibration is external with attachments on the molds or internal via the pouring machine. Often, a combination of both is used.
11. Extract the end bars.
12. Cover the bed with curing enclosure.
13. Begin the accelerated curing cycle.

A good reference for a general discussion on the various methods of manufacturing pretensioned concrete members is [A.1].

Appendix A.2.

Review of Amtrak Specifications

Amtrak's specifications for the pre-2003 Northeast Corridor concrete railroad ties followed standard practice for the period (mid to late 1980s) in which they were generated. Substantial changes were made in 2003 in response to the perceived source of the cracking problem (concerns of ASR distress) that is the subject of the present study. A complete comparison of specification for the concrete material between the pre-2003 and post-2003 are described below:

- Cement/cementitious material: ordinary Type I cement was specified in the early requirements; a change was made in 2003 to Type II or III cement. In addition, the 2003 specification required that the cement be "low alkali", with no more than 0.60% sodium-equivalent alkali.
- Aggregate: While the 1992 specification required that aggregates be innocuous when tested in accordance with ASTM C289 (Standard Test Method for Potential Alkali-Silica Reactivity of Aggregates (Chemical Method)) and C1105 (Standard Test Method for Length Change of Concrete Due to Alkali-Carbonate Rock Reaction) for potential ASR reactivity, the 2003 specification supplemented it by adding the requirements that aggregates shall be hard, strong and durable, clean and free of deleterious material. It specifically stated that the aggregate shall not contain reactive material such as chert, etc.
- Water: The 2003 specification expands this section to protect against chloride-induced corrosion by including a requirement that if at any time the water-soluble chloride content of the concrete approaches the 0.06% limit, the water-soluble chloride content of the individual ingredients used to make the concrete shall be checked as often as necessary until the source of the higher water-soluble chloride content has been identified and corrective action to lower the chloride content has been accomplished.
- Admixtures: The 2003 specification adds that the admixtures shall conform to either ASTM C494 (Standard Specification for Chemical Admixtures for Concrete) or ASTM C1017 (Standard Specification for Chemical Admixtures for Use in Producing Flowing Concrete).
- Curing: While the 1992 specification required low pressure steam or radiant heat with a maximum bed temperature of 140°F, the 2003 Specification significantly expanded the curing temperature criteria by adding requirements that the temperature of the forms before placement shall be no less than 40°F; concrete temperature between casting and transfer of the prestress shall be no less than 50°F; maximum temperature shall not exceed 140°F, and heating rate shall not exceed 35°F/hr.
- Air entrainment: the air entrainment requirement has been evolving over time. The 2003 specification changed the air content to 4% to 7%, increasing the high boundary by 1% as compared to the 1992 specification.

- Strength: The 2003 specification did not revise the design strength of 7000 psi, but it did add a requirement that the strength at the time pre-stress is transferred to the concrete shall be calculated in accordance with ACI 318 but in no case shall be less than 4000 psi vs. 4,250 psi for the pre-2003 specification.
- Concrete material test schedule: The 2003 specification made significant changes to the concrete material test schedule as compared to the 1992 specification, as shown below in Table A.2.1.

Table A.2.1. Comparison of the material test schedule for pre- and post-2003 ties.

Category	1992 Specification	2003 Specification
Aggregate Prescreening	ASTM C289 (Chemical method for potential ASR of aggregate)	ASTM C295 – Petrographic examination of aggregate for concrete, every 3 months.
Aggregate Qualification and Testing	ASTM C1105 (Length change of concrete due to alkali-carbonation reaction, ACR), every 6 months. ASTM C227 – Potential ASR of cement-aggregate combination, min. 12 months duration	ASTM C1260 – Potential ASR of aggregate, mortar bar method, every 6 months. Expansion limit – 0.08% at 16 days after casting ASTM C1293 – Length change of concrete Due to ASR, every 6 months. Expansion limit – 0.04% at one year. ASTM C1105 – Length change of concrete due to ACR, every 6 months.
Concrete Quality Control and Performance Testing	ASTM C457 – Microscopical determination of air content of hardened concrete, every 6 months. ASTM C666 – Resistance of concrete to freeze-thaw, every 6 months.	ASTM C856 – Petrographic examination of hardened concrete, every 3 months. ASTM C457 – Microscopical determination of air content of hardened concrete, every 6 months. ASTM C666 – Resistance of concrete to rapid freezing and thawing, every 6 months. Relative dynamic modulus of not less than 90% at 300 cycles. Duggan concrete expansion test, every 6 months. Expansion limit, 0.15% at 20 days.

Appendix A.3.

Review of Material Testing by Others

Information Related to Pre-2003 Ties

Petrographic Analyses

- Based on petrographic examination and SEM/EDS on twelve core samples, Lankard Materials Laboratory (LML) identified fractured chert aggregate particles with dark reactive rims, fractures passing from the aggregate particles into the matrix phase of the concrete, and ASR gel in all core samples that came from a facility in Bear, Delaware. LML concluded the following:
 - Eleven core samples showed evidence of ASR. The ASR occurred in chert aggregate particles which were a minor constituent (2 to 3%) of the fine aggregate in the concrete represented by all of the core samples.
 - The cracking that was of concern in the present case was not characteristic of cracking typically associated with ASR activity.
 - ASR was the principal factor involved in both initiation of cracking and the subsequent propagation of these cracks. With continued ASR activity due to the ingress of moisture and service-imposed static and cyclic stress conditions, the ASR-initiated cracks propagated and connected and eventually formed a fracture plane through the concrete at one or both of the tendon elevations.
 - There was no major involvement of DEF in the formation of the lateral fractures.
- Based on petrographic examinations of a total of fourteen core samples retrieved from concrete ties provided by Amtrak, LML concluded the following:
 - Evidence of ASR was observed in some of the core samples, but was primarily limited to the infrequent gel deposits in voids and dark rims around some chert, glauconite, and quartzite fine aggregate particles. Cracks and microcracks associated with ASR were not observed. Out of fourteen core samples, the concrete in two core samples showed ASR distress, indicated by dark reactive rims on some of coarse aggregate particles, microcracks extending out of aggregate particles and ASR-gel; and deposits in some microcracks.
 - The causes of the observed lateral cracking were not fully revealed from petrographic examination. Expansive ASR within the body of the concrete may have partially contributed to the occurrences of these cracks; however, ASR did not appear to play a major role in the cracking and did not initiate the cracking.
 - No evidence of DEF was found in the majority of the core samples.
- In addition to the typical observed horizontal cracking, a few questionable concrete ties under the study exhibited significant map cracking on the exterior exposed surface of the ties. Both CTLGroup (CTL) and LML had the opinion that delayed-ettringite-formation

(DEF) may have contributed to the extensive cracking at these ties. CTL commented that the severity of the cracking on the exterior surfaces and within those two concrete ties was primarily related to DEF, with minor contribution from ASR. LML's SEM/EDS analysis, however, primarily identified ettringite in the microfracture planes of the core samples, and they then concluded that the extensive cracking was primarily due to ASR, and was further propagated by DEF.

- Although CTL and LML both noted marginal air content of the concrete in multiple core samples, neither stated that freeze-thaw cycling played a major role in the cracking distress.

Physical Tests – Compression

CTL and Valley Forge Laboratories (VFL) tested a total of seventeen core samples in compression. The compressive strengths ranged from 4,550 psi to 9,020 psi, with an average of 7,840 psi. There is no apparent relationship between the observed cracking and the compressive strength.

Chemical Tests – Chloride Analyses

The total acid-soluble chloride analyses on fourteen concrete samples by CTL and VFL indicate that the chloride concentration ranges from less than 0.001% to 0.007%, which is below the chloride-ion content considered for initiation of corrosion of embedded reinforcing steel. Both CTL and VFL concluded that ingress of chloride ions does not appear to have played a role in the performance of the concrete rail ties.

Duggan Tests – Potential DEF/ASR

CTL conducted Duggan tests (described as a method to test for deleterious expansion in concrete) on two core samples. The method is described in Reference [4.11]. The average expansions of both concrete tie samples in the test were above the 0.1% at 20 days criterion for potentially deleterious reactivity given by the article.

Concrete Test Results from the Manufacturing Period

CTL tested more than twenty concrete specimens in accordance with ASTM C666 (Resistance of Concrete to Rapid Freezing and Thawing) periodically from 1990 and 2000 as part of the production quality control. The test results show that the concrete had sufficient freezing and

thawing resistance, with a durability factor ranging from 92 to 100. CTL tested more than fifteen concrete specimens in accordance with ASTM C457 (Microscopical Determination of Parameter of the Air-Void System in Hardened Concrete) periodically from 1990 and 2000. The test results show that the concrete has a variable (from marginal to sufficient) air content (ranging from 3.1% to 7.6%), a variable but sufficient spacing factor (ranging from 0.003 to 0.008 in.) and a specific surface area of more than 600 in.²/in.³ in all the tests.

CTL tested the potential reactivity of fine and coarse aggregates periodically using the chemical method (ASTM C289, Potential Alkali-Silica Reactivity of Aggregates), with the test results showing that the aggregate were considered as “innocuous.” CTL also periodically tested the potential reactivity of fine and coarse aggregates tested using the mortar-bar method (ASTM C227, Potential Alkali Reactivity of Cement-Aggregate Combinations). All the test results indicate that the average expansions for the cement-aggregate combinations were well below the 0.1% expansion criterion given in the test.

Although not required by the specification, we noted two test reports indicating that the fine aggregate has been tested in accordance with ASTM C295 by two different companies (E.L Conwell in their report dated 14 September 1990, and Ambric in their report dated 11 March 1991). E.L Conwell acknowledged that small amount of chert particles are present in the fine aggregate but considered the fine aggregate composition not to be highly reactive, and Ambric concluded that the sand is sound and lacks any potentially deleterious constituents. In addition, Conwell also tested the coarse aggregate in accordance with ASTM C295 and found it to be nonreactive.

Information Related to Post-2003 Ties

Petrographic Analyses

A report from DRP Consulting, Inc. (DRP) [4.12] revealed that the coarse and fine aggregate were a manufactured (crushed) material from Hanson materials, and consisted primarily of gray dolomitic marble; the aggregate was clean, dense, and hard. The quartz in the aggregates is metamorphic quartz and do not contain chert. They concluded that the aggregates were sound and suitable for use as an aggregate in portland cement concrete. Petrographic examinations on the core samples from a total of eight concrete ties conducted by DRP [4.13, 4.14] and CTL [4.15] indicated that the concrete was proportioned with portland cement, fly ash, dolomitic limestone coarse and fine aggregate; the concrete was air-entrained; and the concrete was well consolidated with no significant segregation and bleeding. Neither DRP nor CTL found any evidence of distress associated with alkali-aggregate reaction (ASR or ACR) or cyclic freeze-thaw damage. During petrographic examination on six core samples, CTL estimated the air content of the concrete to be from 3 to 5% to 4 to 6%. Using the modified point count method outlined in ASTM C457 (Microscopical Determination of Parameters of the Air-Void System in

Hardened Concrete), DRP determined the air content of a concrete sample from a concrete tie manufactured in 2007 to be 5.9%.

Expansion Tests

CTL tested the potential for alkali-silica reaction (ASR) and alkali-carbonation reaction (ACR) of the coarse and fine aggregate. Three reports from CTL noted that they conducted expansion tests in accordance with ASTM C1293 (Determination of Length Change of Concrete Due to Alkali-Silica Reaction), ASTM C227 (Potential Alkali Reactivity of Cement-Aggregate Combinations), and ASTM C1105 (Length Change of Concrete Due to Alkali-Carbonate Rock Reaction). The test results indicated that the potential for deleterious ASR or ACR was considered to be low for the coarse and fine aggregates from the Hanson Aggregate Pit in use for the manufacture of the ties.

Duggan Tests – Potential DEF/ASR

CTL's 7 August 2007 report indicates that the Duggan Test performance of laboratory-cast samples made using the manufacturer's materials and proportions was acceptable.

Cyclic Freezing and Thawing

CTL's 6 March 2007 report noted that they cast three prisms using Hanson aggregates and conducted rapid freeze-thaw tests in accordance with ASTM C666 (Resistance of Concrete to Rapid Freezing and Thawing), Procedure A. They reported that the durability factor of these concrete samples was 93%. This value exceeded the minimum requirement by 2003 specification (90%) and is generally considered to be acceptable.

University of Illinois at Urbana-Champaign (UIUC) Report [4.16]

This report described a study evaluating the adequacy of ties (including the concrete material performance and concrete tie manufacturing process) currently being produced by Rocla at its Bear, Delaware, plant using the 2003 Amtrak Engineering Concrete Cross Tie and Fastening Assembly specification. The consulting team analyzed the 2003 Amtrak plans and specifications, and conducted two site visits (25 April 2008 and 25 November 2008) to the Rocla tie manufacturing plant in Bear, Delaware. The report addressed three areas of focus: evaluation of all processes and procedures in use by Rocla in the manufacture of the concrete ties supplied to Amtrak; evaluation of the internal QA/QC processes that Amtrak uses to ensure the concrete ties received from Rocla meet or exceed the 2003 Amtrak Plans and Specifications; and

arrangement for petrographic analysis of a selection of ties manufactured by Rocla for Amtrak since 2003 and commenting on the petrographic reports. The report concluded the following: the manufacturing process complied with the 2003 Amtrak Plans and Specifications as well as industry recommended practices for the manufacture of precast concrete products; Rocla's QA/QC procedures aligned with Precast/Prestressed Concrete Institute's (PCI) MNL-116; the concrete mixture used by Rocla was an appropriate material for this application; and the raw materials and production methods were consistent with current industry best practices.

Appendix A.4.

SGH Petrographic Examination

Petrographic Findings – From Vertical Core Samples

Concrete in Pre-2003 Tie – General Quality of Concrete:

- In general, the quality of the concrete appears to be fair-to-good, with none-to-minor indications of aggregate segregation near the top surface. The areas of minor aggregate segregation are likely caused by concrete placement deficiencies such as incomplete consolidation or over-consolidation during placement.
- The coarse aggregate is primarily composed of particles of igneous and meta-igneous rock, with minor amounts of diabase or diorite metamorphic rock that are potentially reactive due to the presence of strained quartz. Our studies of the petrology and composition (mineralogy) of the coarse aggregate indicate that the coarse aggregate in all concrete ties in this category appears to be from the same quarry, but may be from different ledges or different parts of the quarry. The latter conclusion is based on the variability and relative amounts of potentially reactive particles that we observe in each core sample.
- The fine aggregate is primarily composed of quartz, with lesser amounts of feldspars, chert, micaceous minerals, quartzite, and igneous rock particles.
- Our examination of prepared ultrathin sections reveals a normal-to-advanced degree of cement hydration. The paste structure consists of hydrated grains of portland cement with no supplemental pozzolanic or alternative cementitious materials such as fly ash or ground granulated blast furnace slag (ggbfs). We do not observe any evidence of retarded hydration or inadequate cement contents in any of the core samples.
- Based on the color, texture, and overall composition of the paste structures, the concrete in water-to-cementitious material (w/cm) ratio varies from very low (0.34 to 0.41) to moderately low (0.40 to 0.46). The estimated w/cm ratio values for each of the core samples are summarized in Table 4.3.
- Based upon a comparison with known laboratory standards, we estimate that the total air content of the hardened concrete varies from 1-1/2% to 4-1/2% and that the overall quality of the air-void systems is marginal-to-well distributed.
- We observe no significant difference with respect to these characteristics between the uncracked and cracked pre-2003 case study ties.
- We observe no indications of cyclic freeze-thaw damage, such as surface scaling and/or the formation of sub-parallel cracking.
- We observe no indications of external or internal sulfate attack, or other chemical alterations of the cement paste.

- There are no indications of delayed-ettringite formation (such as paste cracks, separation gaps around aggregate particles, or alteration of the paste structure with the formation of secondary ettringite deposits) within the paste structure.

Concrete in Post-2003 Ties – Petrographic Findings:

Table A.4.1 provides the summary of our findings for these ties.

- In general, the quality of the concrete appears to be good with low water-to-cementitious material ratio ranging from 0.32 to 0.40.
- The paste structure consists of hydrated grains of portland cement with supplemental fly ash replacement. We did not observe any evidence of retarded hydration or inadequate cement contents in the hardened concrete.
- We did not note any evidence of ASR distress, DEF distress, cyclic freeze-thaw damage, or chemical alternation of paste structure.
- The concrete mix proportions are comparable to those presented in the Amtrak concrete tie 2003 Specification.

Table A.4.1. Petrographic examination summary of concrete ties from Case Study 3: post-2003 NEC.

Feature	Tie 16	Tie 21
General condition	Good: no evidence of excessive bleeding or aggregate segregation	Good: uniform aggregate distribution
Air content	4% to 5%	3% to 4%
Quality and distribution of air-void system	Uniformly distributed	Uniformly distributed
Estimated w/cm	0.34 to 0.40	0.32 to 0.38
Cement hydration	Normal to advanced	Normal to advanced
Supplemental Cementitious material?	Fly ash	Fly ash 10 to 15%
ASR Distress Level	None observed	None observed
DEF Distress Level	None observed	None observed
Cyclic Freezing and Thawing Damage?	None observed	None observed

Concrete in San-Vel Tie – Petrographic Findings:

- In general, the quality of the concrete appears to be good. The concrete is well consolidated and does not exhibit evidence of excessive bleeding or aggregate segregation
- The number and frequency of air voids in the hardened concrete are very low and not indicative of intentional air entrainment (Figure A.4.1).
- Based on the color, texture, and overall composition of the paste structure, the concrete in the examined core samples exhibits variable water/cement ratio values that we estimate to be in the range of 0.34 to 0.42. The paste structure exhibits a normal to advanced degree of cement hydration. We did not observe any gross differences in the constituents or proportions of materials in the core samples from two different ties.
- The concrete in Core S1-3 (horizontal core sample from Tie S1) appears to have suffered cyclic freeze-thaw damage near one of the two exposed lateral surfaces of the tie, as evidenced by the formation of near-horizontal cracks that are oriented subparallel to the exterior (lateral) surface of concrete tie S1 (Figure A.4.2). However, we did not observe evidence of cyclic freeze-thaw damage in any of the other core samples. We attribute this phenomenon to the localized conditions resulting in moisture being trapped against the lateral surface of the concrete tie below the level of the stone ballast.
- Except for the cracking near the exterior surface on one end of Core S1-3, we did not observe any significant cracking within this or the other concrete core samples. Occasionally, we observe indications of early-age shrinkage cracking that disrupts only the paste portions of the core samples. In each case, early shrinkage cracks exhibit autogenous healing¹, as evidenced by the presence of well-formed crystals of calcium hydroxide that completely fill the cracks.
- We observe evidence of a tight bond between the prestressing tendons and the surrounding paste in each of the examined core samples (Figure A.4.3). We observe no gaps along the paste-to-tendon bond interface in any of the core samples.
- Frequently, we observe that the paste surrounding the prestressing tendons is slightly darker than the surrounding paste structure. This observation suggests that the paste immediately surrounding the tendons was dewatered during placement.
- We observe no evidence of DEF (such as paste cracks, separation gaps around aggregate particles, or alteration of the paste structure and formation of secondary ettringite) within the paste structure.
- We observe no evidence of ASR (such as gel-filled fractures extending from aggregate particles into the surrounding paste) in any of the examined core samples.

¹ Autogenous healing is the self-healing of fine (less than 0.008 in. wide) cracks due to the continued hydration of nearby cement grains and due to the deposition of calcium carbonate. It is commonly observed in concrete exposed to moisture.

Table A.4.2 provides our observations on the San-Vel ties.

Table A.4.2. Petrographic examination summary of concrete ties from Case Study 5: San-Vel.

Feature	Tie S1	Tie S2
General condition	Good Well consolidated no evidence of excessive bleeding or aggregate segregation	Good Well consolidated no evidence of excessive bleeding or aggregate segregation
Air content	<1% (not air-entrained)	<1% (not air-entrained)
Quality and distribution of air-void system	N/A	N/A
Estimated w/cm	0.34 to 0.42	0.34 to 0.42
Cement hydration	Advanced	Advanced
Supplemental Cementitious material?	None observed	None observed
ASR Distress Level	None observed	None observed
DEF Distress Level	None observed	None observed
Cyclic Freezing and Thawing Damage?	Yes – only at one side face about 3/4 in. from surface into the concrete body.	None observed

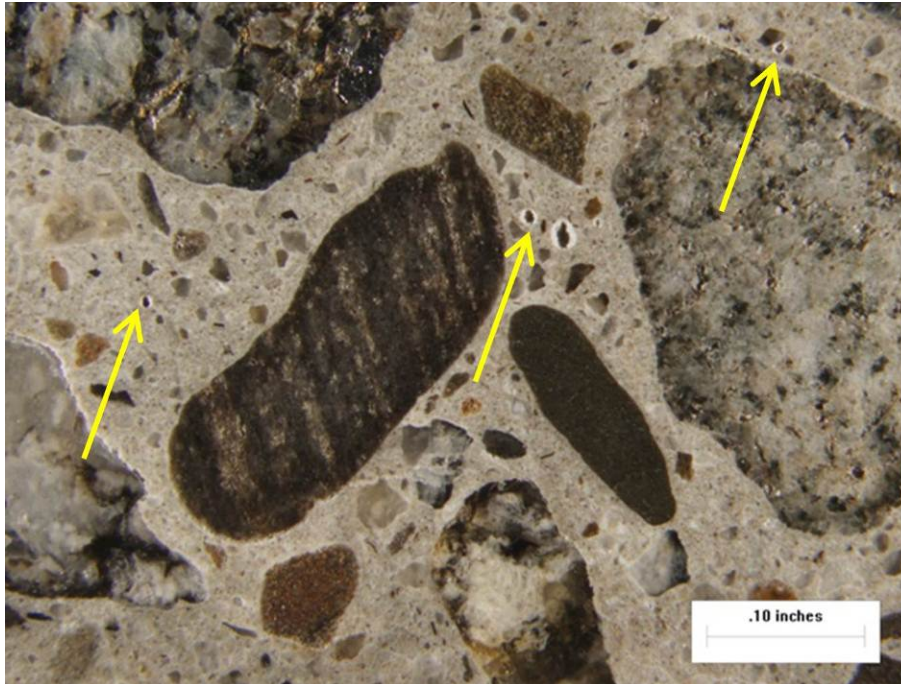


Figure A.4.1. A magnified view of the polished cross-section in Core S1-3 showing very few air voids in the paste structure.

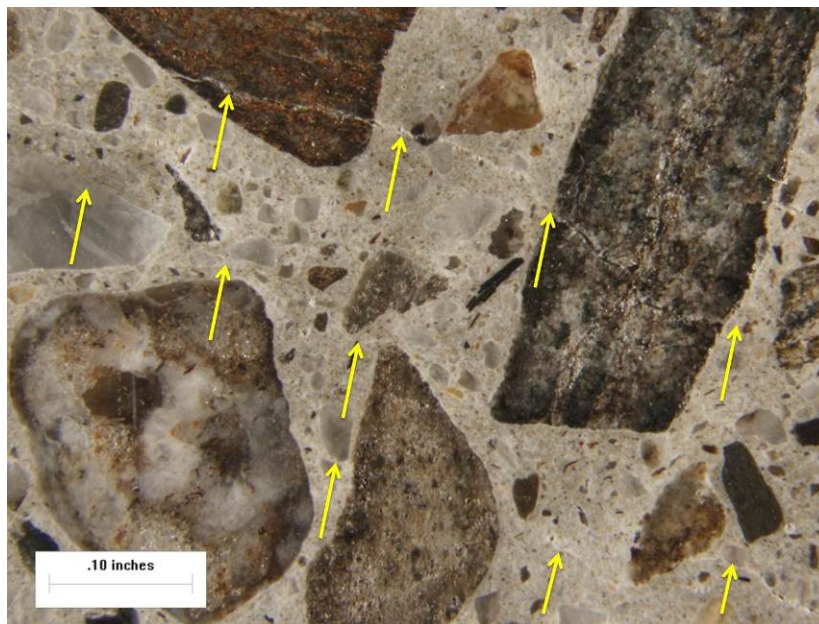


Figure A.4.2. A magnified view of the polished cross-section in Core S1-3 showing very few air voids in the paste structure.

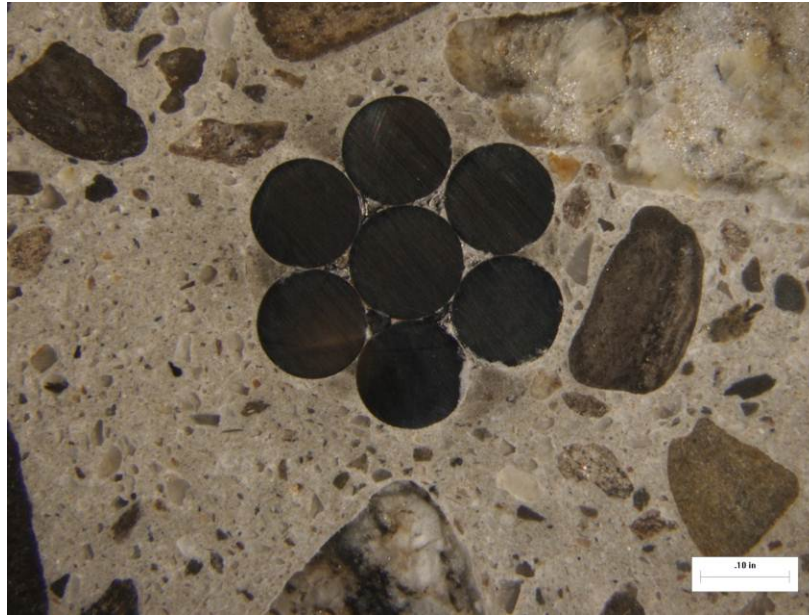


Figure A.4.3. A magnified view of the polished cross-section in Core S1-3 showing a tight intimate bond between the tendon strands and the surrounding paste.